AD 721421

ARL 70-0342
DECEMBER 1970

Aerospace Research Laboratories

CONFIGURATION OPTIMIZATION OF A CLASS OF HYPERSONIC CRUISE VEHICLES

RICHARD C. WALKER, MAJOR, USAF

HYPERSONIC RESEARCH LABORATORY

PROJECT NO. 7064

This document has been approved for public release and sale;
its distribution is unlimited.

Reproduced by
NATIONAL TECHNICAL
INFORMATION SERVICE
Springfield, Va 22151

AIR FORCE SYSTEMS COMMAND

United States Air Force

DDC
RECEIVED
APR 13 1971
C

ARL 70-0342

CONFIGURATION OPTIMIZATION OF A CLASS OF HYPERSONIC CRUISE VEHICLES

RICHARD C. WALKER, MAJ, USAF

HYPERSONIC RESEARCH LABORATORY

DECEMBER 1970

PROJECT 7064

This document has been approved for public release and sale; its distribution is unlimited.

AEROSPACE RESEARCH LABORATORIES
AIR FORCE SYSTEMS COMMAND
UNITED STATES AIR FORCE
WRIGHT-PATTERSON AIR FORCE BASE, OHIO

Foreword

The author would like to acknowledge the guidance of Dr. W. L. Hankey (ARL) throughout the course of this research. This report was prepared by the Hypersonic Research Laboratory, Aerospace Research Laboratories, Air Force Systems Command, United States Air Force, under Project 7064, entitled "High Velocity Fluid Mechanics." This work was also submitted in partial fulfillment of the requirements for the degree of Doctor of Philosophy at the Air Force Institute of Technology.

Table of Contents

List of Figures

List of Tables

Nomenclature

Symbol	
A	area
AR	wing aspect ratio
b	fuselage width
b_w	exposed wing span at midcord
c	longitudinal length of wing
c_p	pressure coefficient, $c_p = \frac{p - p_1}{q}$
C_D	drag coefficient, $C_D = \frac{D}{q \ell_b b}$
C_{D_b}	nondimensional fuselage drag, $C_{D_b} = \frac{D_b}{p_1 \ell_1 b}$
C_{D_w}	nondimensional wing drag, $C_{D_w} = \frac{D_w}{p_1 \ell_1 b}$
C_f	local skin friction coefficient
C_{L_b}	nondimensional fuselage lift, $C_{L_b} = \frac{L_b}{p_1 \ell_1 b}$
C_{L_w}	nondimensional wing lift, $C_{L_w} = \frac{L_w}{p_1 \ell_1 b}$
C_T	nozzle force coefficient, $C_T = \frac{F_n}{p_1 \ell_1 b}$
D	drag
D_b	fuselage drag
D_w	wing drag
F_n	resultant nozzle force
f	fuel-air ratio
g_c	conversion constant
H	altitude; enthalpy
h	fuselage height at station 5 (combustor exit)
h_4	vertical distance of cowl from under surface of fuselage

h_b	fuselage base height
Isp	specific impulse
i	initial
$\hat{i}, \hat{j}, \hat{k}$	unit vector in x, y, z direction respectively
L	lift
L_b	fuselage lift
L_n	nozzle-aftfuselage lift
L_o	length of ray in design space
ℓ	longitudinal dimension on fuselage
ℓ_b	longitudinal length of the fuselage
ℓ_{ew}	longitudinal length from the nose of the vehicle to the leading edge of the wing
ℓ_1	scale factor; longitudinal length of first inlet ramp
M	Mach number
m	number of constraint relations
N	number quantities defining model
n	number of degrees of freedom in model
$\hat{n}$	vehicle surface outward normal unit vector
nm	nautical mile
p	static pressure
$\dot{Q}_c$	heat absorbing rate of the regenerative coolant
$\dot{Q}_h$	convective heat transfer rate to a surface
$\dot{Q}_{\ell e}$	convective heat transfer rate to a leading edge
q	dynamic pressure, $q = \frac{\gamma}{2} p M^2$

R	cruise range; gas constant
RF	Breguet range factor, $RF = \frac{L}{D} Isp \frac{V_1}{1 - V_1^2 / V_o^2}$
r_e	earth radius
r_n	leading edge radius
$\bar{S}$	structural parameter set
S_t	Stanton number
S_p	exposed wing planform area
T	static temperature; thrust
SF	Breguet structural factor, $SF = \ln \frac{W_i}{W_f}$
t	time
$\hat{t}$	vehicle surface tangent unit vector aligned with the local flow direction
V	magnitude of velocity vector
$\forall$	volume
V_o	orbital velocity (26,000 ft/ sec)
W	weight
$\dot{w}$	weight rate of flow
$\bar{X}$	design variable set, $\bar{X} = (X_1, X_2 \ldots . X_n)$
$(X_1, X_2, \ldots, X_n)$	components in a n-dimensional design variable space
x, y, z	rectangular cartesian coordinate system

Greek Symbols

α	angle of attack
γ	ratio of specific heats; flight path angle
γ_s	vehicle surface area-structural weight proportionality constant

δ vehicle surface orientation angle

ζ heat absorbing capacity of coolant fuel per pound mass

θ shock wave angle

θ_T resultant nozzle force direction angle measured from a plane normal to the flight path

ρ density

σ ambient-sea level density ratio

τ shear stress

ϕ equivalence ratio, $\phi = \frac{f}{f_s}$

ψ range angle

$\Delta\omega$ grid size parameter in method of characteristics analysis

Subscripts

a air

av average

abw adiabatic wall condition

b body; base

c calculated; cooling; capture; combustor

e equipment; station on nozzle-aftfuselage surface at termination of fuselage

f final; friction

fc cruise fuel

$f\ell$ total available fuel

i initial

max maximum

o nominal

opt	optimum
p	payload; propulsive stream; pressure
s	structure; stoichiometric
st	stationary
stag	stagnation point
to	takeoff
w	wetted; wing; wind; wall
1	free stream properties; first inlet ramp
2	properties behind first inlet shock; second inlet ramp
3	properties behind second inlet shock; inlet cowl
4	properties behind third inlet shock; station at combustor entrance
5	station at combustor exit; nozzle-aftfuselage surface
6	nozzle cowl
7	upper surface of fuselage
8	vehicle base
9	upper surface of wing
11	lower surface of wing
12	side surface of wing

Abstract

An optimization of air breathing hypersonic cruise vehicles was performed in order to determine basic configuration characteristics and performance trends. A distinctive feature of the investigation is that prediction techniques such as the method of characteristics were used to determine the flow field surrounding the vehicle; therefore, any interaction between the aerodynamic and propulsive flow fields is accounted for in a fundamental manner. The general class of vehicles considered in the study cruise in the Mach 8 - 12 speed regime, utilize a hydrogen fueled supersonic combustion ramjet engine, and can be geometrically characterized as two-dimensional wedgelike shapes. Configurations were optimized for maximum cruise range as determined from the Breguet range equation which incorporates a measure of the aerodynamic, propulsive, and volumetric efficiencies of a configuration. A generalized configuration model was defined by discrete parameters which transformed the variational problem to a static or discrete optimization problem. The direct method of function optimization, utilizing search algorithms such as random point and adaptive creeper techniques, was employed to determine the value of the parameters defining the optimum configuration for cruise at design Mach numbers of 8, 10, and 12. The design parameter space in the vicinity of the optimum point was explored to show performance sensitivity. Results of this study showed that optimum cruise configurations are characterized by small wings. Approximately three-fourths of the total lift is provided directly from the propulsive system in accordance with an expression for optimum propulsive force vectoring derived in the study. The results also indicated that Breguet range factors of approximately 10,000 nautical miles are attainable by vehicles which cruise in the Mach 8 to 12 speed regime.

CONFIGURATION OPTIMIZATION OF A CLASS OF HYPERSONIC CRUISE VEHICLES

I. Introduction

Background

The problem considered in this dissertation is the configuration optimization of air breathing hypersonic cruise vehicles. This study is unique in that vehicle shape will be related directly to the flow field surrounding the vehicle. Previous configuration studies relating geometry directly to the flow field have dealt only with components of the vehicle such as the wings (Ref 1). Complete vehicle optimization studies, on the other hand, usually relate the shape of the vehicle indirectly to the flow field through the use of force coefficients and geometric ratios (Ref 2). At hypersonic speeds the interaction between the aerodynamic and propulsive characteristics of the vehicle can become significant, making questionable the use of force coefficients and geometric ratios to relate vehicle shape to the actual flow field surrounding the vehicle.

Kuchemann, writing in "Progress in Aeronautical Sciences" (Ref 3), points out the danger of carrying over concepts derived for components to a system composed of the components. He also indicates the need for a fundamental analysis of systems which includes the combined effect of the aerodynamic and propulsive flow field, which is the overall goal of this dissertation.

Optimization Process

The statement of the overall goal of the optimization study is the first step in the optimization process. According to Pun (Ref 4), the steps involved in the solution of a general optimization problem include: (1) definition of the overall goal, (2) definition of the level of solution, (3) mathematical formulation of the optimization problem, (4) selection of the optimizing method, and (5) realization of results. These steps also serve as a logical outline for the development of the

optimization problem considered in this dissertation.

Level of Solution. In a problem as broad and complex as the optimization of cruise vehicles, the definition of the level of solution becomes very important. For example, the level of solution could range from a cursory feasibility study to a study for implementing a prototype hypersonic cruise vehicle which would be complete in every detail.

The level of solution adopted for this investigation was between the extremes cited in the above example. The investigation can be characterized as a shape study with emphasis placed on relating vehicle geometry directly to the flow field. The level of solution is reflected in the mathematical formulation of the optimization problem which is the next step in the optimization process.

Problem Formulation. In analytical aerodynamic configuration studies, the mathematical formulation of the optimization problem consists of selection of a performance criterion and a model to relate vehicle configuration to the performance criterion. In the literature, the performance criterion is also referred to as a payoff, return, or cost function. Chapter II contains the development leading to the selection of cruise range as the performance criterion for this study.

The ideal vehicle model in an optimization study would be completely general with all variables and factors determined directly from the physics of the problem. In order to make the problem tractable, however, it was necessary to limit the investigation to a particular class of vehicles. Chapter II contains a discussion of the factors involved in the selection of the vehicle model. The selected class of vehicles cruise in the Mach 8 to 12 speed regime, utilize a constant area supersonic combustion ramjet engine which burns hydrogen fuel, and can be characterized geometrically as two-dimensional wedgelike wing body vehicles.

Chapter II also contains a description of the force and flow field prediction methods which are essential to relating vehicle shape directly to the surrounding flow field. Once the mathematical formulation of the problem is complete, the next step in the optimization process becomes the selection of a method to optimize the performance criterion.

Optimizing Method. The two general optimizing methods used in aerodynamic configuration studies are the indirect and direct methods. Until recently, most configuration optimization studies have utilized indirect methods such as the calculus of variations. With the advent of the digital computer, the direct method has become practical in the solution of optimization problems. Chapter III contains a discussion of the application of the direct method of optimization to the cruise vehicle optimization problem considered in this investigation.

Realization of Results. The last step in the optimization process, the realization of results, is closely related to the definition of the level of solution. The level of solution adopted for this study does not reveal all the possible performance and configuration characteristics of optimized hypersonic cruise vehicles. However, the results and conclusions of this study, contained in Chapter IV and V respectively, do answer a number of fundamental questions concerning the performance and configuration of hypersonic cruise vehicles.

II. Problem Formulation

One of the most difficult steps in the process of optimizing a system such as a complete vehicle configuration is the formulation of the problem. At all times, the objective or overall goal of the investigation must be kept in mind as well as the adopted level of solution. Since the goal of the present investigation was to relate optimum vehicle shape directly to the flow field, emphasis was placed on model selection and flow field prediction techniques which allows the flow field quantities to be determined quite accurately.

The problem formulation consists of selecting a performance criterion and model to relate vehicle configuration to performance. Culminating the problem formulation is an IBM 7094 computer program which evaluates the performance of a generalized configuration defined by various sets of design parameters. A discussion of the selection of performance criterion, model, and design parameters is contained in this section, while details of the computer program formulation as well as a listing of the program are contained in Appendix E.

Performance Criterion

For cruise vehicles the primary objective is either to carry a given payload for the maximum distance, or to carry the maximum payload over a given distance. Thus, either payload or range is a reasonable choice for the performance criterion. Maximum range with a fixed payload was chosen as the measure of performance in this investigation. Total range of a vehicle includes range covered in ascent, cruise, and descent. In order to make the problem tractable and still directly relate vehicle shape to flow field quantities, only the cruise phase of the mission profile was considered. Thus, the optimized configuration represents the optimum cruise configuration of a class of vehicles in which the range covered in the cruise phase of the mission profile is most significant.

The cruise range is obtained in general by numerical integration of the vehicle trajectory equations from initiation to termination of cruise. However, if it is assumed during cruise that: (1) flight path angle is zero, $\gamma = 0$; (2) cruise speed is constant, $\frac{dV_1}{dt} = 0$; and (3) the product $\frac{L}{D}$ Isp is constant, then the cruise range R can be expressed by the familiar Breguet range equation (see Appendix A)

$$R = \frac{L}{D} Isp \frac{V_1}{1 - \frac{V_1^2}{V_o^2}} \ell n \frac{W_i}{W_f} \qquad (1)$$

subject to the restrictions of

$$L = W \left(1 - \frac{V_1^2}{V_o^2} \right) \qquad (2)$$

and

$$T = -Isp \frac{dW}{dt} = D \qquad (3)$$

The above version of the range equation yields great circle range over a spherical nonrotating earth.

The Breguet range equation is an appropriate performance criterion in that it incorporates three fundamental measures of vehicle efficiency (aerodynamic, propulsive, and volumetric) in one equation. The first two are easily recognized in Eq 1 as the L/D and Isp respectively; however, the volumetric efficiency is implicitly related to the structural factor term ($\ell n\ W_i/W_f$) as shown in Appendix E. Volumetric efficiency for the purpose of this investigation is the ratio of configuration volume to the enclosing surface area, $\forall / A_w$.

Vehicle Model Selection

Once the performance criterion has been selected, a vehicle model is needed to relate vehicle configuration to performance. In order to proceed with the formulation of the problem it is necessary at this point to limit further the problem by specifying the cruise Mach

number regime, combustion process, fuel, and geometrical configuration class.

Mach Number Regime and Combustion Process. The lower limit of the Mach number regime investigated (M = 8) was coupled to the selection of combustion process. Previous studies (Ref 5) have shown that the subsonic combustion process is more efficient below flight Mach numbers of about M = 8, while supersonic combustion is more efficient for the higher speeds. Mach number design points of M = 10 and M = 12 were also included in this study to determine the possibility of a cruise range increase with cruise velocity, as suggested by the velocity term in the Breguet range equation. Thus, the supersonic combustion process was utilized as the model for the Mach 8, 10, and 12 design points.

Fuel. The specification of the flight Mach number regime of M = 8 to M = 12 limited the choice of fuel for the vehicle to liquid hydrogen. The main factor in the fuel selection was the high heat sink capacity of LH_2 compared to the other candidate fuels shown in Table I.

TABLE I

Candidate Fuel Properties

Fuel	Heat of Combustion Btu/lb	Heat Sink Btu/lb	Density lb/ft^3	M_{max}
Liquid H_2	51,600	6000	4.5	16
Methane	21,500	1100	26.4	7
JP-4	18,600	165	50.0	3

At hypersonic speeds, it is necessary to cool actively at least the combustor of the vehicle. The higher the speed--the higher the cooling requirement. A limiting speed in a sense occurs when the fuel required for cooling (which is then used for propulsion) equals that required for stoichiometric combustion. A qualitative estimate of the limiting speed can be obtained by equating the heat sink of the fuel to

the total enthalpy of the air flow (Ref 6). The last column in Table I indicates the maximum cruise Mach number for this condition. From the table it can be seen that only LH_2 has enough cooling capacity for the Mach number range considered in this investigation.

The density of LH_2 is approximately the same as the density of passenger compartments of transport type vehicles; therefore, to the first order, passengers and fuel can be interchanged. Since passenger type cruise vehicles were considered in this investigation, configurations optimized for maximum cruise range with a given payload will be the same as configurations optimized for maximum payload over a given cruise range.

Geometrical Class. One of the major steps in the formulation of the optimum cruise vehicle problem is the selection of a geometrical class of vehicle shapes to optimize. The two-dimensional wedgelike wing body class of vehicles was selected as the model for this investigation for several reasons. Since one of the basic goals of the study was to relate vehicle configuration directly to the flow field caused by volume, lift, and heat addition, the generalized model must be amenable to these flow field calculations. Two classes of vehicle models which are amenable to the required flow field calculations are a two-dimensional wedgelike class and an axisymmetric conelike class. In an investigation of hypersonic lifting bodies which included both of the classes, Hankey found that when sharp leading edges could be maintained the two-dimensional wedgelike class had superior aerodynamic and volumetric efficiencies--two of the factors in the performance criterion of this investigation (Ref 7). The cooling capacity of the hydrogen fuel allows regenerative cooling of the leading edges of the two-dimensional configuration which permits the leading edges to be aerodynamically "sharp." Thus, on the basis of potential performance considerations the wedgelike class was selected over the conelike class as the geometrical model for this investigation.

A final consideration in the selection of the model was from the standpoint of the evolution of the optimization model level in the solution of optimization problems. Williams (Ref 8) considered a wedgelike geometrical model at a lower level of solution. Some results of the present investigation will be compared with the work of Williams to gain insight into the effect of the level of solution on the realization of results in the optimization process.

Due to the numerical nature of the algorithm for computing the flow field surrounding the vehicle, variational optimization methods, such as the calculus of variations, were not convenient to apply to this problem. Therefore, a generalized configuration model was defined by discrete parameters. Thus, the optimization problem was transformed from a variational problem to a discrete or static problem (Ref 4). The generalized configuration and the geometric parameters used to define the configuration are shown in Figure 1. The parameters chosen to define the geometrical model were balanced by two factors: (1) the desire to have many design parameters in order to keep the model as general as possible; and (2) the knowledge that each additional design parameter increases the number of possible combinations of design parameters which complicates the search for the optimum.

Force Prediction Model

At this point, methods are needed to relate the vehicle model to the performance criterion. The first two terms of the performance criterion, the L/ D and Isp, can be determined from a knowledge of the flow field surrounding the vehicle and the amount of hydrogen fuel added to the propulsive stream. A unique feature of the present investigation is that a complete inviscid flow field solution was performed for each change in configuration geometry. Thus, any interaction between components of the vehicle was accounted for in a fundamental manner. Although described in more detail in Appendix E, a summary of the model used to obtain the aerodynamic and propulsive forces on the

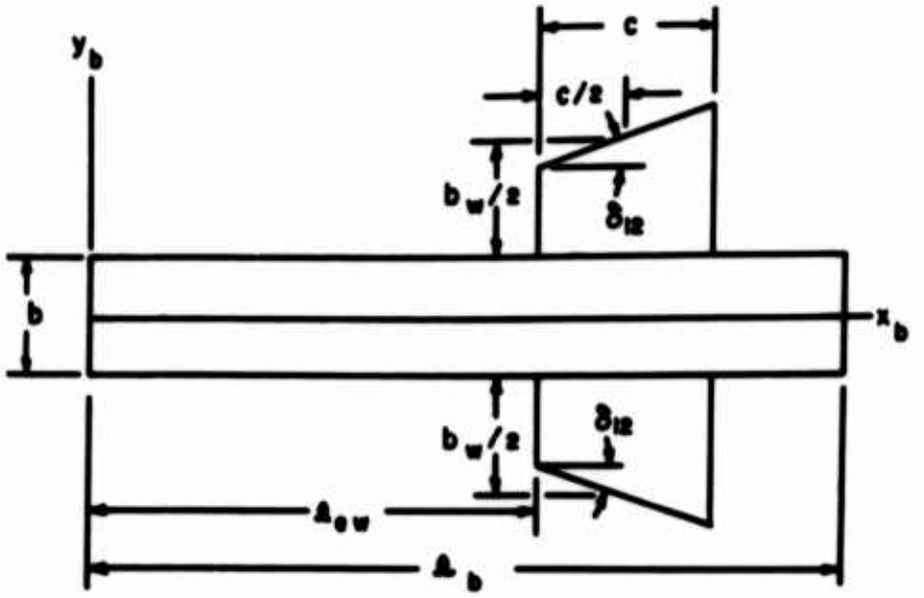

PLANFORM VIEW

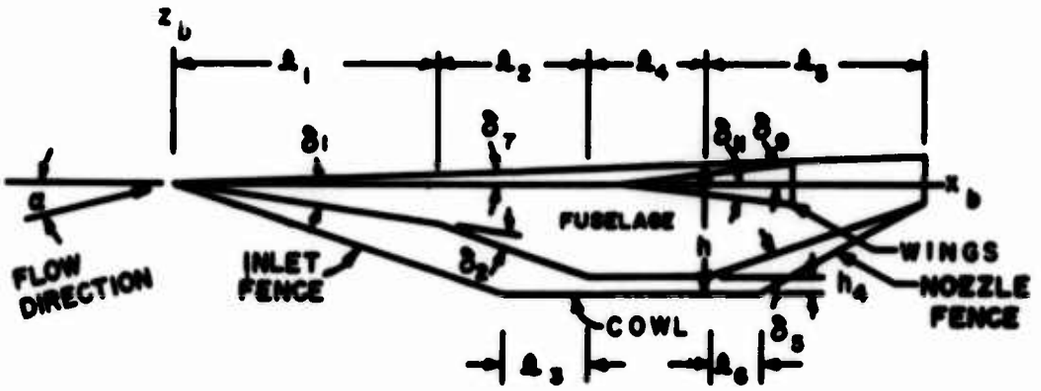

PROFILE VIEW

FIG 1 Generalized Shape

vehicle is presented here. In describing the model, it is convenient to divide the vehicle into components: inlet-forebody, combustor, nozzle-aftfuselage, fuselage, and wing.

Inlet-forebody. The inlet-forebody is a two-dimensional double ramp inlet with a three-shock wave external compression system. Fences (Fig 1) extend from the nose of the vehicle to the leading edge of the inlet cowl to contain the inlet airflow. Thus, the vehicle is a wave rider (Ref 9) in the sense that the forebody "rides" on the contained plane shock waves. Forces on the inlet-forebody were obtained using the oblique shock relations with skin friction superimposed.

The geometry of the inlet was constrained to produce shock on the cowl lip, thus all of the air flow deflected by the forebody is captured by the inlet cowl and is used in the combustion process as depicted schematically in Figure 2. The inlet geometry was also constrained to produce a combustor entrance temperature of at least 2000R corresponding to the auto-ignition value of the hydrogen fuel-air mixture. The method of incorporation of these constraints in the mathematical model is discussed in the section on constraints.

Combustor. Length of the combustor and the midsection of the vehicle was defined by the length ℓ_4 as shown in Figure 1. The combustor inviscid flow field was computed using a constant area one-dimensional supersonic combustion process. Turbulent skin friction was superimposed on the inviscid solution to determine the combustor duct forces, as it is shown in Appendix E that combustor drag does not appreciably affect the inviscid solution.

Nozzle-aftfuselage. The underside of the aftfuselage of the vehicle serves as an expansion surface for the combustor gases thereby forming, along with the nozzle cowl and fences, a two-dimensional asymmetric nozzle or half nozzle as shown in Figure 1. The nozzle forces were determined by using the method of characteristics solution to determine the pressure forces to which skin friction was superimposed.

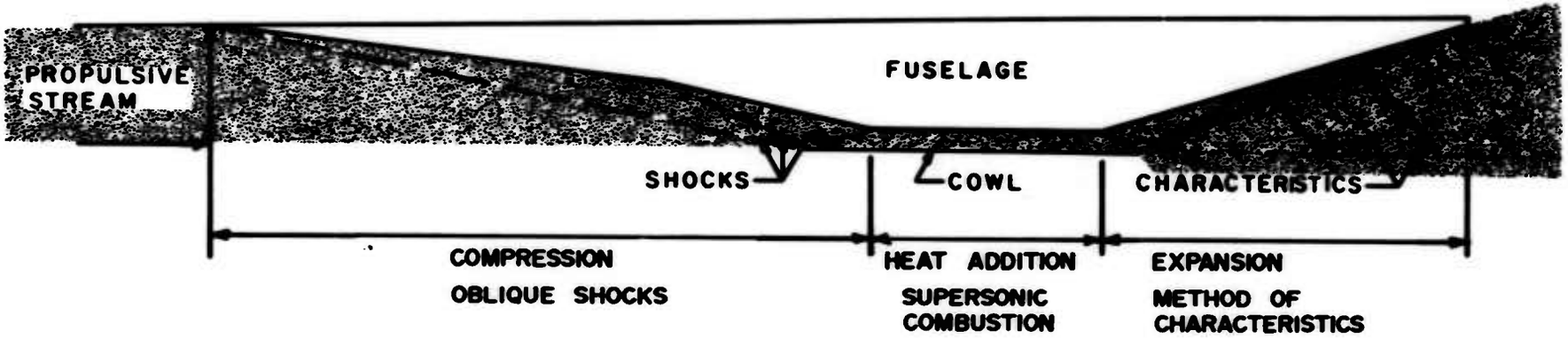

FIG 2 Propulsive Flow Field Model

Fuselage and Wing. Oblique shock or Prandtl-Meyer relations and superimposed skin friction were used to determine the forces on the top surface of the fuselage, underside of the cowl, and wing surfaces depending on the orientation of the surfaces with respect to the free-stream flow direction. Base pressure drag and leading edge drag of the fuselage and wings were included in the summation of vehicle forces. Regenerative cooling requirements of the sharp leading edges of the vehicle (one tenth of an inch diameter) were also determined for the model.

Placement of wings on the fuselage was determined by the requirement that the pitching moment about the center of gravity (assumed to be at centroid of the fuselage profile area) be zero. Rolling and yawing moments are zero due to symmetry of the model. Thus, although stability and control devices (reaction controls, thrust vectoring, and control surfaces) were not included in the analysis, the vehicle model can be characterized as being trimmed about all three axes.

In Appendix E, it is shown that in order to obtain the flow field solution it was necessary to specify the cruise Mach number M_1, ambient temperature T_1, and pressure p_1 at cruise altitude, as well as the amount of fuel added to the propulsive stream which can be expressed in terms of the equivalence ratio ϕ. These quantities (M_1, T_1, p_1, ϕ), in addition to the vehicle geometry parameters, became variables in the problem, although not necessarily independent variables as will be explained in the section on constraints.

The problem formulation thus far has accounted for relating vehicle geometry directly to the first three terms of the performance criterion which are collectively referred to as the range factor RF given by

$$RF = \frac{L}{D} Isp \frac{V_1}{1 - \frac{V_1^2}{V_o^2}} \qquad (4)$$

The range factor is an indication of the range potential of a vehicle from a propulsive and aerodynamic point of view. The range factor is meaningful, however, only if the aerodynamic and propulsive characteristics are calculated in light of the constraint that the configuration provides a volume for payload, fuel, and equipment. This constraint is contained implicitly in the last term of the performance criterion--the structural factor $\ell n(W_i / W_f)$. A method is needed at this point in the formulation to relate vehicle geometry to the structural factor and hence, to the performance criterion.

Structural Factor

The structural factor SF for the cruise segment of the trajectory can be written as

$$SF = \ell n \frac{W_i}{W_f} = \ell n \left[1 + \frac{\dfrac{W_{fc}}{W_{f\ell}} \dfrac{W_{f\ell}}{W_{to}}}{\dfrac{W_p}{W_{to}} + \dfrac{W_e}{W_{to}} + \dfrac{W_s}{W_{to}}} \right] \quad (5)$$

where

$W_{fc} / W_{f\ell}$ = cruise fuel fraction
$W_{f\ell} / W_{to}$ = total available fuel fraction
W_p / W_{to} = payload fraction
W_e / W_{to} = equipment fraction
W_s / W_{to} = structural weight fraction

The objective here is to relate the volumetric efficiency of a configuration to the structural factor. It is shown in Appendix E that this can be done by assuming the structural weight W_s to be a function of the surface area

$$W_s = \gamma_s A_w \quad (6)$$

and by assuming typical values for a set $\bar{S}$ of structural parameters which become reference parameters for the evaluation of the structural

factor. The set consists of three weight fractions which characterize the mission of vehicles, material densities which relate weight to vehicle volume, and the proportionality constant γ_s which relates area to structural weight

$$\bar{S} = \left\{ \frac{W_p}{W_{to}} = .05, \quad \frac{W_e}{W_{to}} = .15, \quad \frac{W_{fc}}{W_{f\ell}} = .5, \quad \rho_p = 4.5 \text{ lb/ ft}^3, \right.$$

$$\left. \rho_{f\ell} = 4.5 \text{ lb/ft}^3, \quad \rho_e = 180 \text{ lb/ft}^3, \quad \gamma_s = 7.5 \text{ lb/ ft}^2 \right\} \tag{7}$$

The assumed values of the structural set members are characteristic of hydrogen fueled passenger transport type vehicles (Ref 10). Appendix C contains a range performance sensitivity analysis of each member of the structural set.

The main purpose of forming the structural set $\bar{S}$, however, was not to evaluate the absolute level of performance but rather to evaluate the change in the performance as a function of the volumetric efficiency of the configurations. This can now be done. Thus, three basic measures of vehicle efficiency (aerodynamic, propulsive, and volumetric) are incorporated in the performance criterion.

Constraints

Constraints incorporated in the mathematical formulation can either help or hinder the optimization process. Constraints are helpful if the information from the constraints can be used to calculate configuration variables thereby reducing the number of search variables. Besides reducing the number of search variables, it will be shown in the next chapter that constraints can provide explicit information on the boundaries of the feasible region of the design space.

Constraints complicate the optimization process if they cannot be used to reduce the design space and must, for example, be adjoined to the performance criterion to form a penalized performance

criterion (Ref 11). Considerable effort was made in this investigation, therefore, to use constraint information to limit the dimensions and feasible region of the design space. The two general types of constraints incorporated in the mathematical formulation were the equality and inequality constraints.

Equality. Relationships derived from equality constraints can be used to reduce the number of search variables as shown in Appendix E. In addition to geometric interrelationships, the following equality constraints were imposed on the formulation: equilibrium flight, from selection of performance criterion; trimmed condition, to provide a gross measure of longitudinal stability; ambient pressure-temperature relationship, from the physics of the atmosphere; and shock on inlet cowl lip, from ramjet inlet design practice to give optimum performance. The shock on inlet lip constraint also reduces the dimensions of the design space which still contains the optimum. Two nongeometric parameters, combustor entrance temperature T_4 and takeoff weight W_{to}, were also introduced to replace two geometric parameters, δ_2 and ℓ_1, (see Fig 1) as design variables. The motivation for the substitution becomes apparent later when discussing inequality constraints. Although the substitution of design variables added two parameters to the number necessary to define the generalized configuration, two equality constraint relations were also added keeping the effective number of independent variables constant.

Inequality. Equality constraints have a direct influence on all design points in the design space whereas inequality constraints influence the design only when the constraint is encountered. Two forms of inequality constraints were present in the problem investigated in this study. One form was applied directly as an upper and or lower bound on the design variable. A lower bound of 2000R (auto-ignition value of fuel-air mixture) was imposed on the combustor entrance temperature. An upper bound of 500,000 lb was placed on the takeoff weight as a

typical value since the results will show range performance to increase monotonically with takeoff weight. Inequality constraints placed directly on the design variables are easily handled. In fact, they are even desirable from an optimization search standpoint since they explicitly define the boundaries of the feasible region of the design space.

On the other hand, inequality constraints which are functions of the independent design variables are more difficult to handle. The inequality constraint functions are calculated along with the performance criterion. If the value of the constraint function exceeds the specified amount, then the value of the performance criterion for that set of design variables is penalized. Thus, the function type inequality constraint also limits the feasible region of the design space, although after the fact since the numerical calculations have already been performed.

The following functional type inequality constraints were incorporated in the mathematical formulation:

(1) A cooling constraint, such that the fuel required for regenerative cooling (see Appendix D) was less than or equal to fuel required for propulsion.

(2) A wing placement constraint (see Fig 1) such that the attachment point of the leading edge of the wing was on the fuselage ($\ell_{ew} < \ell_b$) and in the xy-plane of the body axis system ($\delta_7 \geq 0$) for trimmed flight.

(3) A wing area constraint, such that planform area was greater than or equal to zero ($S_p \geq 0$). Since in this formulation (see Appendix E) the wing area was directly proportional to thrust minus fuselage drag, a wing area greater than zero indicates constant velocity flight can be maintained. Notice that the wing area of the optimized configurations will reflect the cruise point. Takeoff and landing considerations, not included in this investigation, would perhaps require the lower bound on the wing area constraint to be increased.

The problem formulation contained in this chapter reflects one level of solution of the general problem of configuration optimization of hypersonic vehicles. The selections and assumptions made during the formulation of the problem have resulted in a particular class of configurations to be optimized for a specific set of conditions. Since the mathematical formulation of the problem does not include all classes of configurations and a consideration of all constraints, limitations, and influences; the optimized configuration is not expected to offer a final solution to the optimum vehicle problem. The present formulation of the problem is expected, however, to contribute to a final solution by answering some fundamental questions concerning the performance and configuration trends of optimum cruise vehicles when vehicle geometry is related directly to the surrounding flow field.

Appendix E contains the development and a listing of the Fortran IV computer program which resulted from the problem formulation discussion presented in this chapter. The program relates the performance criterion (cruise range R) to the parameterized configuration shown in Figure 1. So that functionally

$$R = f(\overline{X}) \tag{8}$$

where $\overline{X}$ is a set of independent design variables consisting of

$$\overline{X} = (\delta_1, T_4, \phi, \ell_4, \delta_5, \ell_5, \ell_6, \delta_9, \delta_{11}, \delta_{12}, AR, b, \delta_7, a, W_{to}, M_1)$$

Due to the numerical methods necessary to predict the flow field and to integrate the forces on the vehicle, the algebraic form of Eq 8 is not known. However, the value of the performance criterion can be determined numerically for values of the independent variables. Thus the relationship between the performance criterion and independent design variables is characterized as computational as opposed to mathematical. This distinction becomes important in the selection of optimizing methods which is discussed in the next chapter.

III. Optimizing Method

Introduction

Once the problem is formulated, the next step in the optimization process is the selection of an optimizing method. The methods can be classified into two groups--indirect and direct. Indirect methods are mathematical in the sense that necessary conditions are used to find the extremum. In ordinary maxima and minima theory, the value of x is sought which causes the first derivative of f(x) with respect to x to vanish, or in the case of the calculus of variations the curve is sought which satisfies the Euler necessary condition. In the direct method, on the other hand, the value of x which makes f(x) an extremum is determined by direct comparison of the value of the function at two or more points in the operating space (Ref 12). Problems formulated by the indirect methods can be solved either numerically or analytically; whereas, the direct method implies a numerical solution. With the advent of the digital computer, the direct method of optimization has become practical.

The cruise vehicle optimization problem has been formulated so that the performance criterion R can be evaluated for values of the independent design variables $\bar{X}$ by the computational algorithm contained in Appendix E. The objective now becomes to determine the combination of independent design variables $\bar{X}_{opt}$ which maximizes the cruise range R

$$R_{max} = f(\bar{X})_{opt} = f(X_1, X_2, \ldots, X_{15})_{opt} \qquad (9)$$

for design cruise Mach numbers of 8, 10, and 12.

In order to understand the factors involved in the direct search for the maximizing set of design variables, it is helpful to introduce some geometric concepts of the design variable space and response surface such as those discussed by Wilde (Ref 12). The design variable plane and response surface are schematically depicted in Fig 3

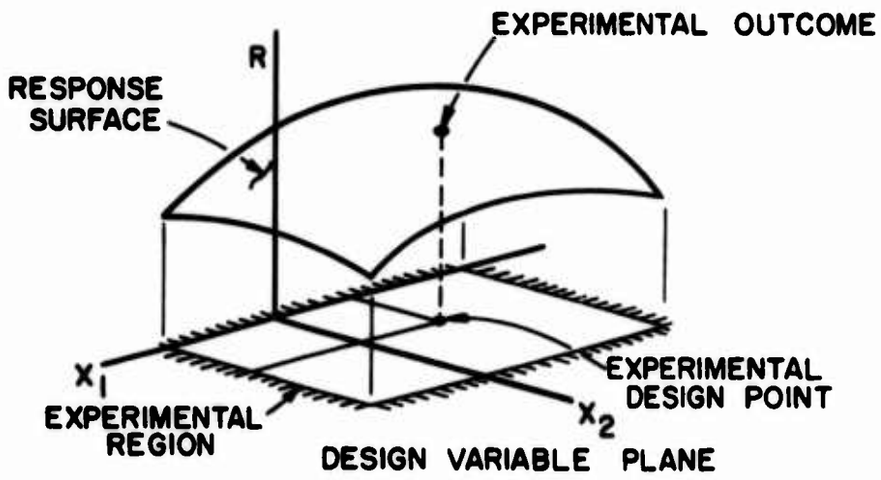

FIG 3 Graphical Representation of Direct Search Problem for Two Design Variables

for a function of two independent variables. In the case of configuration optimization, for example, each point in the design variable plane represents a configuration and comprises the input for a possible numerical experiment. The point above it on the response surface (the value of the function) represents the experimental outcome. The feasible values which each of the independent variables can assume form a bounded region in the design variable plane. This bounded region is referred to as the experimental region or design space.

Geometrically, the direct search method of function optimization locates the summit of the response surface by performing numerical experiments with points contained in the design space. The methods used to select the points with which to perform the numerical experiments are called search techniques which are discussed later. Although impossible to represent physically for functions of more than two independent variables, the concepts of the design space and response surface can be extended to functions of n independent variables.

Optimum Configuration Search

The search for the optimum cruise vehicle configuration can be divided into three phases. The first phase is the definition of the design space or experimental region from the design variable plane; the second phase is the systematic exploration of the design space for the optimum; and the third phase is the termination of the search.

Design Space Definition. The experimental region or design space is the portion of the design variable plane which contains the candidate optimum configurations. The upper and lower bounds on each of the design variables (X_1, . . . , X_{15}) define the design space. Inequality constraints on the independent variables and care to include the true optimum configuration in the design space were factors in placing upper and lower bounds on the 15 design variables comprising the design space. The minimum combustor inlet temperature T_4 is an example of a design space boundary formed by an inequality constraint. Initially upper and lower bounds on the unconstrained design variables are chosen such that the design space represents all feasible configurations. As knowledge of the response surface is gained, the size of the design search space which still contains the optimum configuration can be reduced. Once the design space is defined, multivariable search techniques are used to systematically explore the design space for the optimum configuration at the specified design Mach number.

Direct Search Algorithms. Several well known direct search algorithms (Table II) have been combined into a single computer program called the Automated Engineering and Scientific Optimization Programs - AESOP (Ref 14). The program AESOP is independent of the problem being solved. In aerodynamic configuration problems, for example, the computer program containing the algorithm for the evaluation of the configuration performance is linked to AESOP to perform a systematic search for the optimum configuration. In the cruise vehicle problem, for a given design Mach number M_1, points

TABLE II

Basic Search Algorithms Contained in Program AESOP

1. Sectioning - Succession of one-dimensional optimization calculations parallel to coordinate axes. Variables may be perturbed in random or natural order.

2. Pattern - A Ray Search in the gross direction defined by a previous search or search combination.

3. Magnification - Straightforward magnification or diminution about the origin.

4. Steepest Ascent - Search along the weighted gradient direction. Several weighting options available.

5. Adaptive Creeping - Search in small incremental steps parallel to the coordinate axes. Step-size adjusted automatically in the algorithm. Variables may be perturbed in random or natural order.

6. Quadratic - Second-order multivariable curve fit to the function being optimized, followed by search in direction of second-order surface optimum.

7. Davidon's Method - An attempt to achieve the advantages of second-order search from an ordered succession of first-order (steepest ascent) searches.

8. Random Point - Function to be optimized is evaluated at a set of uniformly distributed random points in a specified region.

9. Random Ray Search - Function is optimized by search along a sequence of random rays having a uniformly distributed angular orientation in the multivariable parameter space.

from the design space were selected by a specified search algorithm in AESOP and evaluated by the vehicle Design and Evaluation Computer Program - DECP (Appendix E) until the maximum cruise range performance and corresponding configuration were obtained.

Although nine search algorithms were available in AESOP, it became evident in early searches that search algorithms (steepest ascent, quadratic, and Davidon's method) requiring derivatives of the performance function with respect to each of the search variables were too time consuming. For example, since the derivatives must be determined numerically, to find the gradient of the performance function at one point on the response surface of a 15 search variable problem required 30 evaluations by DECP. This required approximately 10 minutes of 7094 computer time. Furthermore, in the steepest ascent method, the path of steepest ascent and the positive gradient of the performance function coincide only if unit perturbations of each of the search variables produce a similar change in the performance function (Ref 14). In the case of the cruise vehicle problem, the effect on the performance function of a unit perturbation of the equivalence ratio $\Delta\phi = 1$ is large; whereas, a unit perturbation of the takeoff weight $\Delta W_{to} = 1$ is negligible. A weighting matrix can be chosen in an effort to account for varying effects of a unit perturbation on the performance function. The necessity of choosing a weighting matrix in order to determine the true path of steepest ascent, however, makes it questionable if the computational time required to determine accurately the gradient of the performance function was used most effectively. Search algorithms available in AESOP which produced satisfactory results for the cruise vehicle problem were the random point, sectioning, and adaptive creep algorithms.

In the random point method, a series of design points are selected from points which have uniform distribution throughout the design space. The performance at these design points is evaluated one by one and the design point with the highest value of the performance

function is retained. This method has an advantage in that its effectiveness is independent of the shape of the response surface. The method works as well on multimodal as on unimodal (single peak) response surfaces. One disadvantage of the method is that, due to the size of the design space, for most problems many points must be evaluated before attaining a high probability that the best point selected is actually at or near the optimum. The random point method was used in this investigation during the early exploration of the design space when the response surface of the criterion function was unknown.

Another method which is useful in the early phases of the optimum configuration search is sectioning. Search by sectioning is a series of one-dimensional searches along the entire ray in design space parallel to each of the coordinate axes as shown in Figure 4.

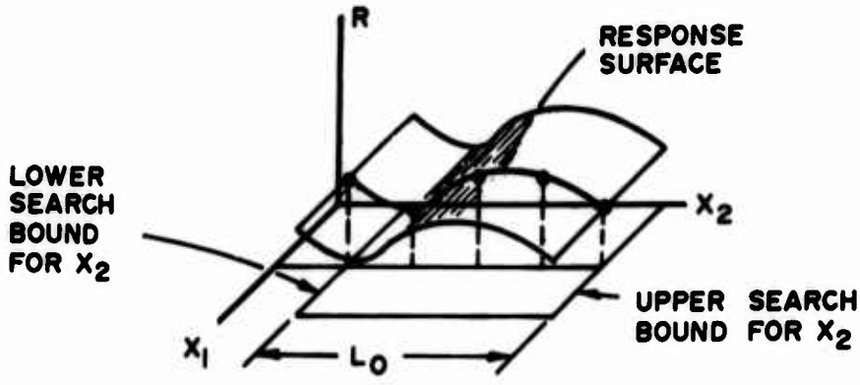

FIG 4 Sectioning Search for Extremal Along Ray Parallel to X_2 Axis

The one-dimensional ray in design space is formed by fixing all the search variables except the one on which the search is to be performed. The length L_o of the ray is determined by the upper and lower bound of the design variable. Points are evaluated along the ray in order to find the value of the sectioned variable which results in the highest value of the performance function. The value of the variable giving

the maximum performance is retained and the process repeated for each of the remaining design variables.

The adaptive creeper search method is another form of sectioning. However, instead of searching along the entire length of the ray parallel to the coordinate axis as in the section search, only small perturbations are made in one of the independent variables. Perturbations in the independent variable are continued until no further improvement in performance is possible. When the process has been repeated for each independent variable in turn, a creeper search cycle is completed. In the case where there is no interaction between the independent variables only one search cycle is required to locate a peak in the response surface. This case is illustrated in Fig 5 for the contours of a performance function which has two independent variables. Usually, however, interaction between the independent variables is present so that more than one search cycle is required to locate the optimum. This case is also illustrated in Fig 5 where three

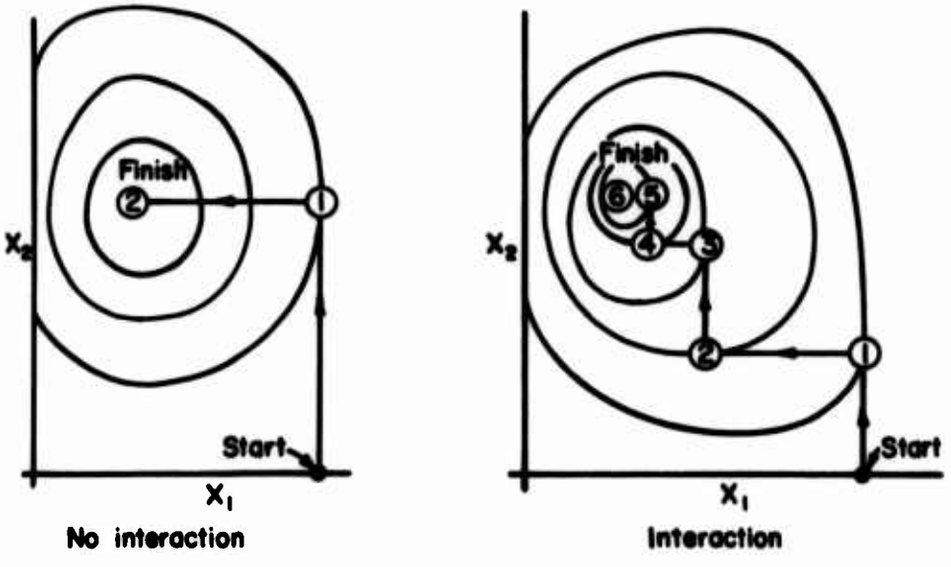

FIG 5 Creeper Search With and Without Interaction of Design Variables

adaptive creeper search cycles would be required to locate the optimum. The creeper method was effective in the cruise vehicle optimization in the latter phases of the systematic search.

Figures 6 - 9 illustrate the performance of the random point, sectioning, adaptive creeper, and steepest ascent optimum seeking algorithms on a test function J

$$J = 10 - ((X_2 - X_1)^2 + (1 - X_1)^2) \qquad (10)$$

where the shape of the response surface is known. Contours of the response surface of the test function are shown in the figures as well as the starting point and search limits for all search techniques. Although the response surface is unimodal, the search problem is not a particularly easy one since a mild ridge is present in the response surface.

All searches in the above example were terminated after 50 evaluations of the performance function. Progress during the search is indicated in the figures by arrows and the number of evaluations of the performance function required to arrive at the point. The results of the example show the adaptive creeper to be most efficient while the steepest ascent is least efficient in this example. It should be pointed out, however, that the best search technique depends on design space and response surface characteristics which, of course, are a function of the particular search problem.

Termination of Search. The last step in the direct search for the optimum cruise vehicle configuration is the termination of the search. A total of approximately 3000 numerical experiments were made on a IBM 7094 computer to obtain the optimum configuration for the design cruise Mach number 8, 10, and 12 shown in the next chapter. Searches were terminated when the gain in the performance function R was less than 1% between search cycles. Searches were also started from different points in the design space to examine the possibility of a multimodal performance response surface. The response surface

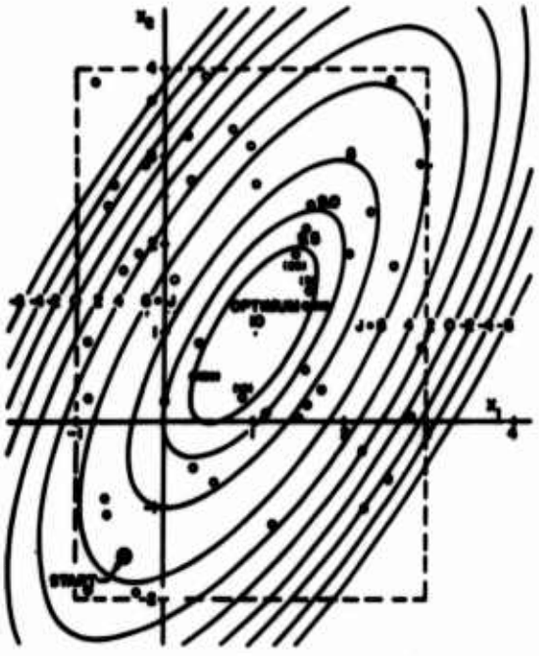

FIG 6 **Random Point Search**

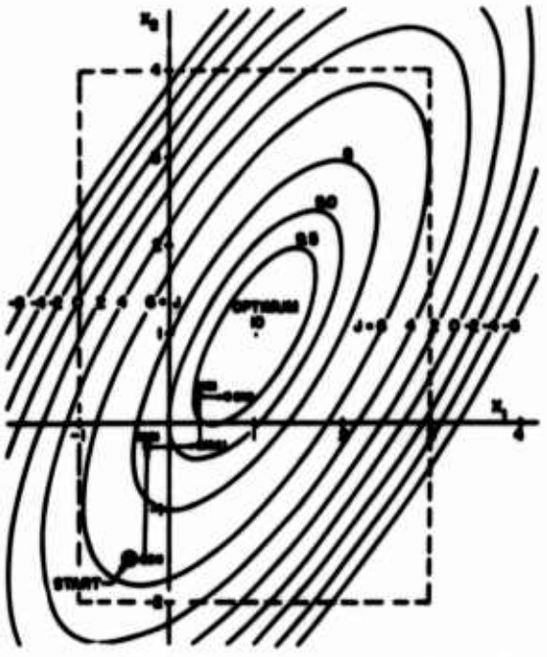

FIG 7 **Sectioning Search**

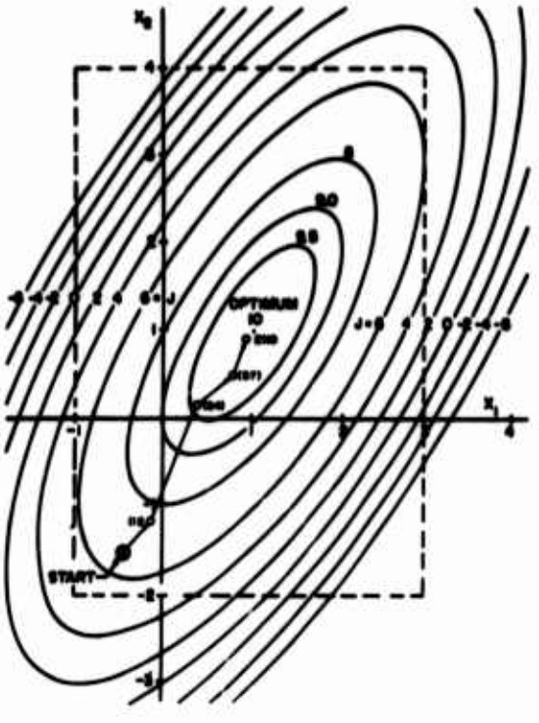

FIG 8 **Adaptive Creeper Search**

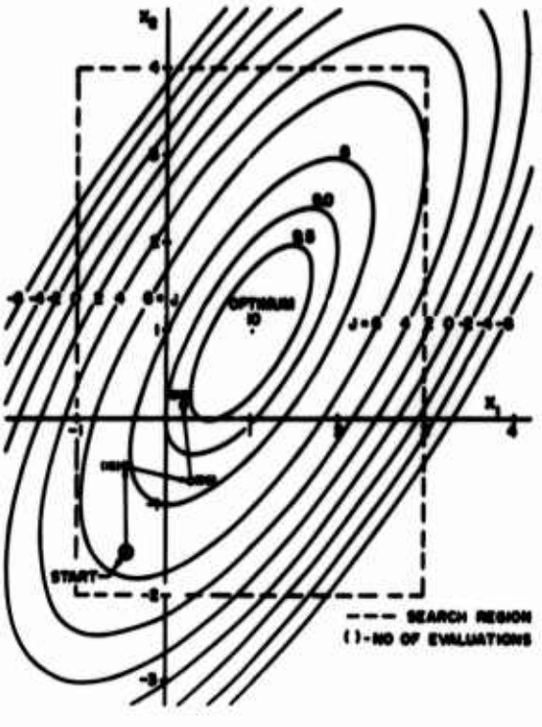

FIG 9 **Steepest Ascent Search**

appeared to be unimodal, however, for a large region around the optimum design point. In the region of optimum point the response surface was relatively "flat" so that a large number of configurations correspond to nearly equal performance. This is illustrated in the performance sensitivity analysis contained in the next chapter.

IV. Analysis of Results

Results of this study are presented in two parts. The first section deals with configuration characteristics of optimum range hypersonic cruise vehicles; whereas, the second section deals with performance.

Optimum Configuration Characteristics

The overall goal of this investigation was a fundamental analysis of configurations in which the optimization process included the effects of the interaction of the aerodynamic and propulsive flow fields. Table III contains the values of the independent variables which were determined by the direct search methods discussed in the previous chapter. The table also contains the dependent variables which were calculated from equality constraint relationships as developed in Appendix E. Together, the independent and dependent variables define the vehicle configuration. The fuselage of the shapes shown in Figs 10, 11, and 12 are waveriders in that the edge of the inlet fences coincides with the shock waves produced by the inlet-forebody. Thus, the forebody of the vehicle "rides" on the contained plane shock waves. Nozzle fences, also evident on the configurations maintain two-dimensional pressure distribution on the aftfuselage.

The shapes were determined by directly relating geometry to the flow field quantities surrounding the vehicles. Some of the flow field quantities associated with the propulsive stream are shown in Figs 10 - 12. The Mach number can be seen to decrease between the entrance and exit of the combustor which is characteristic of the constant area supersonic combustion process. Figures 10 - 12 illustrate that the wall static pressures at termination of the aftfuselage were above free-stream pressure for the optimum configuration. Aftfuselage length and hence nozzle expansion was terminated by the zero fuselage base constraint in the case of the Mach 10 and 12 designs. Figure 11 shows that further nozzle expansion was possible in the case of the Mach 8

TABLE III

Configuration Definition Quantities[a] for Design Mach Numbers of 8, 10, and 12

QUANTITIES		DESIGN MACH NUMBER		
		8	10	12
Independent				
Inlet				
δ_1	deg	11.36	8.21	6.40
T_4	R	2000.	2000.	2000.
Combustor				
ϕ		.449	.530	.795
ℓ_4/h_4		5.00	5.00	5.00
Nozzle				
δ_5	deg	15.15	14.02	12.92
ℓ_6/h_4		1.51	2.36	2.85
ℓ_5/ℓ_1		1.23	1.29	1.11
Wing				
δ_{11}	deg	8.80	7.41	7.18
δ_9	deg	-5.32	-5.21	-5.25
δ_{12}	deg	0.	0.	0.
AR		.345	.240	.245
Fuselage				
α	deg	.747	1.01	1.05
δ_7	deg	0.	0.	0.
W_{t_o}	lb	500,000.	500,000.	500,000.
b/h		1.21	1.33	1.36
Dependent				
δ_2	deg	5.48	4.81	4.12
ℓ_2/ℓ_1		.781	.771	.777
ℓ_3/ℓ_1		.219	.206	.204
h_4/ℓ_1		.0390	.0271	.0214
$Sp/b\ell_1$		.374	.306	.239
ℓ_{ew}/ℓ_1		3.20	3.17	2.99
bw/ℓ_1		.273	.185	.148
c/ℓ_1		.791	.769	.606
p_1	lb/ft^2	13.73	12.10	9.44
ℓ_1	ft	52.84	64.41	76.12
T_1	R	438.3	443.2	453.0

[a] Data obtained with structural parameter set $\bar{S}$ values of: $W_p/W_{t_o} = .05$ $W_e/W_{t_o} = .15$, $W_{f_c}/W_{f_\ell} = .5$, $\rho_p = 4.5$ lb/ft^3, $\rho_f = 4.5$ lb/ft^3, $\rho_e = 180$ lb/ft^3, $\gamma_s = 7.5$ lb/ft^2.

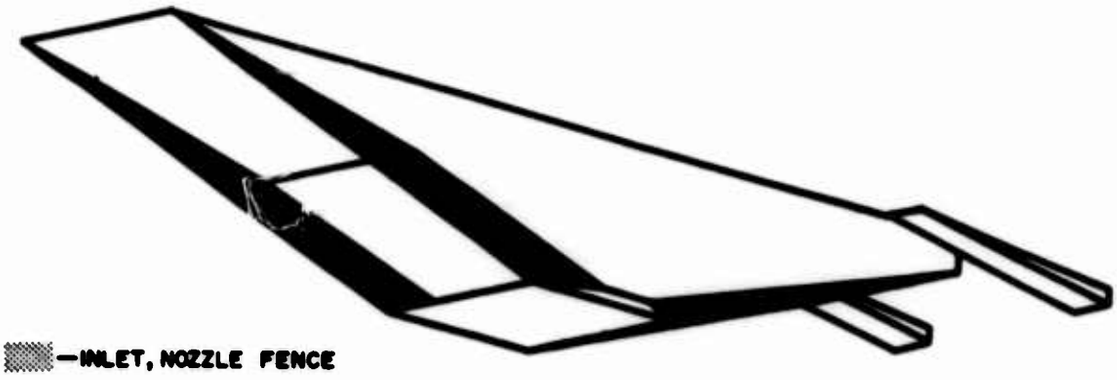

Performance (cruise)				**Propulsive**		
Altitude (initial)	112000.	ft		Inlet		
Range	4591.	nm		capture area	799.59	ft^2
Velocity	4861.	nm/hr		entrance		
Breguet Range factor	9878.	nm		pressure	.00649	atm
Structural				Mach	8.	
				exit		
Fuselage Dimensions				pressure	.444	atm
length	169.79	ft		Mach	3.18	
height	25.17	ft				
width	30.46	ft		Combustor		
				entrance		
Weight				pressure	.444	atm
takeoff	500000.	lb		Mach	3.18	
fractions				temperature	2000.	R
payload W_p/W_{to}	.050			exit		
structural W_s/W_{to}	.258			pressure	1.273	atm
fuel W_{fl}/W_{to}	.542			Mach	1.84	
equipment W_e/W_{to}	.150			temperature	4475.	R
				specific heat ratio	1.269	
Breguet Structural						
factor $\ln(W_i/W_f)$	.465			Nozzle-afterbody		
				exit pressure ratio $\frac{P_2}{P_1}$	1.83	
Aerodynamic						
				Equivalence ratios		
Angle of attack	.747	deg		propulsive	.449	
Dynamic pressure	602.	lb/ft^2		coolant	.125	
Lift-drag ratio	2.453					
(power on)				Specific impulse	2678.	sec

FIG 10 Configuration and Characteristics of a Hydrogen-Fueled Mach 8 Cruise Vehicle

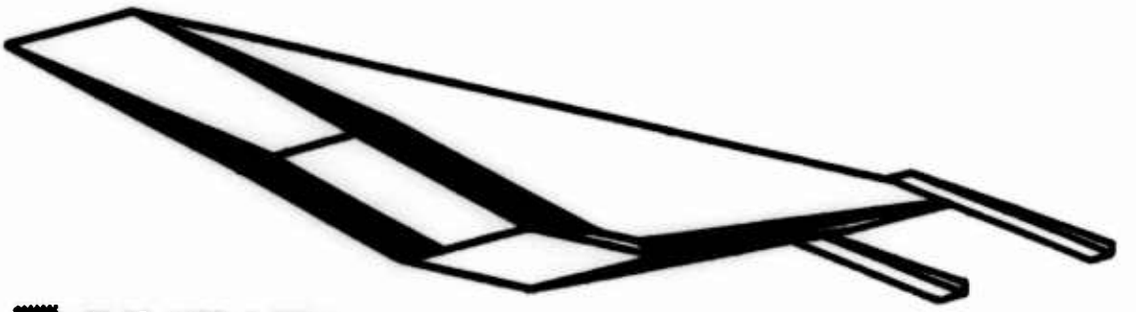

[redacted]—INLET, NOZZLE FENCE

Performance (Cruise)			
Altitude (initial)	115000.	ft	
Range	4777.	nm	
Velocity	6110.	nm/hr	
Breguet Range factor	11191.	nm	
Structural			
Fuselage Dimensions			
length	205.90	ft	
height	22.52	ft	
width	29.96	ft	
Weight			
takeoff	500000.	lb	
fractions			
payload W_p/W_{to}	.090		
structural W_s/W_{to}	.284		
fuel W_{ff}/W_{to}	.516		
equipment W_e/W_{to}	.150		
Breguet Structural factor $ln(W_i/W_f)$	.427		
Aerodynamic			
Angle of attack	1.01	deg	
Dynamic pressure	847.	lb/ft^2	
Lift-drag ratio (power on)	2.70		

Propulsive			
Inlet			
capture area	727.71	ft^2	
entrance			
pressure	.00572	atm	
Mach	10.		
exit			
pressure	.3944	atm	
Mach	4.28		
Combustor			
entrance	.3944	atm	
pressure	4.28		
Mach			
temperature	2000	R	
exit			
pressure	1.12	atm	
Mach	2.56		
temperature	4630.	R	
specific heat ratio	1.266		
Nozzle-afterbody exit pressure ratio $\frac{P_e}{P_t}$	1.77		
Equivalence ratios			
propulsive	.530		
coolant	.218		
Specific impulse	2053.	sec	

FIG 11 Configuration and Characteristics of a Hydrogen-Fueled Mach 10 Cruise Vehicle

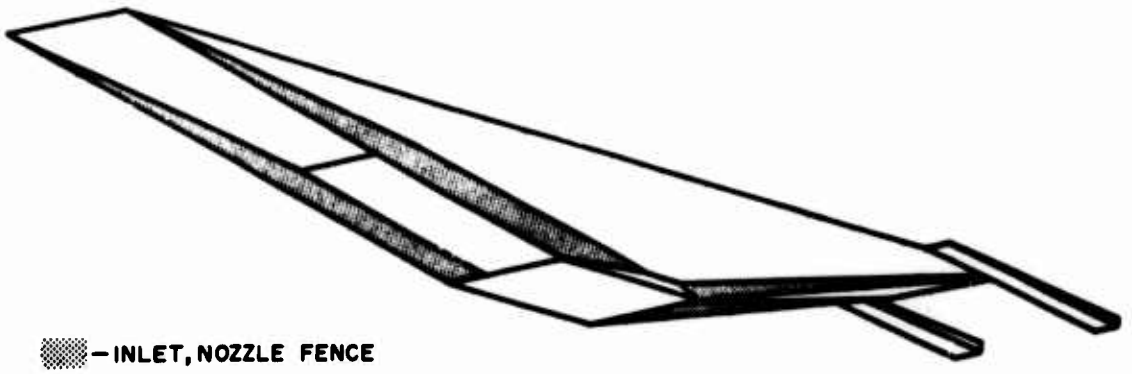

▒ — INLET, NOZZLE FENCE

Performance (cruise)			
Altitude (initial)	121000.	ft	
Range	4388.	nm	
Velocity	7413.	nm/hr	
Breguet Range factor	10688.	nm	
Structural			
Fuselage Dimensions			
length	228.56	ft	
height	21.14	ft	
width	28.76	ft	
Weight			
takeoff	500000.	lb	
fractions			
payload W_p/W_{to}	.050		
structural W_s/W_{to}	.296		
fuel W_{ff}/W_{to}	.504		
equipment W_e/W_{to}	.150		
Breguet Structural factor $\ln(W_i/W_f)$	.410		
Aerodynamic			
Angle of attack	1.05	deg	
Dynamic pressure	951.	lb/ft^2	
Lift-drag ratio (power on)	3.05		

Propulsive			
Inlet			
Capture area	668.98	ft^2	
entrance			
pressure	.00460	atm	
Mach	12.		
exit			
pressure	.2985	atm	
Mach	5.36		
Combustor			
entrance			
pressure	.2985	atm	
Mach	5.36		
temperature	2000.	R	
exit			
pressure	.9881	atm	
Mach	3.01		
temperature	5015.	R	
specific heat ratio	1.262		
Nozzle-aftfuselage exit pressure ratio $\frac{P_a}{P_t}$	2.34		
Equivalence ratios			
propulsive	.795		
coolant	.339		
Specific impulse	1314.	sec	

FIG 12 Configuration and Characteristics of a Hydrogen-Fueled Mach 12 Cruise Vehicle

design since the fuselage base is not zero; however, the additional nozzle forces which would be obtained by further expansion did not compensate for the additional structural weight associated with the increased fuselage length.

Takeoff weight, which was an independent design variable in this study, and members of the structural set $\bar{S}$ listed in Table III determined the scale or dimension of the vehicles shown in Figures 10 - 12. The cruise range also depends explicitly on the assumed values of the set members; therefore, a range sensitivity analysis with respect to each member of the set is contained in Appendix C. The sensitivity analysis indicated that the cruise range either increased or decreased monotonically in the investigated domain of the set members. Payload density ρ_p, for example, did not have a natural optimum--higher payload density produced higher cruise range. While the cruise range depends explicitly on the values assumed for the structural set $\bar{S}$, the range factor shown in Fig 10 - 12 does not. The range factor will be considered more fully when discussing the performance aspects of the vehicle. First, however, the configuration characteristics of the vehicle will be examined.

Insight into why a particular configuration was optimum can be gained by exploring the design space in the vicinity of the optimum point. Each figure in the series of Figs 13 - 14 and Figs 16 - 28 illustrates, for the Mach 10 configuration, the influence of the independent design variables on the range factor, structural factor, and cruise range R. The variation of cruise range R with each of the independent variable represents one-dimensional "cuts" in the response surface around the optimum point. Aerodynamic and propulsive efficiencies variations are reflected by the range factor; whereas the volumetric efficiency is reflected by the structural factor of the Breguet range equation repeated here for convenience

$$R = \overbrace{\frac{L}{D} \, Isp \frac{V_1}{1 - V_1^2 / V_o^2}}^{\text{range factor}} \overbrace{\ell n \, (W_i / W_f)}^{\text{structural factor}} \qquad (1)$$

Figures 13, 14 and 16 through 28 were generated by perturbing one independent design variable at a time while holding the other independent quantities (except nozzle length and equivalence ratio) at the optimum values for the Mach 10 design. The nozzle length was automatically reoptimized during the solution of Eq 1 and the equivalence ratio was adjusted when necessary to provide additional thrust to satisfy the equilibrium flight constraint (thrust equal drag). In discussing some of the characteristics of the optimum configuration, it is convenient to divide the vehicle into components: inlet-forebody, combustor, nozzle-aftfuselage, wing, and fuselage.

Inlet-forebody. Two independent design variables define the shape of the inlet-forebody. One is the inlet ramp angle δ_1 which, in addition to defining the profile of the underside of the forebody, also controls the relative shock strength produced by the first and second inlet ramps. From a propulsive efficiency standpoint, the goal of inlet design is to achieve maximum pressure recovery. According to Orlov (Ref 15) maximum pressure recovery occurs for the three shock inlet of type considered in this study when the pressure rise across the first two shock waves is equal. This result was confirmed in this investigation; however, Fig 13 illustrates that, although the response surface is rather flat near the optimum point, the optimum δ_1 for maximum range was greater than the δ_1 producing maximum pressure recovery. The reason for the difference is apparent also from Fig 13 as the volumetric efficiency of the vehicle (reflected by the structural factor) increased as δ_1 increased. Thus, consideration of the volume producing aspects of the inlet-forebody resulted in a slight change from the conventional one-dimensional goal of inlet design--that of maximum inlet pressure recovery. This information could be used in future

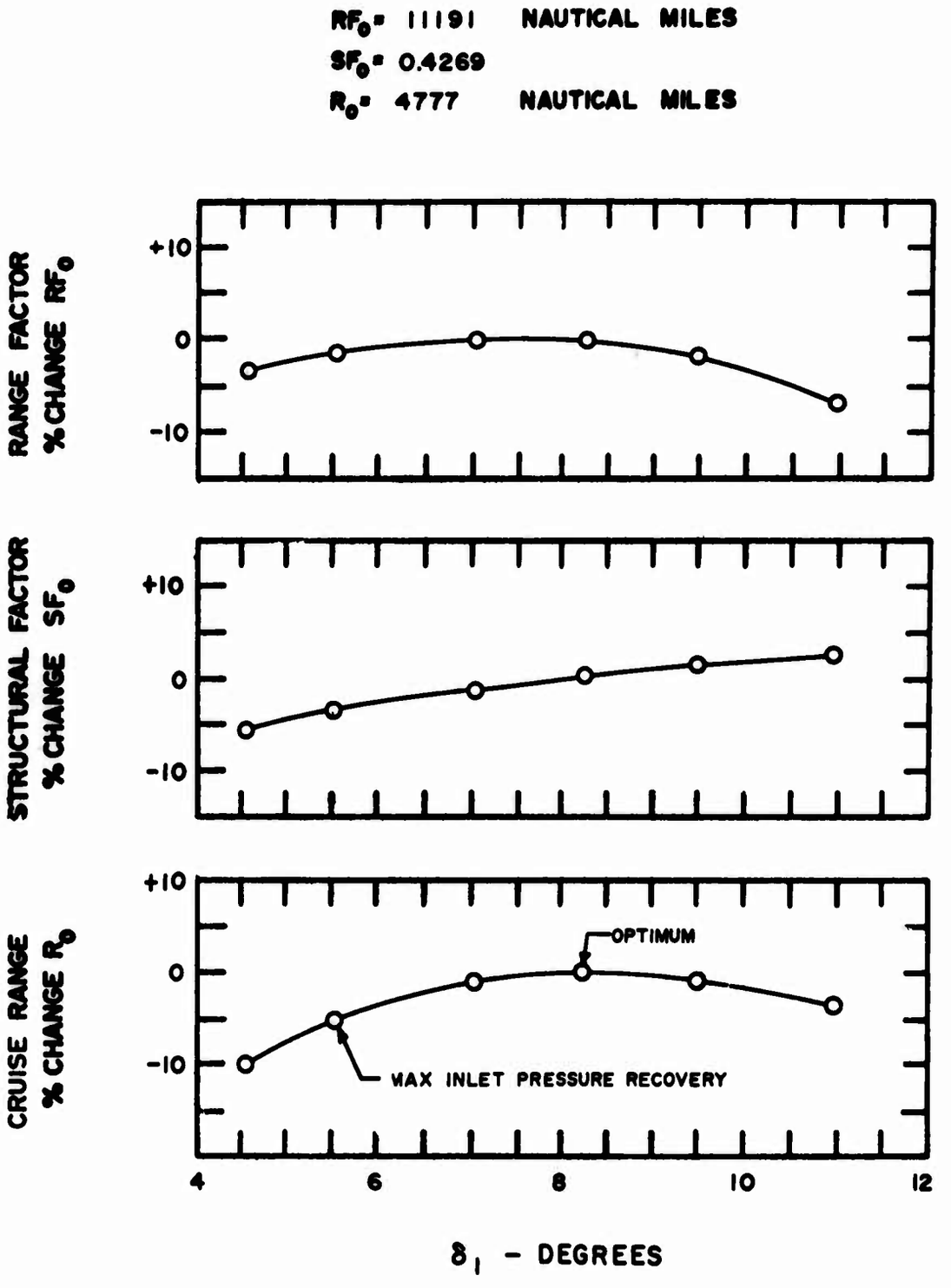

FIG 13 First Inlet Ramp Angle δ_1 Influence on Cruise Range and Factors of Breguet Range Equation

configuration optimization studies of this nature to limit the feasible region of the design space. For example, the maximum pressure recovery configuration inlet-forebody could be used as a starting point with searches in the design space limited to those inlet-forebody configurations with improving volumetric efficiency.

Whereas the first inlet-forebody design variable δ_1 defines the inlet profile and relative shock wave strengths from the inlet ramps, the second inlet design variable, combustor entrance temperature T_4, defines the total strength of the shock wave system. A higher combustor entrance temperature requires a stronger inlet shock wave system which in turn demands a greater deflection of the propulsive stream. Thus, in terms of configuration geometry, the combustor entrance temperature defines the inlet-forebody length to thickness ratio. Figure 14 illustrates that the trade off between the structural factor and range factor with varying combustor entrance temperature resulted in a rather flat response surface; however, in the region of allowable solutions ($T_4 \geqq 2000$ R) a combustor entrance temperature of $T_4 = 2000$ R produced maximum range. This is an interesting result since vehicle thickness, necessary to provide volume in the vehicle, is automatically provided by the propulsive constraint ($T_4 \geqq 2000$ R autoignition temperature for hydrogen air mixture). The thickness ratio of the Mach 8, 10, and 12 designs can be observed from Fig 10 - 12 to become progressively finer as the flow deflection needed to produce the required shock strength is reduced as Mach number increases.

An interesting characteristic of the forward section of the vehicle is that it produced very little lift as shown in Figure 15. In fact, neglecting friction, at zero angle of attack and zero angle of incidence of the upper surface of the fuselage, the lift produced by the forward section of the vehicle is zero. The force in the lift direction produced by pressure acting on the underside of the forebody is cancelled by the downward pressure force acting on the inlet cowl. The zero lift result

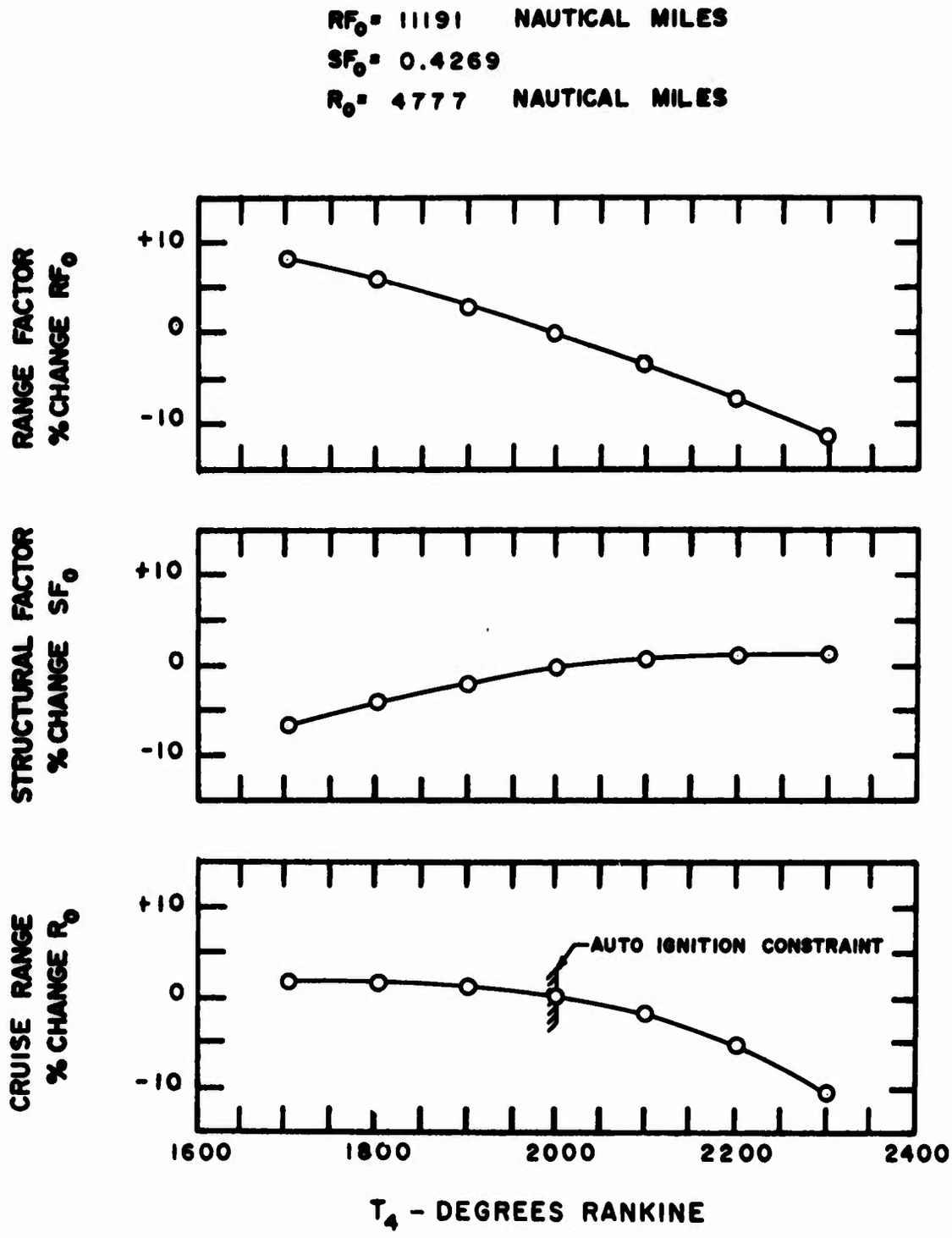

FIG 14 Combustor Entrance Temperature T_4 Influence on Cruise Range and Factors of Breguet Range Equation.

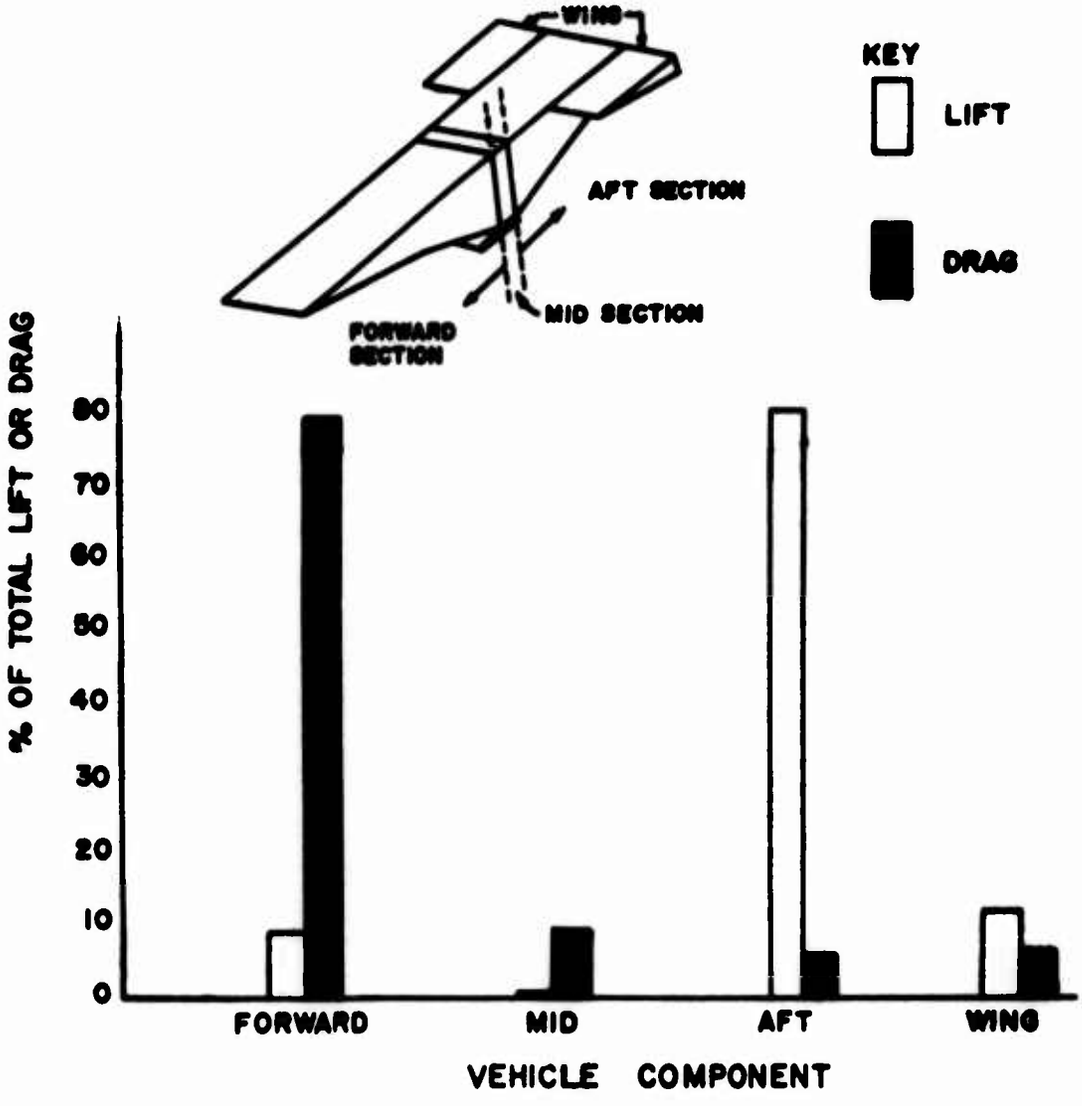

FIG 15 Vehicle Component Contribution to Lift and Drag of Mach 10 Configuration

may also be deduced from a simple momentum stream tube analysis, since for zero angle of attack and the shocks focused on the cowl lip, the inlet-forebody does not produce a net downward deflection of the inlet flow. A pitch up moment was produced by the forward section of the vehicle, however, which is reflected by the rearward placement of the wing on the configuration shown in Figures 10, 11, and 12.

An argument for the shock on lip at the design point constraint used in this study can be made using the stream tube analysis and some results of the study. When the shock pattern is focused ahead of the cowl lip, a downward deflection of the flow field occurs and the inlet-forebody becomes a wing in the sense that it produces lift, although with a highly compressed air flow. According to Kuchemann (Ref 3), it is not aerodynamically efficient to produce lift with a strong shock wave system. This fact was also evident from the range factor variation with lower wing surface angle δ_{11} shown in Figure 21. The aerodynamic efficiency, as reflected by the range factor, decreased with increasing shock strength since the strength of the shock wave produced by the wing increased with increasing lower wing surface angle. Thus, air which has been compressed by the inlet-forebody should be used in the propulsive stream (shock on lip) rather than to provide lift (shock ahead of lip) for optimum performance at the design point. Off design performance of the inlet was not included in this investigation; however, other studies (Ref 16, Ref 17) have shown the performance penalty to be small when fixed geometry inlets of the type considered in this investigation are operated below the design Mach number.

Combustor. Equivalence ratio ϕ and nondimensional combustor length ℓ_4 / h_4 are the independent design variables associated with the combustor midsection of the vehicle. As explained in Appendix E, the vehicle design problem was formulated such that the wing planform area was adjusted to generate drag to balance thrust produced at a given equivalence ratio. This is the inverse of the conventional

situation where vehicle geometry is fixed and the equivalence ratio is adjusted (by throttle setting) to maintain equilibrium flight during cruise. Hence, in the present vehicle design formulation, wing planform area S_p increased with increasing equivalence ratio ϕ. This is reflected by Fig 16 as the structural factor decreased with increasing equivalence ratio illustrating that wings were not volumetrically efficient compared to the fuselage of the vehicle.

As the planform area S_p of the wing decreased, the center of pressure of the wings moves rearward in order to maintain a trimmed condition. The trim constraint indicated in Fig 16 occurred when the wing had moved rearward to a position such that the common wing-fuselage length was zero ($\ell_b - \ell_{ew} = 0$). Although the optimum equivalence ratio occurred at the trim constraint, from a practical standpoint, some common wing-fuselage length ($\ell_b - \ell_{ew}$) would be necessary in order to attach the wings to the fuselage without resorting to booms or other such devices. Figure 16 illustrates that the performance penalty for increasing the common wing-fuselage length was slight. The configurations in Figs 10 - 12 are shown with a common wing-fuselage length of $(\ell_b - \ell_{ew})/\ell_1$ equal to three tenths. Figure 16 also illustrates that only a small performance gain could be obtained by relaxing the trim constraint, since the range for a wingless body ($S_p = 0$) was only slightly greater than for a configuration with sufficient wing to maintain trimmed flight.

The combustor length ℓ_4 specifies the length of the combustor as well as the length of the midsection of the vehicle. Although the structural factor increased with increasing vehicle midsection length, the range factor decreased at an even faster rate due to skin friction drag in the combustor as shown in Figure 17. Since the chemical kinetics of mixing, ignition, and burning were not considered in the combustor synthesis (only the initial and final states of the fuel-air mixture are considered), nothing can be said about the optimum length of the combustor from this investigation other than that the combustor

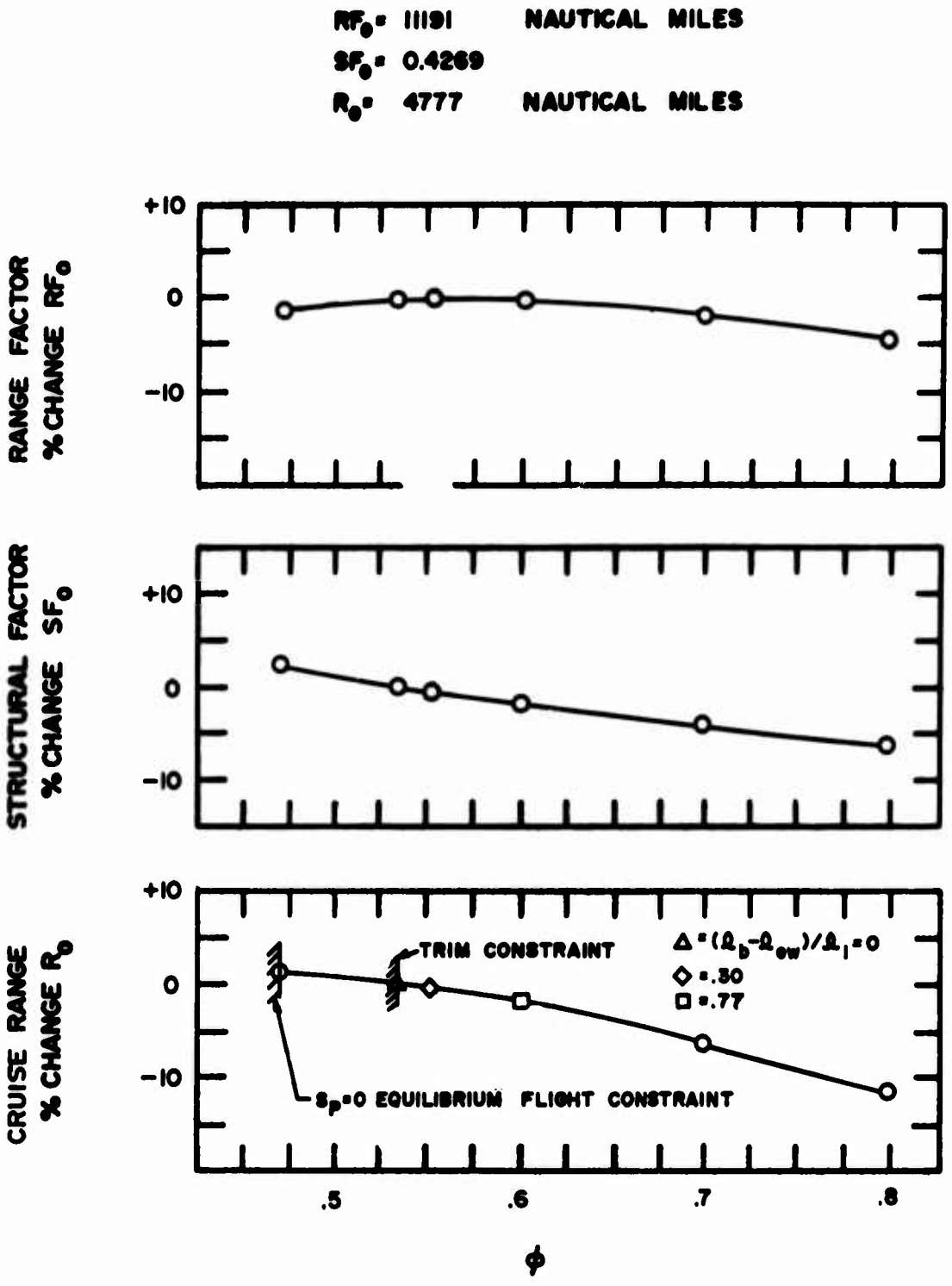

FIG 16 Equivalence Ratio ϕ Influence on Cruise Range and Factors of Breguet Range Equation

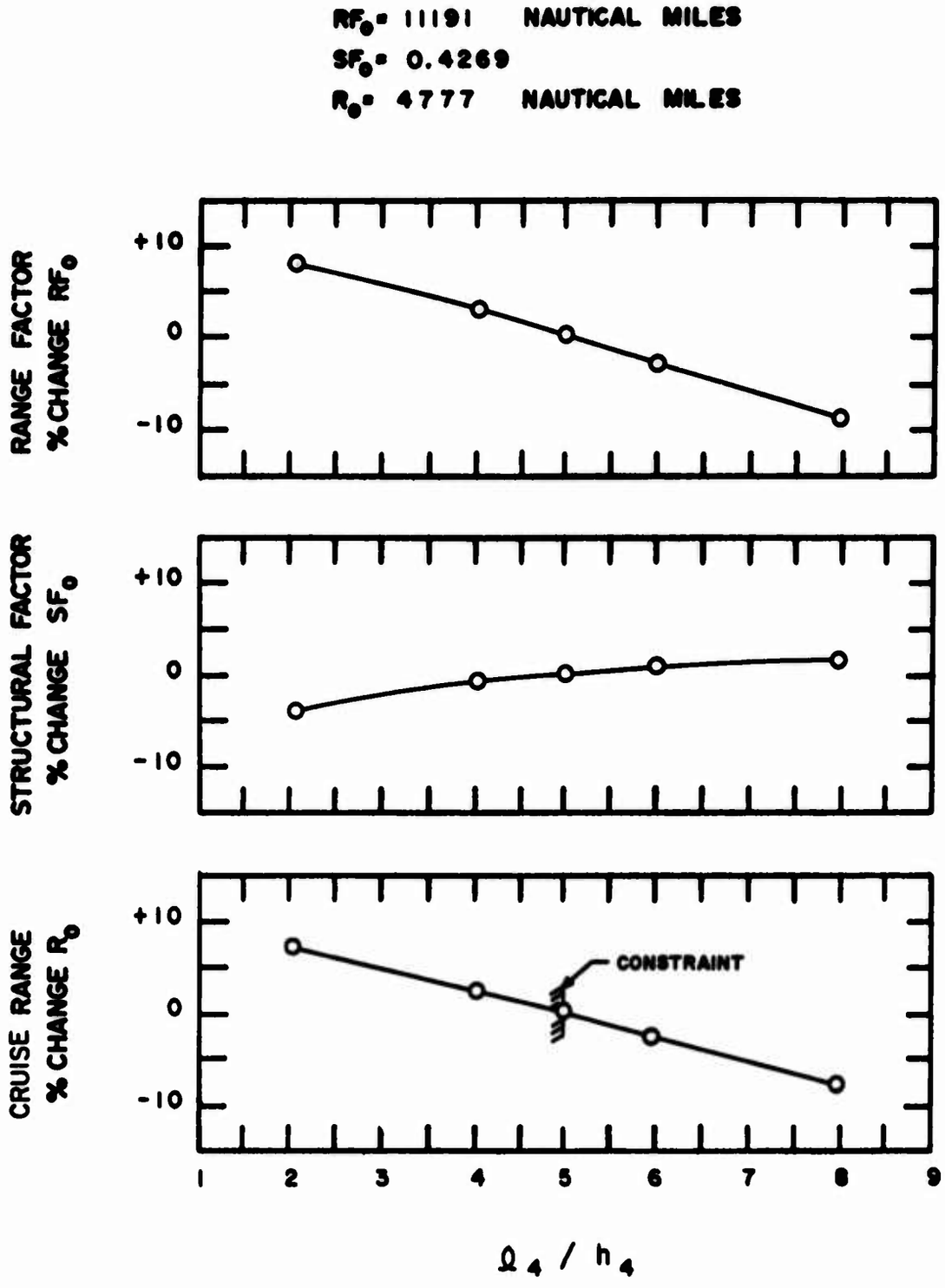

FIG 17 Nondimensional Combustor Length ℓ_4 / h_4 Influence on Cruise Range and Factors of Breguet Range Equation

should be as short as possible. A combustor length to height ratio of $\ell_4 / h_4 = 5$, which was chosen as a lower constraint, resulted in a physical combustor length of $\ell_4 \sim 10$ ft for the three Mach number designs which provides a reasonable length for combustion to take place (Ref 18).

Nozzle-aftfuselage. Three independent design variables (δ_5, ℓ_5, ℓ_6) determine the geometry of the nozzle-aftfuselage of the configuration shown in Figures 10 - 12. The underside of the aft-fuselage provides an expansion surface for the combustor gases, thereby forming, along with the nozzle cowl and fences, a two-dimensional asymmetric nozzle. The nozzle can be configured so that the resultant nozzle force direction θ_T (θ_T measured from a plane perpendicular to the flight path) is in the direction of lift ($\theta_T = 0^\circ$) or in the direction of thrust ($\theta_T = 90^\circ$). Thus, the possibility of an optimum force direction θ_T exists.

Swithenbank (Ref 17) suggests the optimum nozzle-aftfuselage configuration for the two-dimensional asymmetrical nozzle would be obtained when the resultant nozzle force direction θ_T, in terms of the quantities defined in this investigation, is given by

$$\tan \theta_T = \left(\frac{L}{D}\right)_w \tag{11}$$

Appendix B contains the development of Eq 12 which is a more general expression than Eq 11 for the nozzle force direction angle θ_T producing a stationary value of the range factor:

$$\tan \theta_{T_{st}} = \frac{\left(\frac{L}{D}\right)_w + \frac{1}{C_T} \frac{\partial C_T}{\partial \theta_T}}{1 - \left(\frac{L}{D}\right)_w \frac{1}{C_T} \frac{\partial C_T}{\partial \theta_T}} \tag{12}$$

If the term $\partial C_T / \partial \theta_T$ which represents the change of nozzle force coefficient C_T with nozzle force direction θ_T is zero, as is usually the case for symmetrical nozzles, then Eq 12 reduces to Eq 11 the

result quoted by Swithenbank.

Equation 12 is essentially an expression indicating how the force recovered from the propulsive stream should be used to obtain optimum performance. If the wing is aerodynamically efficient (high L/ D) and the thrust magnitude is independent of direction ($\partial C_T / \partial \theta_T = 0$), then the nozzle force direction should be nearly aligned with the vehicle flight path ($\theta_T \sim 90^\circ$). This is the case for most classes of subsonic and supersonic vehicles where the axis of the symmetrical engine nozzles are aligned with the reference axis of the vehicle. On the other hand, if the wings are inefficient converters of thrust to lift (low L/D), or if the loss in nozzle force with increasing θ_T is large, then Eq 12 indicates the nozzle configuration should be such that some lift is produced directly from the nozzle. This was the case for the class of vehicle configurations considered in this study, since Fig 15 illustrates that about 75% of the lift was produced directly by the nozzle-aftfuselage of the Mach 10 configuration.

In terms of vehicle geometry, a nozzle-aftfuselage designed to produce a force direction angle indicated by Eq 11 ($\theta_T = 76^\circ$ for $(L/D)_W = 4$) would have a large nozzle expansion half angle δ_5 and/ or a long nozzle cowl ℓ_6. For example, a nozzle force angle of $\theta_T = 76^\circ$ and a nozzle cowl length of $\ell_6 = 0$, implies a nozzle half angle of $\delta_5 = 76^\circ$ for maximum range factor. Figure 18 illustrates maximum range factor was obtained at $\delta_5 \sim 15^\circ$ for the Mach 10 configuration. The consideration of the structural factor shifted the optimum δ_5 for maximum cruise range shown in Fig 18 to a slightly lower value than the δ_5 for maximum range factor. At lower values of δ_5, more nozzle lift is produced allowing a smaller wing which improves the volumetric efficiency of the vehicle. Reference 19 reports that a survey of hypersonic cruise vehicle configurations, submitted by aircraft companies in response to a proposal request by the United States Air Force, revealed the nozzle half angle δ_5 of the configurations to be

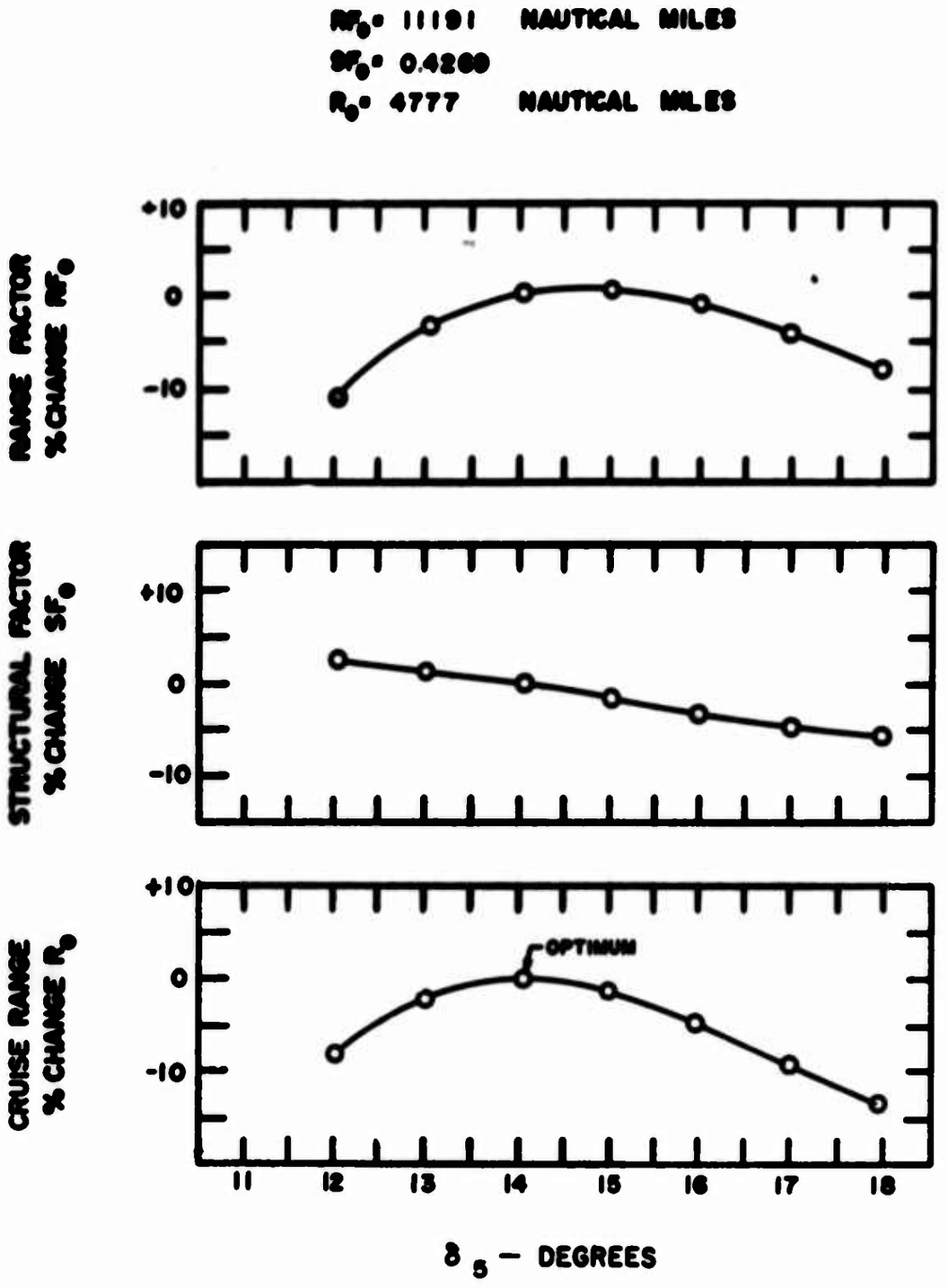

FIG 18 Nozzle Half Angle δ_5 Influence on Cruise Range and Factors of Breguet Range Equation

approximately 15 degrees.

Although Fig 19 shows that nozzle cowl length ℓ_6 for maximum range factor occurred in the search domain, the decrease in structural factor with increasing cowl length caused the value of ℓ_6 for maximum range to occur at the minimum allowable length. As explained in Appendix E. the minimum nozzle cowl length was constrained such that the first down running characteristic or Mach line from the nozzle-aftfuselage expansion corner strikes the trailing edge of the cowl. However, Fig 19 illustrates low sensitivity of cruise range with nozzle cowl length in the region of the constraint, indicating the constraint value was at or near the optimum value.

The optimum nozzle length ℓ_5 occurred in the search interval for the Mach 8 design and at the zero base constraint for the Mach 10 and 12 designs. As shown in Fig 20, range factor increased with nozzle length, while the structural factor decreased. Thus, the sensitivity of range with nozzle length was low in the region of the optimum.

Wing. Optimum values of the independent configuration definition quantities associated with the wing (δ_{11} , δ_9 , δ_{12} , AR) are shown in Table III. The insensitivity of cruise range with respect to the wing parameters, expecially the parameters (δ_9 , AR), accounts for the absence of a trend with design Mach number for optimum values of the wing parameters. Figure 15 illustrates a reason why performance was insensitive to values of the wing parameters as the wing lift is shown to constitute only about 10 per cent of the total vehicle lift. An inspection of Fig 21 reveals that the optimum lower wing surface angle δ_{11} occurred in the domain of the variable as a result of a trade off between the range factor and structural factor of the Breguet range equation. Figure 22 indicates that maximum range was obtained when the upper surface of the wing δ_9 was positioned to provide lift (negative incidence to the freestream flow) rather than to provide wing volume. Figure 23 illustrates that maximum range was obtained when

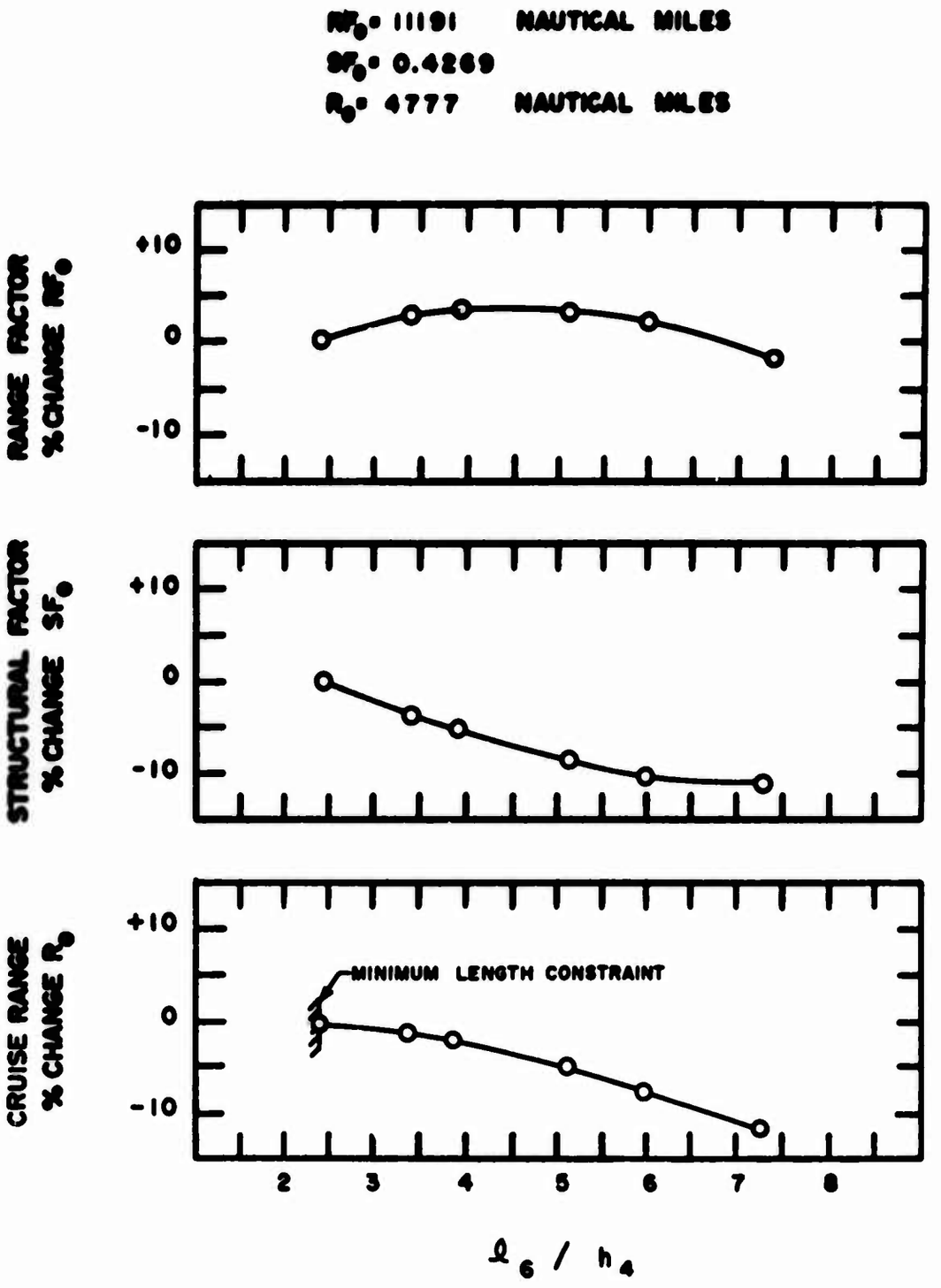

FIG 19 Nondimensional Nozzle Cowl Length ℓ_6 / h_4 Influence on Cruise Range and Factors of Breguet Range Equation

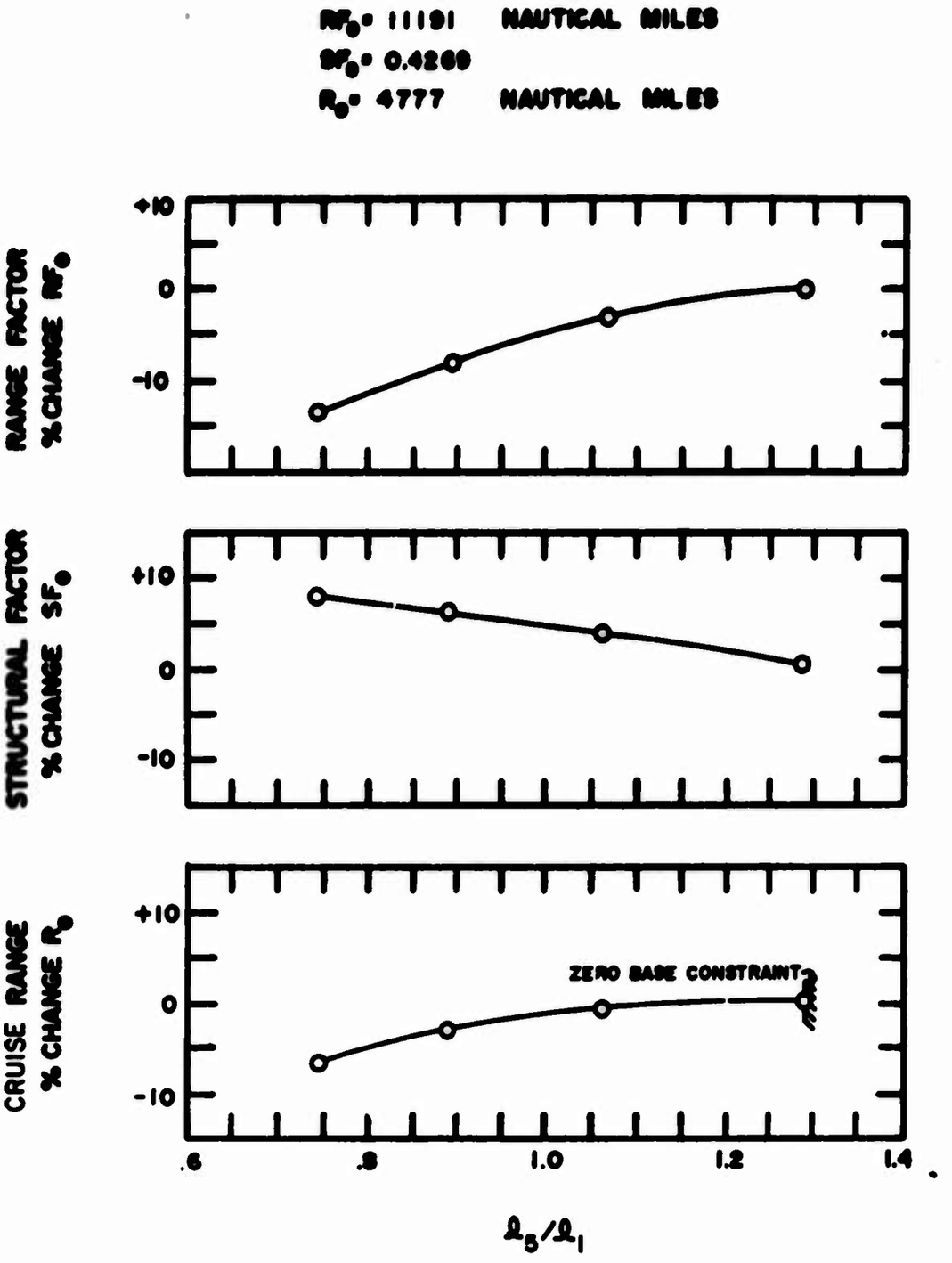

FIG 20 Nondimensional Nozzle Length ℓ_5 / ℓ_1 Influence on Cruise Range and Factors of Breguet Range Equation

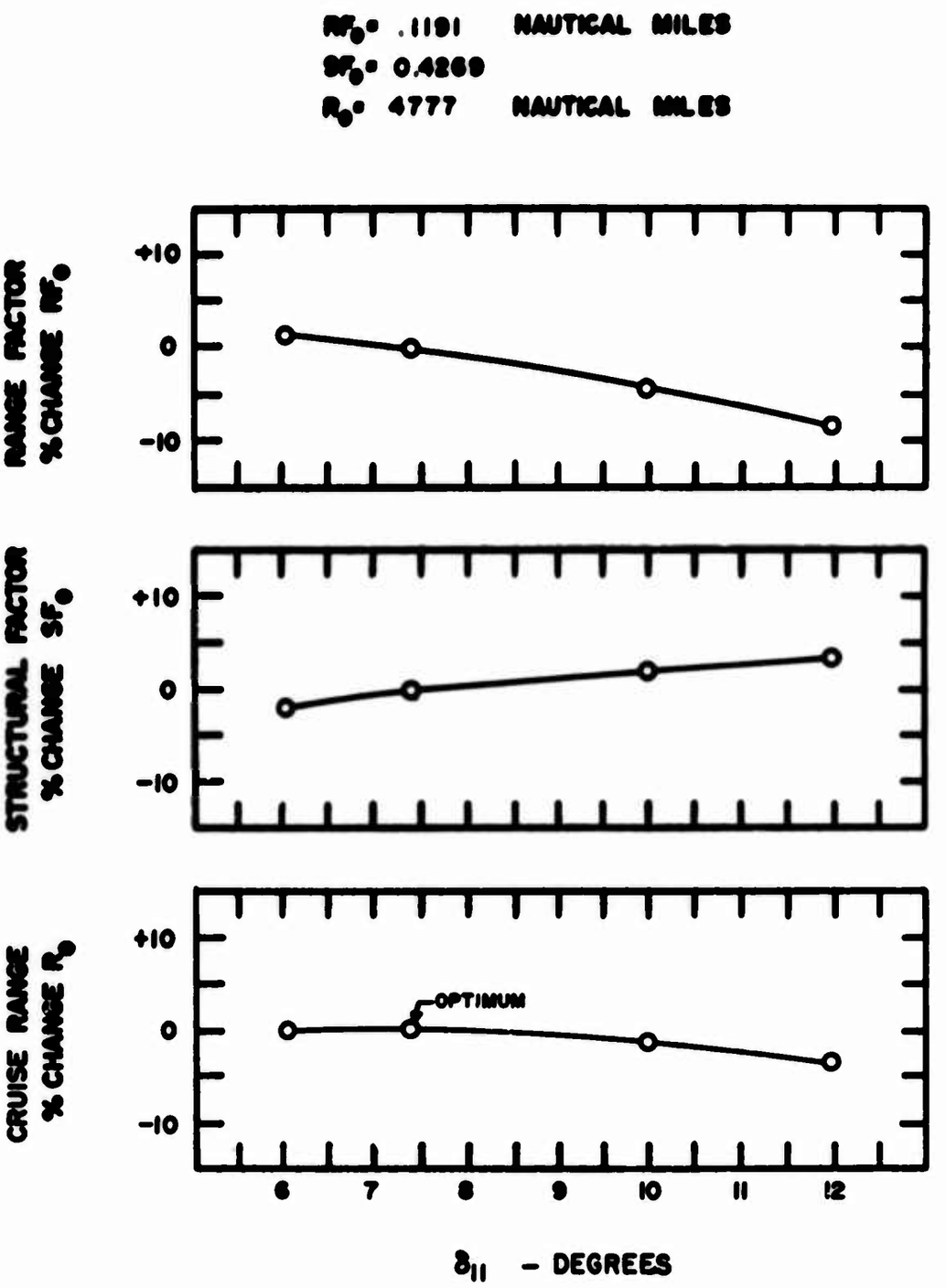

FIG 21 Lower Wing Surface Angle δ_{11} Influence on Cruise Range and Factors of Breguet Range Equation

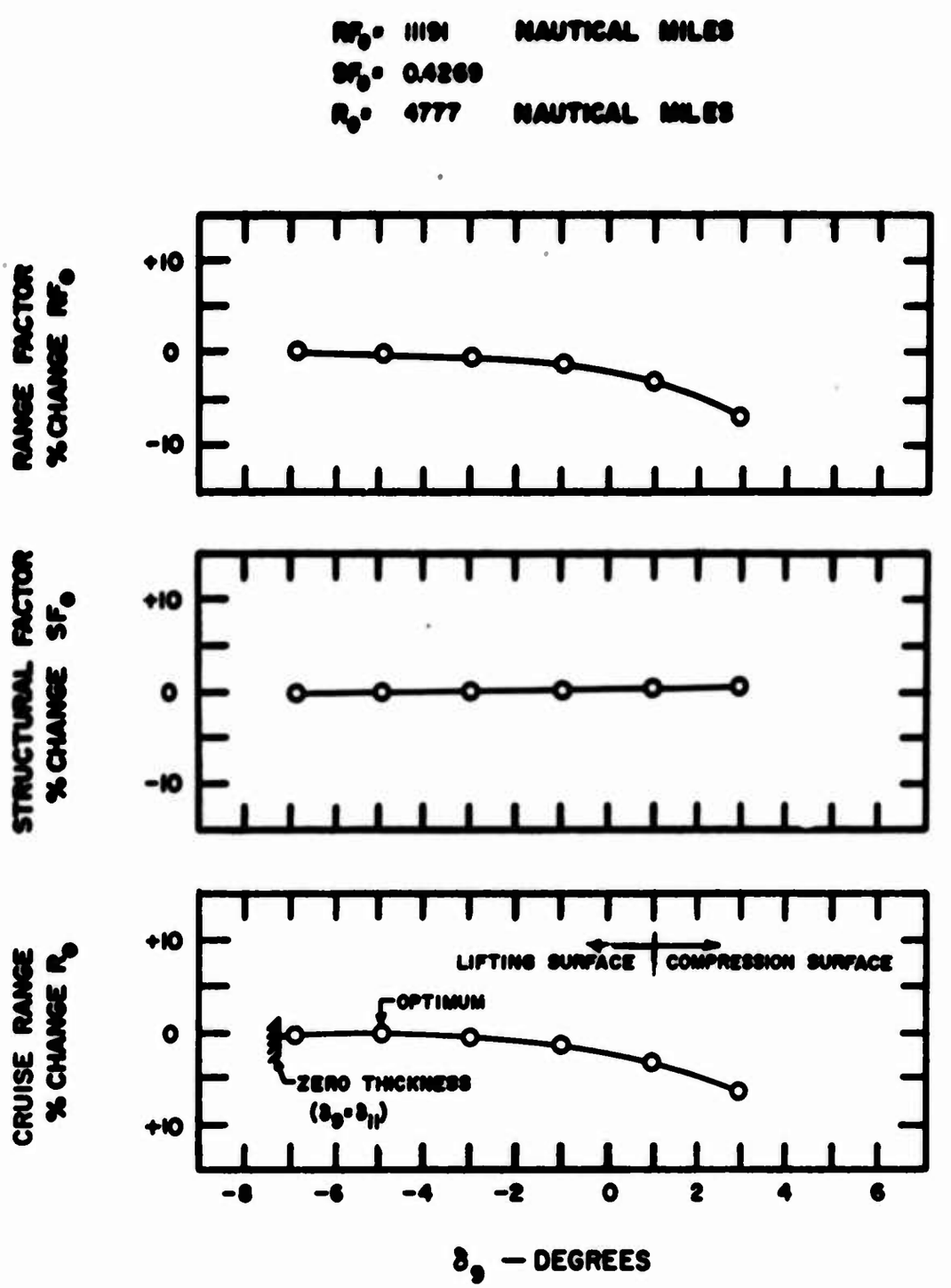

FIG 22 Upper Wing Surface Angle δ_9 Influence on Cruise Range and Factors of Breguet Range Equation

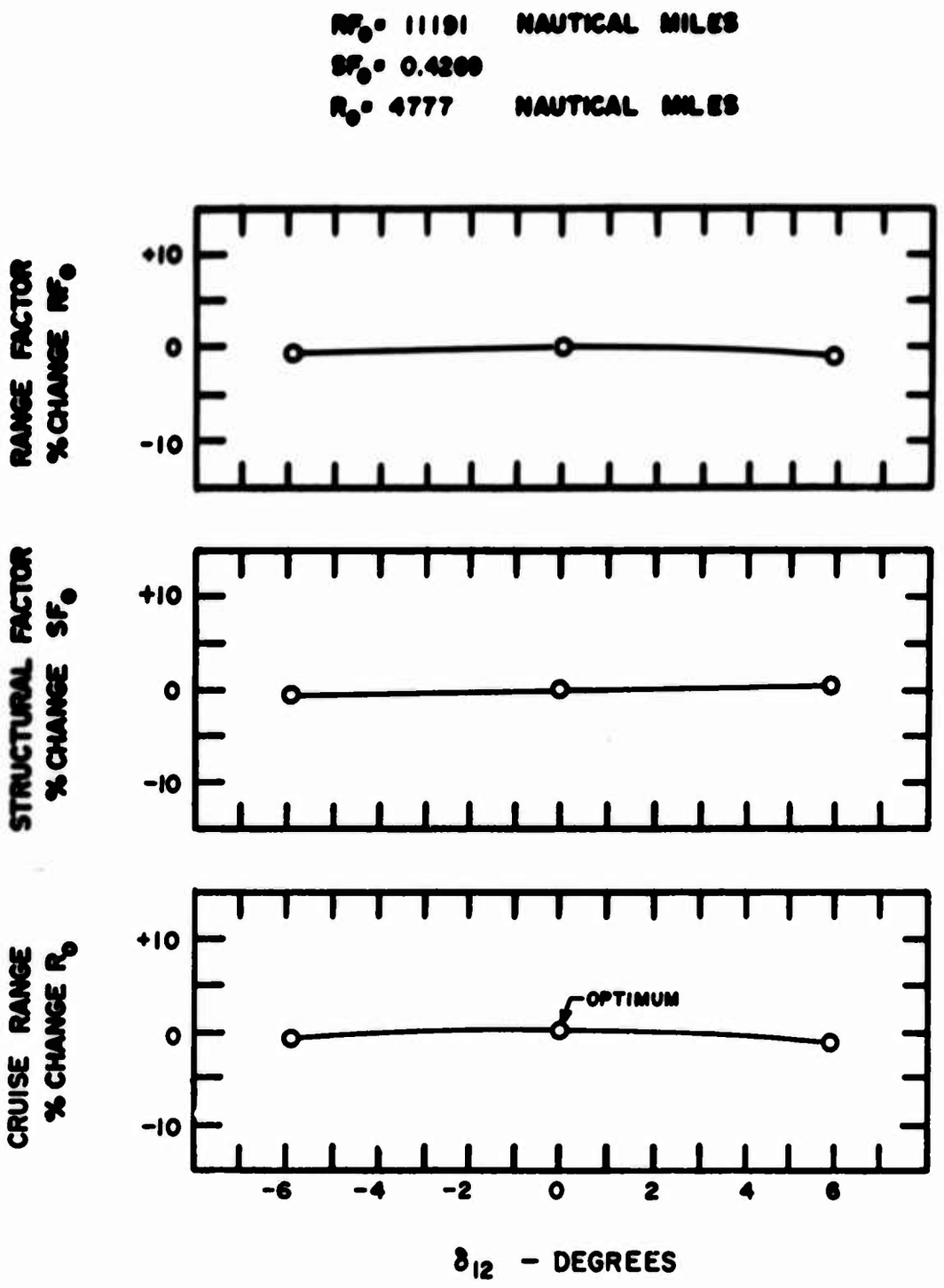

FIG 23 Wing Side Surfaces Angle δ_{12} Influence on Cruise Range and Factors of Breguet Range Equation

the side surface of the wing δ_{12} was at zero incidence with the free stream. Leading edge wing drag was a factor in the optimum wing being of low aspect ratio. However, if it were necessary to increase the wing aspect ratio due to takeoff and landing considerations, for example, Fig 24 shows that the performance penalty would be small.

Fuselage. Four independent design quantities are associated with the fuselage (α, δ_7, W_{to}, b/ h). The optimum angle of attack α for the three design cases, as shown in Table III, was approximately one degree. A positive angle of attack permits the underside of the cowl to become a lifting surface. The lift provided by the cowl reduced the size of the wing which is reflected by the increasing structural factor with increasing angle of attack shown in Figure 25.

Although the upper fuselage surface angle δ_7 was constrained to be positive, a variable angle of attack allowed the upper fuselage surface to assume negative angles of incidence with respect to the free stream flow. Thus, the upper section of the fuselage could be positioned to provide lift or additional fuselage volume. Since Fig 26 was generated with an angle of attack of one degree, Fig 26 shows that more cruise range was obtained when the upper portion of the fuselage provided lift rather than volume, even though volumetric efficiency (as reflected by the structural factor) increased with increasing upper fuselage surface angle. Figure 26 also indicates maximum cruise range was obtained at the lower constraint boundary ($\delta_7 = 0$) as a result of the trade off between the range factor and structural factor.

The vehicle design takeoff weight W_{to} for maximum cruise range occurred at the constraint boundary of 500, 000 lb for all three Mach number designs. The predominant effect of variable takeoff weight is to change the dimensions of the vehicle through the scale factor ℓ_1 of the vehicle. For a given geometrical shape the ratio of enclosed volume $\forall$ to wetted area A_w increases with increasing

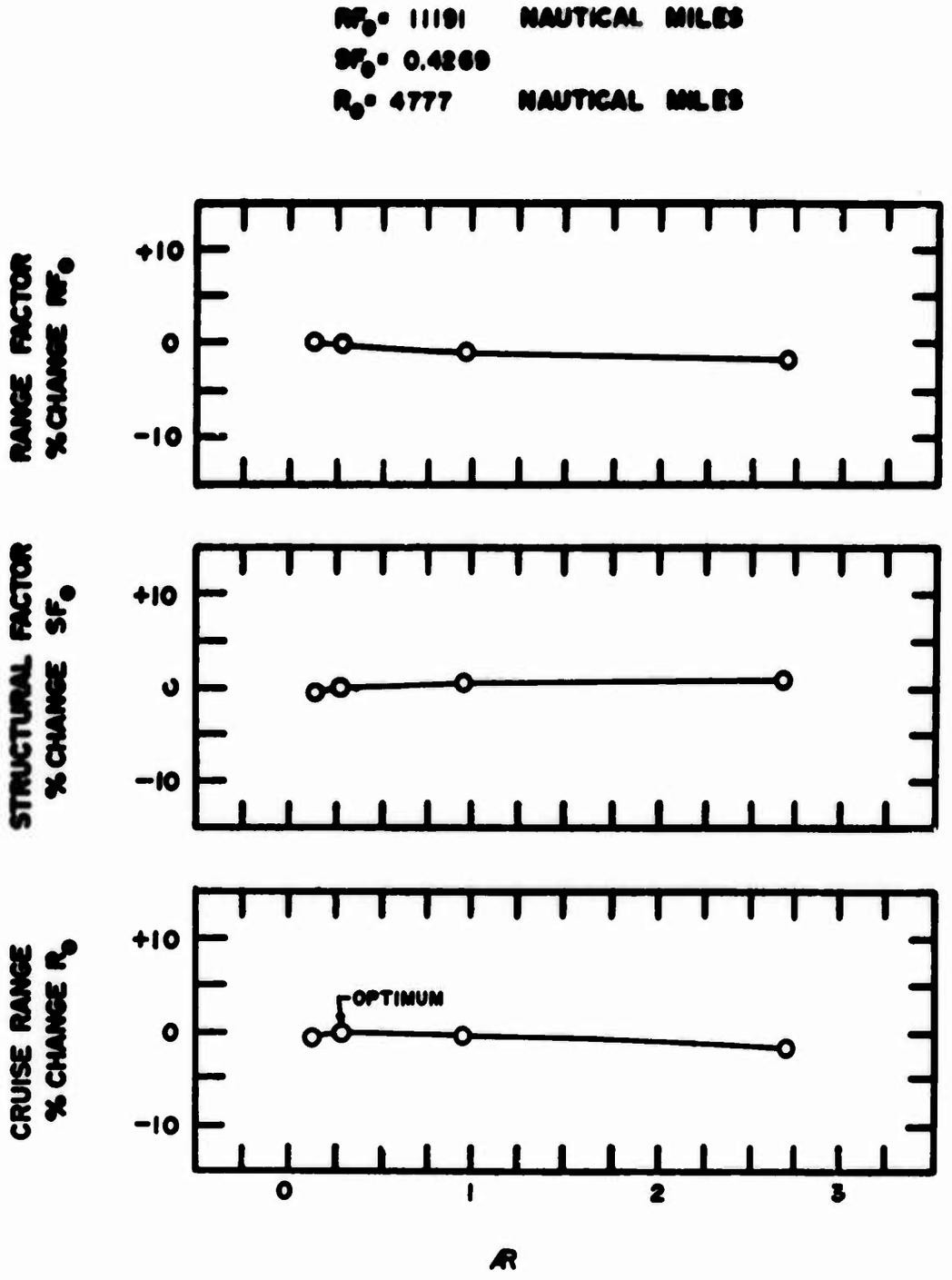

FIG 24 Aspect Ratio AR Influence on Cruise Range and Factors of Breguet Range Equation

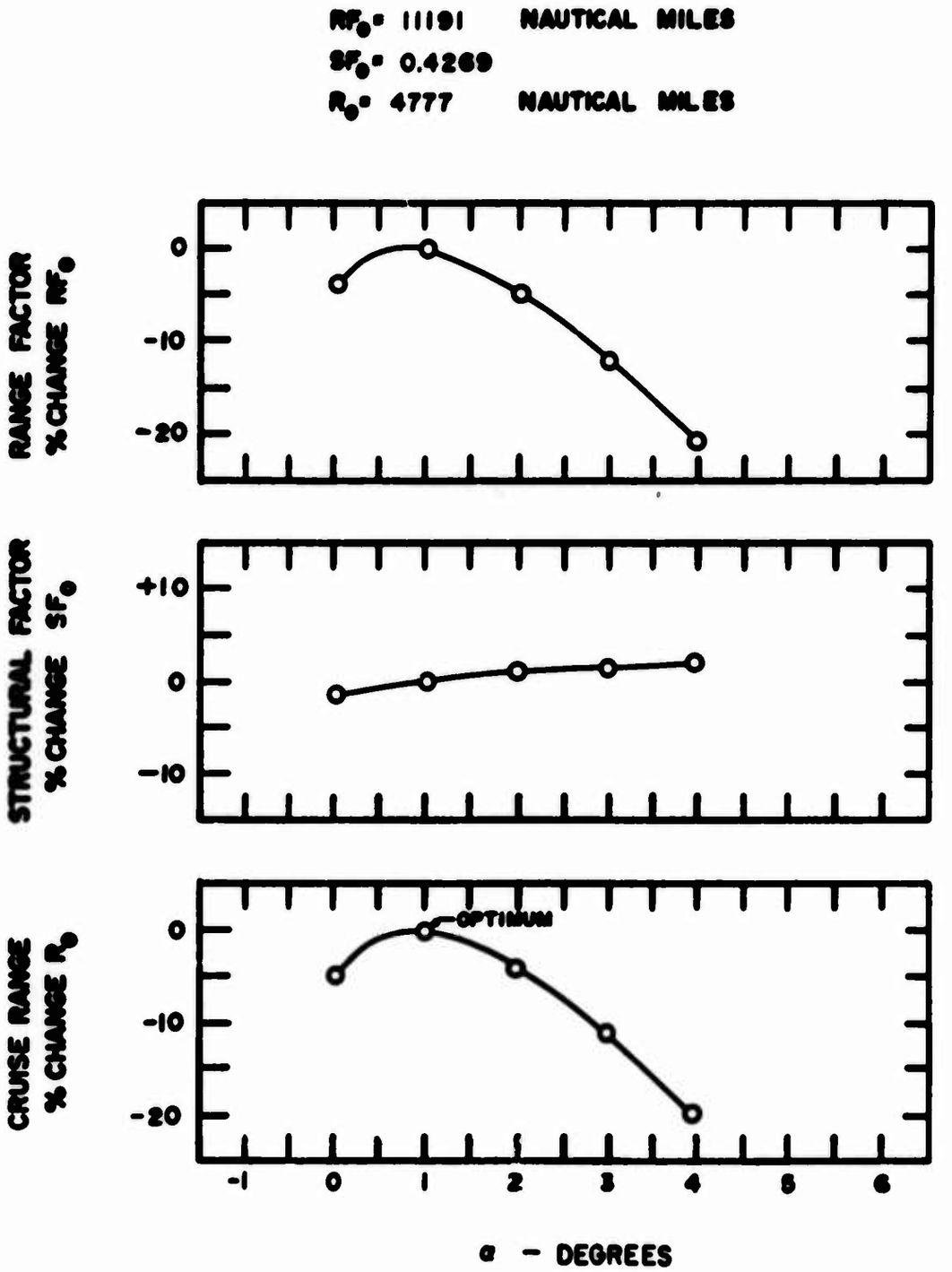

FIG 25 Angle of Attack α Influence on Cruise Range and Factors of Breguet Range Equation

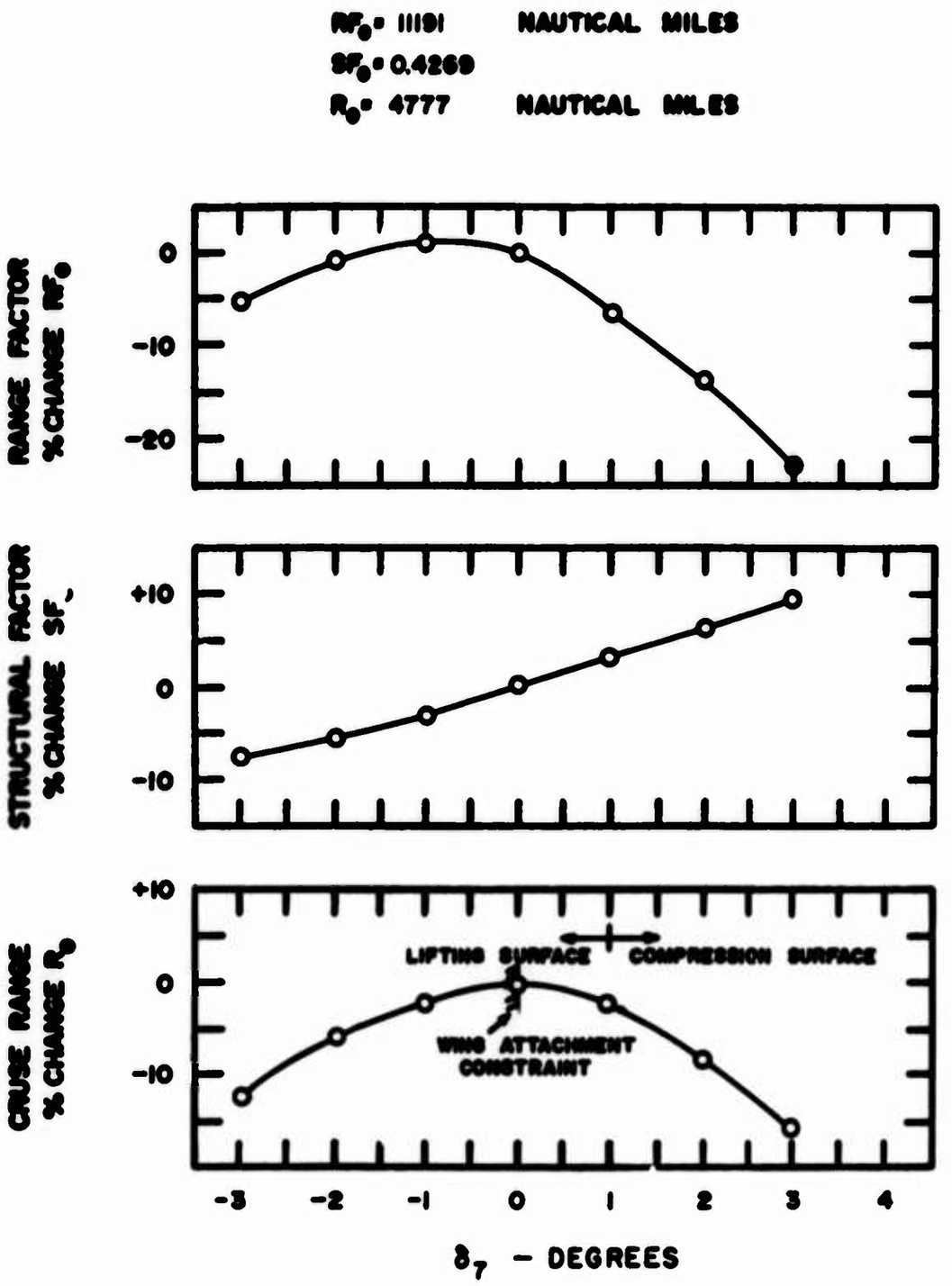

FIG 26 Upper Fuselage Surface Angle δ_7 Influence on Cruise Range and Factors of Breguet Range Equation

dimensions. The volume-wetted area ratio of a sphere, for example, increases in direct proportion to the radius. The increasing volume-wetted area ratio is reflected by the increase in structural factor with increase in design takeoff weight as shown in Fig 27 for the Mach 10 configuration. The trend of increased performance with increased size is evidenced in the subsonic cruise regime also by the appearance of larger jet aircraft such as the Boeing 747.

Width of the fuselage b was specified by the fuselage width to maximum thickness ratio b/h. The optimum value of the width to thickness ratio occurred as a result of a trade off between the range factor and structural factor as shown in Figure 28. Aerodynamic performance increased as vehicle width increased as a result of the friction drag of the vehicle sides (which is nearly constant) becoming a small percentage of the total drag as the width of the vehicle increased. Volumetric efficiency of the vehicle, as reflected by the structural factor in Fig 28, decreased with increasing fuselage width to thickness ratio after obtaining a maximum at width to thickness ratio of approximately one.

Range Potential

In addition to determining characteristics of optimum configurations in which lift, propulsion, and volume are integrated, a second objective of the study was to determine the possibility of range potential increase with increased design cruise Mach number. Range potential, as reflected by the range factor rather than absolute range, is treated here since the detailed weight and trajectory analysis necessary to determine the absolute level of range, was beyond the scope of this investigation. Figure 29 indicates for the cruise Mach number regime considered in this investigation (8 - 12) that the range potential increased with design cruise Mach number for the case without skin friction; however, for the case with skin friction, little change in range potential occurred with cruise Mach number.

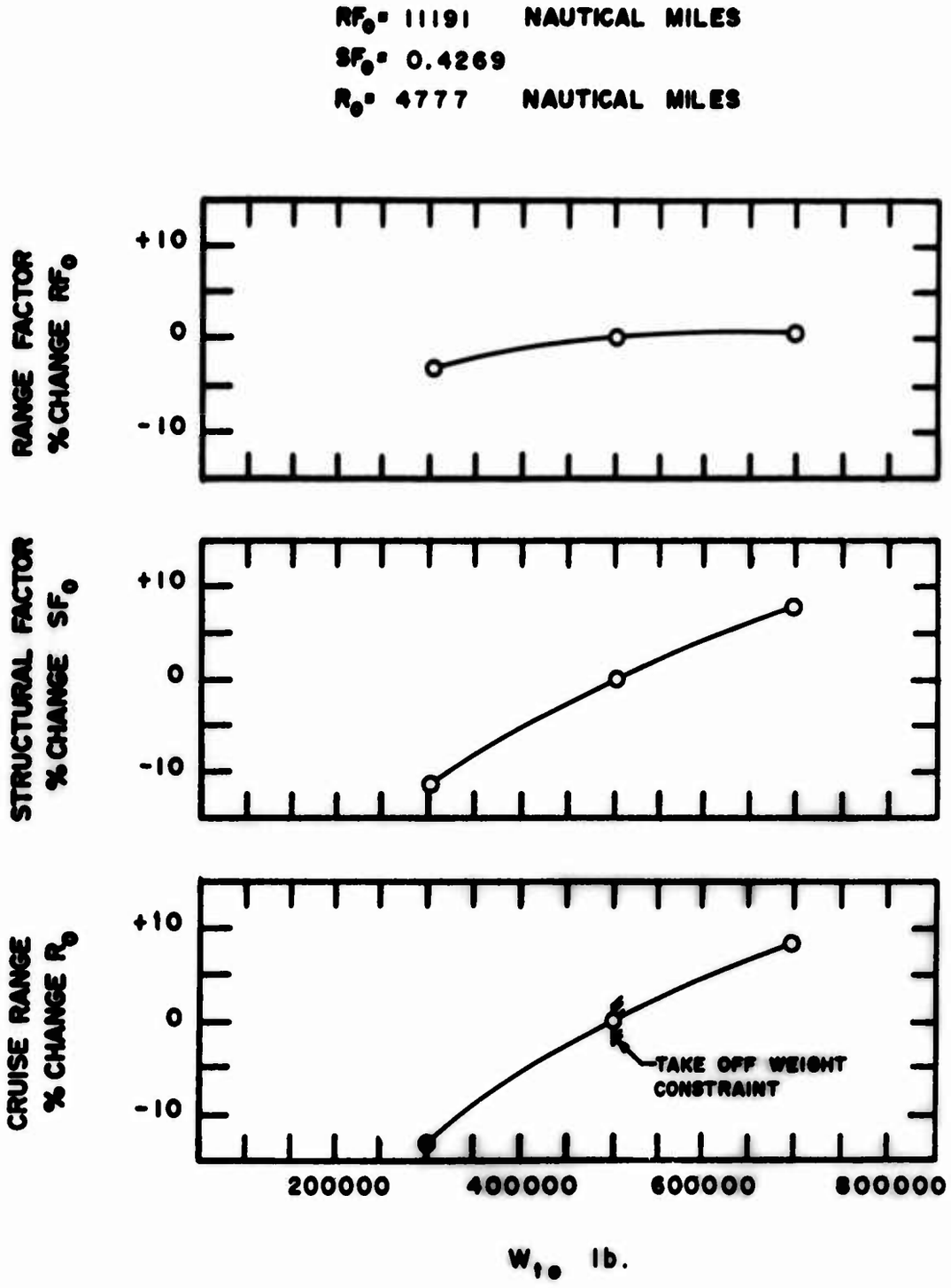

FIG 27 Take Off Weight W_{to} Influence on Cruise Range and Factors of Breguet Range Equation

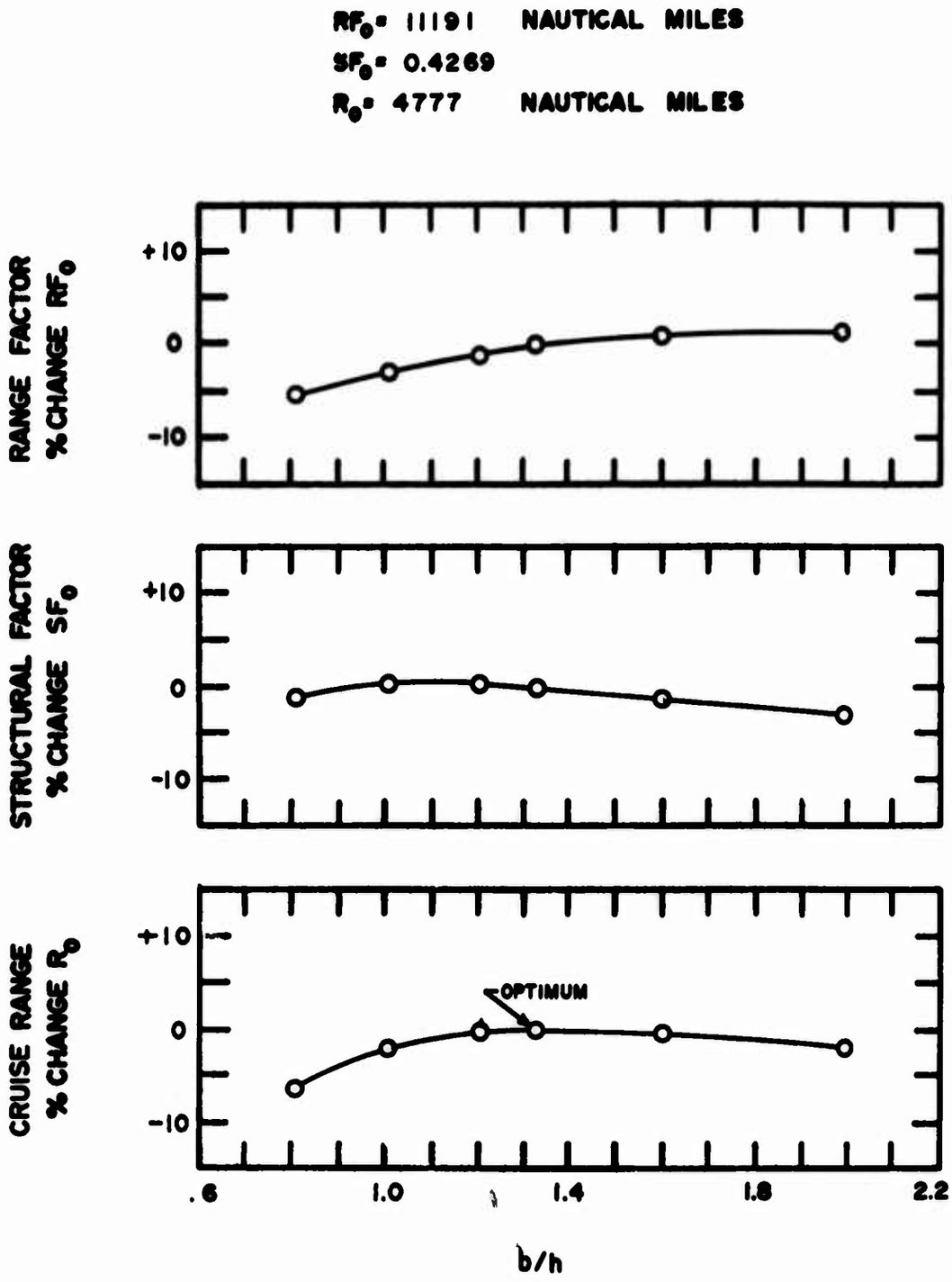

FIG 28 Nondimensional Vehicle Width b/h Influence on Cruise Range and Factors of Breguet Range Equation

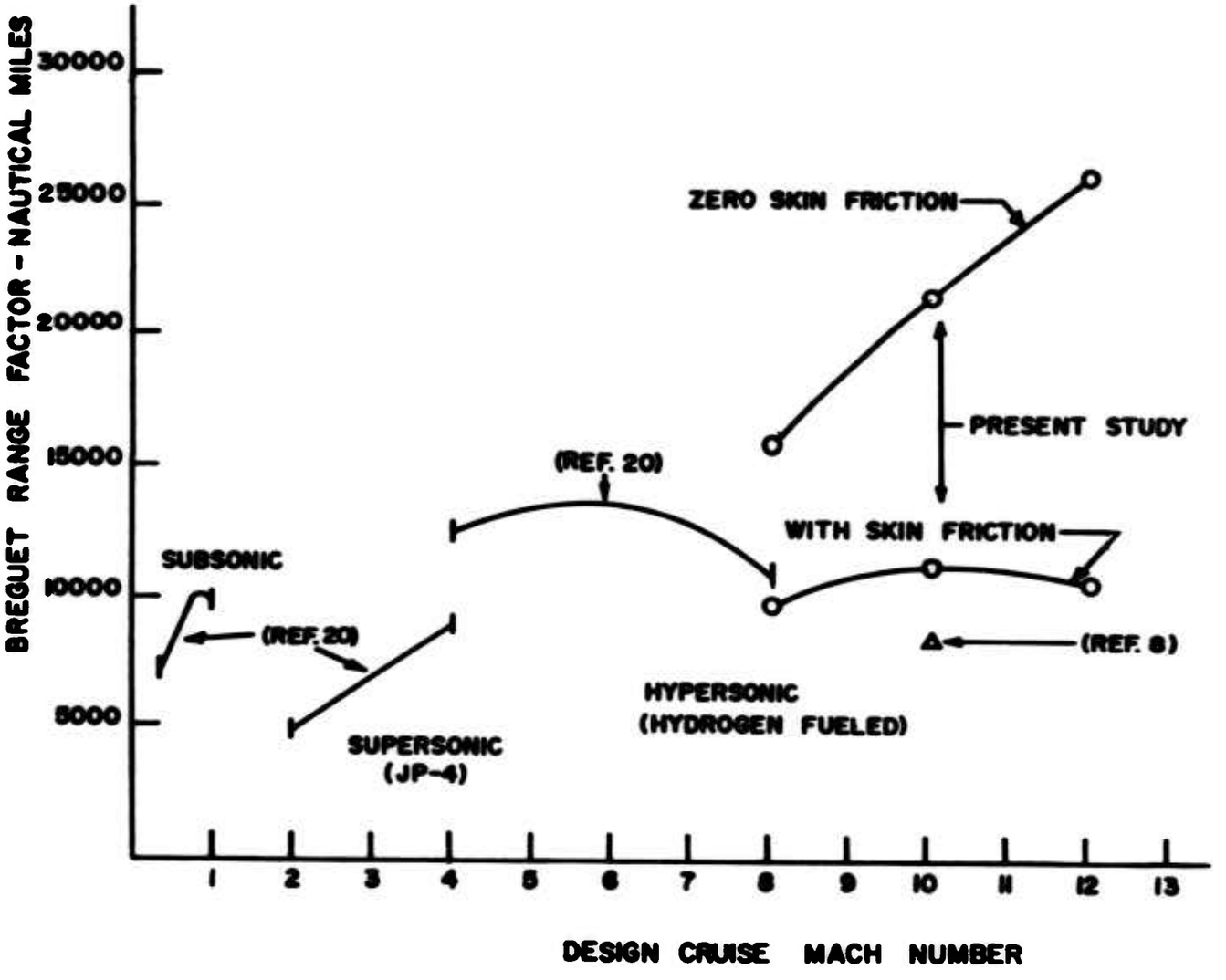

FIG 29 Range Potential of Transports

Figure 29 also indicates that skin friction places an important limitation on the range of vehicles in the Mach 8 to 12 cruise regime. A partial reason for this is illustrated in Fig 30 as friction drag is seen to become an increasingly higher percentage of total drag as the cruise Mach number increases since the pressure drag coefficient decreases. The decreasing pressure drag coefficient with Mach number is due to the decreasing thickness ratio of the vehicle since the deflection required to produce compression waves that will produce a combustor entrance temperature of $T_4 \geq 2000$ R decreases as design Mach number increases.

Another reason for the high sensitivity of hypersonic cruise vehicles to skin friction is the high dynamic pressure of the propulsive stream which comes into contact with certain components of the vehicle, especially in the final stage of compression. In the case of the Mach 10 design, for example, the dynamic pressure at the entrance of the combustor is approximately 12 times that of free stream.

The cooling constraint, fuel required for regenerative cooling of internal surfaces of the propulsion system and the leading edges of the vehicle be less than or equal to fuel required for propulsion ($\phi_c \leq \phi$), was not encountered as shown in Figs 10 - 12; therefore, the constraint did not affect the range potential of the optimum configurations. Appendix D contains a breakdown of the regenerative cooling requirements of the various components of the Mach 12 vehicle. Of the components considered, the combustor required the most active cooling while the leading edges of the vehicle required the least.

Comparison of Performance

The Breguet range factor is shown in Fig 29 for subsonic jet transports, supersonic transports, and a hypersonic (Mach 4 - 8) transport which was based on a performance study (Ref 20). Since the assumptions and conditions under which the values of Breguet range factor of these vehicles were obtained are not the same, the range

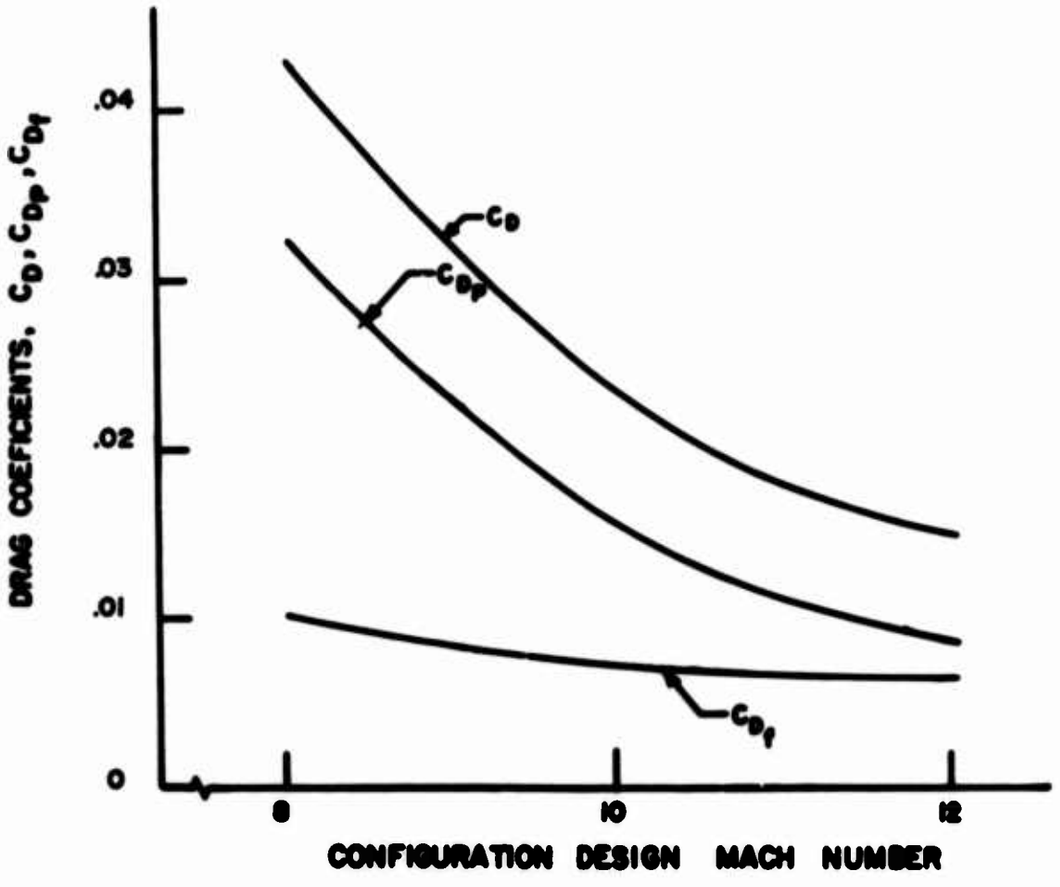

FIG 30 Variation of Drag Coefficients with Design Mach Number

potential of these vehicles is shown only to serve as a general guide to comparison of the cruise regimes. Figure 29 illustrates that the attractiveness of hypersonic cruise in the Mach 8 to 12 speed regime, from the standpoint of range potential increase over cruise below Mach 8, depends heavily on the level of skin friction drag. The lower the skin friction--the more attractive hypersonic cruise becomes.

Also included in Fig 29 is the range factor obtained by Williams (Ref 8) in a cruise vehicle optimization study. The study did not include the effects of skin friction; therefore, his result should be compared to the zero skin friction curve of the present study shown in Figure 29. The model for the optimization study by Williams contained three independent variables which were, in terms of the nomenclature used in this study, (δ_1, δ_7, δ_5). For the case of maximum range factor, which was the performance criterion for his study, the values of δ_1 and δ_7 obtained in both studies agree ($\delta_{1\,opt} \cong \delta_1$ for maximum inlet pressure recovery, and $\delta_{7\,opt} = 0$). However, his optimization model did not contain sufficient degrees of freedom to obtain higher performance which is a danger at any level of solution of optimization problems. If his model had included wings and or a variable equivalence ratio, the nozzle geometry would not have been constrained to produce equilibrium flight which resulted in the lower value of range factor shown in Figure 29.

Figure 31 contains a comparison of specific impulse Isp data obtained in the present study and typical Isp data obtained from one-dimensional supersonic combustion cycle analysis studies of hydrogen and air (Ref 17). Figure 31 illustrates that the specific impulse obtained from the present study decreases at a faster rate with increasing Mach number than the specific impulse obtained from the one-dimensional data. This is due to the fact that propulsive efficiency of the optimized configurations was traded for increased aerodynamic efficiency as design cruise Mach number increased. The objective of

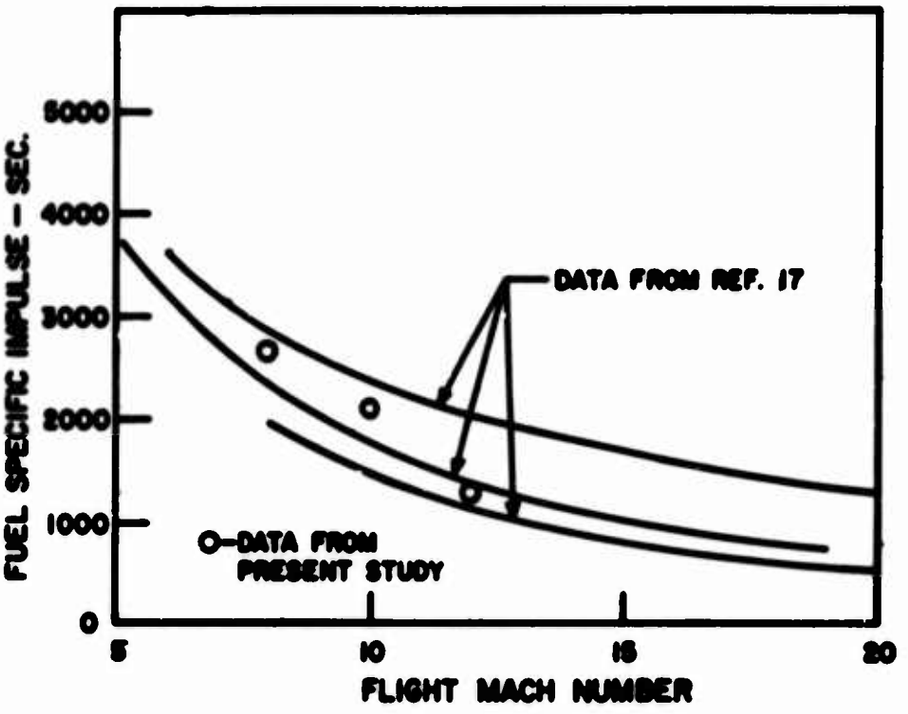

FIG 31 Specific Impulse Comparison

this investigation, however, was not to optimize a configuration based on the propulsive efficiency alone, but rather the geometry of a configuration in light of the combined propulsive, aerodynamic, and volumetric efficiencies. The main ideas of this chapter are summarized in the next chapter.

V. Summary and Conclusions

The optimization process was applied to the design of an air breathing hypersonic cruise vehicle configuration. Emphasis was placed on relating the configuration performance directly to the surrounding flow field so that any interaction between the aerodynamic and propulsive flow field would be accounted for in a fundamental manner. Cruise range, as determined from the Breguet range equation, was selected as the performance criterion for the optimization process with payload fraction becoming one of the constraints. The general class of vehicles which were optimized cruise in the Mach 8 to 12 speed regime, utilize a constant area supersonic combustion ramjet engine which burns hydrogen fuel, and can be characterized geometrically as two-dimensional wedgelike wing-body vehicles.

A generalized configuration model was defined by discrete parameters, transforming the variational optimization problem to a discrete or static optimization problem. Automated direct search algorithms were then used to determine the discrete parameters defining the configurations producing maximum cruise range for design cruise Mach numbers of 8, 10, and 12.

Within the limits of the analytical model used, the following qualitative conclusions can be deduced concerning the cruise configuration of the class of vehicles considered in this investigation:

(1) The optimum configuration flies at about zero angle of attack.

(2) Although developing very little lift, the inlet-forebody produces a pitch up moment.

(3) Inlet-forebody compression ramp configuration for maximum range differs from the inlet-forebody configuration producing maximum pressure recovery (see Fig 13).

(4) Inlet-forebody thickness ratio is determined by the minimum shock wave strength necessary to produce the autoignition air

temperature at the combustor entrance .

(5) Optimum combustor-midsection length of the vehicle is the minimum combustor length which allows for mixing, ignition and burning of the fuel.

(6) Optimum nozzle-aftfuselage configuration is one which produces a resultant nozzle force direction θ_T consistent with the expression derived in Appendix B:

$$\tan \theta_{T_{opt}} = \frac{\left(\frac{L}{D}\right)_w + \frac{\partial \ell n C_T}{\partial \theta_T}}{1 - \left(\frac{L}{D}\right)_w \frac{\partial \ell n C_T}{\partial \theta_T}}$$

(7) Maximum range is obtained when the upper surface of the fuselage is nearly parallel to the free stream flow.

(8) Range performance increases with takeoff weight which is consistent with the "cube-square law" preferring largest possible scale from a volumetric efficiency standpoint.

(9) Volumetric efficiency dictates a fuselage width slightly greater than the fuselage height (at the highest point) for maximum range.

(10) The wings of the optimum cruise configuration are small with approximately three-fourths of the total lift provided directly by the propulsive system.

In addition to the above conclusions concerning the cruise configuration of the vehicles, several qualitative conclusions can be deduced concerning performance trends:

(1) Range potential (Breguet range factor) increases with velocity as anticipated from the Breguet range equation for the case without skin friction. However; for the case with skin friction, little change in range occurs with velocity.

(2) Range factors of approximately 10000 nautical miles are indicated for transport type vehicles which cruise in the Mach 8 to 12 regime.

(3) The cooling capacity available in the liquid hydrogen fuel required for propulsion is adequate for cooling in the Mach range (8-12).

In regard to the direct method of configuration optimization, several factors can be noted.

(1) In this investigation, nongradient search algorithms were more efficient than gradient techniques such as the steepest ascent.

(2) Of the nongradient search algorithms, random point and sectioning were effective in the early phases of the search; whereas, the adaptive creeper search algorithm was effective in the terminal search phase.

(3) The performance response surface appeared unimodal in the region of the optimum and very flat so that a large number of configurations produced approximately the same performance.

Since the mathematical formulation of the problem did not include all classes of configuration or consideration of all constraints, influences, etc., the optimized configurations obtained in this investigation are not expected to offer a final solution to the optimum cruise vehicle problem. However, in addition to the fundamental configuration and performance results enumerated above, the investigation can contribute to a final solution by serving as a guide and as a comparison point for future configuration optimization studies in which the performance is related directly to the flow field.

Future work might include extension of the present model of the wedgelike wing-body class of vehicles to include subsonic combustion, or formulation of a new model to investigate another geometric family of shapes such as the conelike class of vehicles. In the more distant future however, as techniques progress for predicting the flow field about arbitrary three-dimensional shapes, as computers grow in size

and speed, as optimizing search algorithms become more efficient, the goal of configuration design will perhaps be realized. That is--when the configuration is shaped more by the physical aspects of the problem and less by the intuition of the designer.

Bibliography

1. Pritchard, R. E., "Base Drag Effects on Maximum Lift-to-Drag Ratio Airfoils at Moderate Supersonic Speeds," Journal of Optimization Theory and Application, Vol 3, No 2, pp. 115-136 (February 1969).

2. Hague, D. S. and C. R. Glatt, Application of Multivariable Search Techniques to the Optimal Design of a Hypersonic Cruise Vehicle, NASA CR-73202, Moffett Field, California: Ames Research Center, April 1968.

3. Kuchemann, D., "Hypersonic Aircraft and their Aerodynamic Problem," in Progress in Aeronautical Sciences, Vol 6, edited by D. Kuchemann and L. H. G. Sterne. London: Pergamon Press, 1965, pp 271-351.

4. Pun, Lucas, Introduction to Optimization Practice, New York: John Wiley & Sons, Inc., 1969.

5. Dugger, G. L., "Comparison of Hypersonic Ramjet Engines with Subsonic and Supersonic Combustion," Proceedings of Fourth AGARD Colloquim (Milan 1960). London: Pergamon Press, 1961, pp 112-116.

6. Hankey, W. L. and G. A. Elliott, "Hypersonic Lifting Body Optimization" paper given at AIAA Entry Vehicle System and Technology Meeting, Williamsburg, Virginia, 3-5 December 1968. (AIAA Paper No. 68-1157).

7. Hankey, W. L., Some Design Aspects of Hypersonic Vehicles, ARL 70-0044, Wright-Patterson Air Force Base, Ohio: Aerospace Research Lab., 1970.

8. Williams, J. E., Optimization of a Scramjet Configuration, M.S. Thesis, Wright-Patterson Air Force Base, Ohio: Air Force Institute of Technology, 1967.

9. Townend, L. H., On Lifting Bodies Which Contain Two-Dimensional Supersonic Flows, Aero. Res. Council R and M No. 3383, August 1963.

10. Plank, P. P., et al. Hypersonic Cruise Vehicle Wing Structure Evaluation, NASA CR-1568, Washington, DC: National Aeronautics and Space Administration, 1970.

11. Kelly, Henry J., "Method of Gradients," in Optimization Techniques, edited by G. Leitmann, New York: Academic Press, 1962, pp 205-254.

12. Leon, A., "A Classified Bibliography on Optimization," in Recent Advances in Optimization Techniques, edited by A. Lavi and T. P. Vogl, New York: John Wiley & Sons, Inc., 1966, pp 599-649.

13. Wilde, Douglas J., Optimum Seeking Methods, New Jersey: Prentice-Hall, Inc., 1965.

14. Hague, D. S. and C. R. Glatt, An Introduction to Multivariable Search Techniques for Parameter Optimization, NASA CR-73200, Moffett Field, California: Ames Research Center, April 1968.

15. Orlov, B. V. et al Design Principles of Rocket-Ramjet Engines for Unmanned Flight Vehicles, (a translation of "Osnovy Proyektirovaniya Raketno-Prynaotochnykh Dvigateley Dlya Bespilotnykh Letatel' nykh Apparatov," Moscow, Izd-vo Mashinostroyeniye (Russian)), FTD-MT-240108-68, Wright-Patterson Air Force Base, Ohio: Foreign Technology Division, July 1968, pp 17-23.

16. Franciscus, L. C., Off Design Performance of Hypersonic Supersonic Combustion Ramjets, NASA TMX-52032, Washington, DC: National Aeronautics and Space Administration, June 1964.

17. Swithenbank, J., "Hypersonic Air-Breathing Propulsion," in Progress in Aeronautical Sciences, Vol 8, edited by D. Kuchemann, London: Pergamon Press, 1967, pp 259-260.

18. Ferri, Antonio, "Review of Problems in Application of Supersonic Combustion," Journal of the Royal Aeronautical Society, Vol 68, No 645: 575-594, (September 1964).

19. Elliot, Irwin I. et al, Automated Procedures for Evaluating Powered Hypersonic Vehicles from Subsonic Through Hypersonic Speeds, Vol I, Part II, Air Force Flight Dynamics Laboratory, AFFDL-TR-68-25, Wright-Patterson Air Force Base, Ohio: April 1968, pp 688-689.

20. Gregory, T. J.; R. H. Peterson and J. A. Wyss, "Performance Tradeoffs and Research Problems for Hypersonic Transports," Journal of Aircraft, Vol 2, No 4: 266-271, (July - August 1965).

21. Robertson, R. L., Guidance, Flight Mechanics and Trajectory Optimization, Vol XVI Mission Constraints and Trajectory Interfaces, CR-1015, Washington, DC: National Aeronautics and Space Administration, April 1958, pp 14-20.

22. Hildebrand, R. B., "Aerodynamic Fundamentals," Handbook of Astronautical Engineering, edited by H. H. Koelle, New York: McGraw-Hill, Inc., 1961, Chapter IV, pp 30.

23. Lees, Lester, "Laminar Heat Transfer Over Blunt Nosed Bodies at Hypersonic Flight Speeds," Jet Propulsion, Vol 26: 259 (Apr 56).

24. Ames Research Staff, Equations, Tables, and Charts for Compressible Flow, NACA Report 1135, Washington, DC: National Advisory Committee for Aeronautics, 1953.

25. Minzner, P. A., et al The ARDC Model Atmosphere, 1959, August 1959, pp 78-93, AFCRC-TR-59-264, Bedford, Mass.: Air Force Cambridge Research Center (AD-229482).

26. Komar, J. J., Improved Turbulent Skin Friction Coefficient Predictions Utilizing the Spalding-Chi Method, DAC-59801, Long Beach, Calif.: Douglas Missile and Space Division, November 1966.

27. Wilson, Donald M., Digital Computer Program for Making Comparative Aerodynamic Heat Transfer and Skin Friction Drag Calculation, Report No 67-137, August 1957, (AD-660688), Silver Spring, MD: U. S. Naval Ordnance Laboratory.

28. Wyatt, D. D., "The Ramjet Engine," in Jet Propulsion Engines, edited by O. E. Lancaster, Princeton: Princeton University Press, 1959, pp 286-287.

29. Browne, W.G. and D. L. Warlich, Properties of Combustion Gases, System: H_2 - Air, R62FPD-366, Cincinnati, Ohio: General Electric Company, 1962.

30. Shapiro, Ascher H., The Dynamics and Thermodynamics of Compressible Fluid Flow, Vol I, New York: Ronald Press Co., 1953, pp 462-524.

Appendix A

Cruise Trajectory Equations

The purpose of this appendix is to trace the development of a form of the Breguet range equation from the differential equations describing the state of the vehicle during the cruise portion of the mission profile.

With reference to Fig 32, the equations of motion of the vehicle (Ref 21) can be written for a nonrotating spherical earth in a wind axis coordinate system as

$$\frac{W}{g_c}\frac{dV_1}{dt} = T - D - W \sin\gamma \tag{A1}$$

$$\frac{W}{g_c} V_1 \frac{d\gamma}{dt} = L - W\cos\gamma + \frac{W}{g_c}\frac{V_1^2 \cos\gamma}{H + r_e} \tag{A2}$$

From Fig 32 the rate of change of altitude and ground range is given by

$$\frac{dH}{dt} = V_1 \sin\gamma \tag{A3}$$

$$\frac{dR}{dt} = \frac{r_e}{H + r_e} V_1 \cos\gamma \tag{A4}$$

The differential equation describing the rate of change of weight of the vehicle in terms of thrust and specific impulse is

$$\frac{dW}{dt} = -w_f = -\frac{T}{Isp} \tag{A5}$$

Numerical methods are in general necessary to integrate Eqs A1 through A5 simultaneously from start to termination of cruise in order to determine the cruise range. If certain assumptions are made; however, the cruise range can be simply expressed as an ordinary function commonly referred to as the Breguet range equation. The

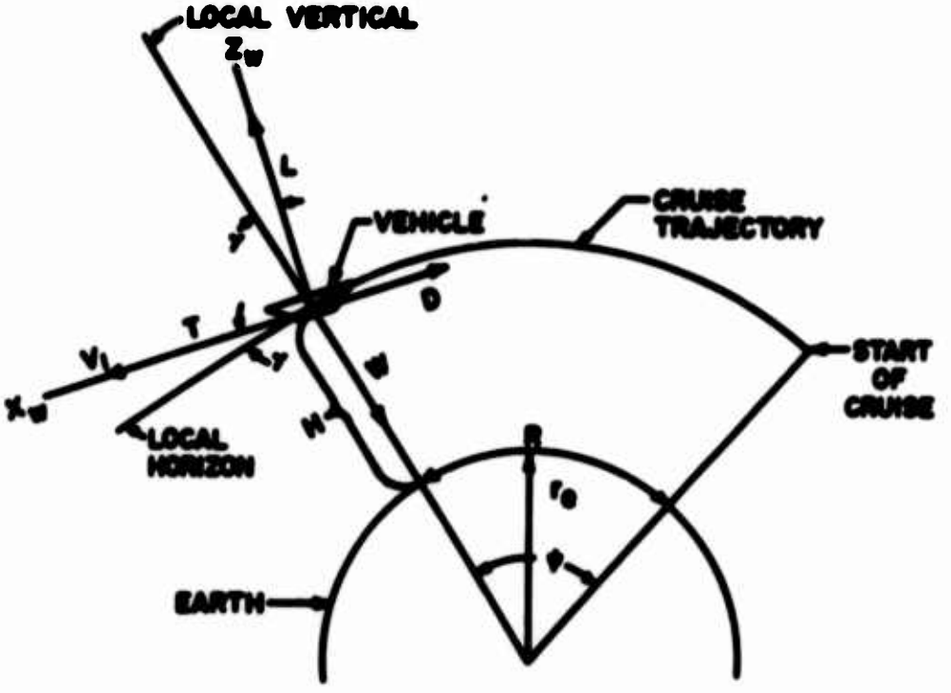

FIG 32 Cruise Trajectory Parameters

required assumptions are:

1. A zero flight path angle, $\gamma = 0$.
2. A constant flight path angle, $\frac{d\gamma}{dt} = 0$.
3. A constant cruise speed, $\frac{dV_i}{dt} = 0$.
4. A cruise altitude small compared to the radius of the earth, $\frac{r_e}{H + r_e} \approx 1$.

With the above assumptions Eqs A1 - A4 respectively become

$$T = D \tag{A6}$$

$$L = W\left(1 - \frac{V_i^2}{g_c r_e}\right) \tag{A7}$$

$$H = \text{constant} \tag{A8}$$

$$R = \int_{t_i}^{t_f} V_i \, dt \tag{A9}$$

Equation A9 is integrated by changing the integration variable from time t to weight W

$$R = \int_{W_i}^{W_f} V_i \, \frac{dW}{(dW/dt)} \tag{A10}$$

and by using Eqs A5 through A 7 in Eq A10

$$R = \int_{W_i}^{W_f} -\left[\frac{L}{D} \, Isp \, \frac{V_i}{1 - \frac{V_i^2}{g_c r_e}}\right] \frac{dW}{W} \tag{A11}$$

The final form of the Breguet range equation is obtained by assuming that the bracketed term in Eq A11 is a constant for constant velocity cruise and noting that $g_c r_e = V_o^2$

$$R = \frac{L}{D} \, Isp \, \frac{V_i}{1 - V_i^2 / V_o^2} \, \ln \frac{W_i}{W_f} \tag{A12}$$

The form of the Breguet equation used as the performance criterion is obtained by substituting Eq A5 and A6 into Eq A12

$$R = \left[\frac{L}{\dot{w}_f} \quad \frac{V_i}{1 - V_i^2 / V_o^2} \right] \ell n \frac{W_i}{W_f} \qquad \text{(A13)}$$

The range of each trial configuration during the optimization process was estimated with a range factor (the bracketed terms in Eq A11 and A13) evaluated at initiation of cruise. In order that the range factor remains constant for the cruise segment (necessary for the integration of Eq A11), the vehicle is assumed to climb during cruise as fuel is depleted (maintain W/ρ_i = const.). A slight acceleration is induced, however, for a constant Mach number cruise as temperature of the standard atmosphere increases with altitude. For example, the initial and final cruise altitudes of the Mach 10 cruise vehicle were 115,000 ft and 124,000 ft respectively, which resulted in an ambient temperature increase of 14 R and an acceleration, to maintain constant Mach number cruise, of $dV_i / dt = 1.88 \times 10^{-3} g$.

The change which occurs in flight path angle γ due to the altitude change is also slight. Thus, estimating the range at initial cruise and flying the constant Mach-varying altitude trajectory results in a reasonable cruise range prediction for the trial configurations evaluated during the optimization process.

Appendix B

Expression for Optimum Nozzle Thrust Angle

The purpose of Appendix B is to develop an expression for the nozzle thrust angle θ_T which produces a stationary or extremum value (if one exists) of the Breguet range factor.

Starting with the expression for the range factor

$$RF = \frac{L}{\dot{w}_f} \frac{V_1}{1 - V_1^2 / V_o^2} \tag{B1}$$

and noting that for a fixed cruise speed the only variable term in Eq B1 is $L / \dot{w}_f$ which can be expressed as

$$\frac{L}{\dot{w}_f} = \frac{L_w + L_b + L_n}{(p_1 / R_1 T_1) A_c V_1 \phi f_s} \tag{B2}$$

where the wing lift L_w is given by

$$L_w = (F_n \sin \theta_T - D_b) \left(\frac{L}{D}\right)_w \tag{B3}$$

and the nozzle lift is given by

$$L_n = F_n \cos \theta_T \tag{B4}$$

Dividing numerator and denominator of Eq B2 by $\ell_1 b$ and nondimensionalizing the forces by $p_1 \ell_1 b$ results in the following expression

$$\frac{L}{\dot{w}_f} = \frac{\left(C_T \sin \theta_T - C_{D_b}\right) \left(\frac{L}{D}\right)_w + C_{L_b} + C_T \cos \theta_T}{(A_c V_1 \phi f_s) / (R_1 T_1 b \ell_1)} \tag{B5}$$

Applying the necessary conditions for an extremum with respect to the nozzle thrust angle to Eq B5, and noting that terms in the denominator of Eq B5 as well as C_{L_b}, C_{D_b}, and $(L/D)_w$ are independent of θ_T results in

$$\frac{\partial(L/\dot{w}_f)}{\partial\theta_T} = \left(\frac{L}{D}\right)_w \left(C_T \cos\theta_T + \frac{\partial C_T}{\partial\theta_T} \sin\theta_T\right) + \frac{\partial C_T}{\partial\theta_T} \cos\theta_T - C_T \sin\theta_T = 0 \tag{B6}$$

Dividing Eq B6 by $\cos\theta_T$ and rearranging, produces an expression for the nozzle force direction angle producing a stationary value of the range factor:

$$\tan\theta_{T_{st}} = \frac{\left(\frac{L}{D}\right)_w + \frac{1}{C_T}\frac{\partial C_T}{\partial\theta_T}}{1 - \left(\frac{L}{D}\right)_w \frac{1}{C_T}\frac{\partial C_T}{\partial\theta_T}} = \frac{\left(\frac{L}{D}\right)_w + \frac{\partial \ln C_T}{\partial\theta_T}}{1 - \left(\frac{L}{D}\right)_w \frac{\partial \ln C_T}{\partial\theta_T}} \tag{B7}$$

Since the nozzle thrust direction θ_T is a function of the nozzle half angle δ_s, Eq B7 can also be used to determine the δ_s producing an extremum value of the range factor.

As an example, Figs 34 and 35 show the variation of nozzle force coefficient C_T and direction θ_T respectively as a function of nozzle half angle δ_s for a configuration of the class investigated in this study. In order to determine $\theta_{T_{st}}$ and $\delta_{s\,st}$ for a configuration with a wing lift-drag ratio of $(L/D)_w = 5.5$ and an equivalence ratio of $\phi = .8$, a trial value of $\delta_{s_t} = 16^\circ$ is assumed. This allows the unknown term in Eq B7 to be evaluated graphically from Figs 34 and 35

$$\frac{1}{C_T}\frac{\partial C_T}{\partial\theta_T} = \left(\frac{1}{C_T}\frac{\partial C_T}{\partial\delta_s}\right)\left(\frac{\partial\delta_s}{\partial\theta_T}\right) = (-3.25)\left(\frac{1}{2.63}\right) = -1.27 \tag{B8}$$

substituting into Eq B7

$$\tan\theta_{T_{st}} = \frac{5.5 - 1.27}{1 + (5.5)(1.27)} = .530 \tag{B9}$$

which implies $\theta_{T_{st}} = 27.9^\circ$, and from Figure 35, $\delta_{s_c} = 15.8^\circ$.

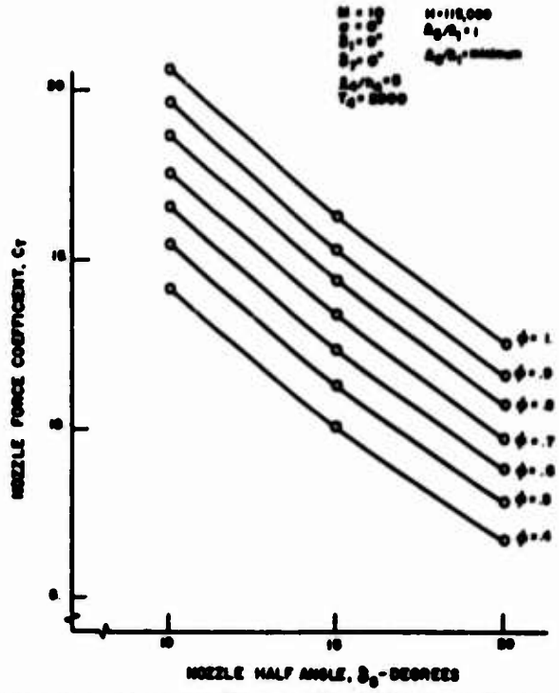

FIG 33 Nozzle Force Coefficient Variation with Nozzle Half Angle

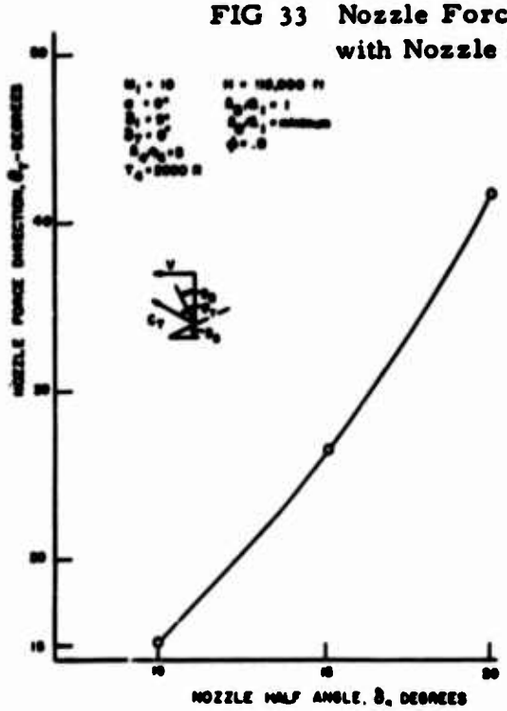

FIG 34 Nozzle Force Direction Variation with Nozzle Half Angle

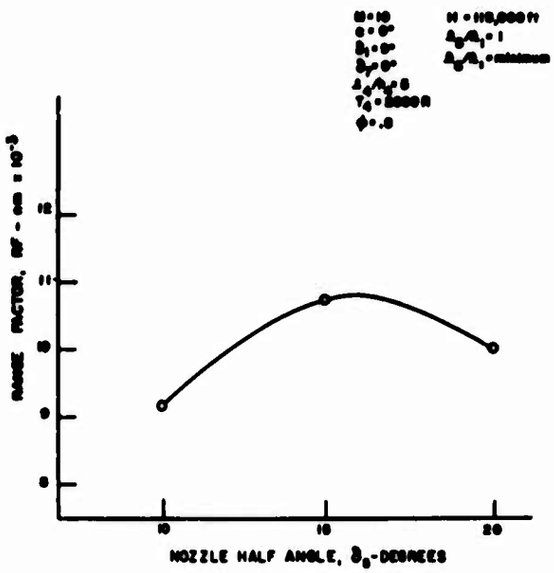

FIG 35 Range Factor Variation with Nozzle Half Angle

This indicates the optimum nozzle half angle for maximum range factor predicted by Eq B7 is in the neighborhood of 16^{o} which agrees reasonably well with the numerical solution of the range factor (Eq B1) as shown in Figure 36.

Appendix C

Performance Sensitivity with Respect to the Structural Set Parameters

In order to evaluate the structural factor (hence the cruise range) during the optimization of independent design variables, it was necessary to specify values of certain parameters. These parameters were termed the structural parameter set $\bar{S}$ and consisted of

$$\bar{S} = \left[\rho_e, \rho_p, \rho_f, \frac{W_{fc}}{W_{f\ell}}, \frac{W_e}{W_{to}}, \frac{W_p}{W_{to}}, \gamma_s \right] \qquad (C1)$$

Sensitivity of the cruise range and structural performance with each member of the set $\bar{S}$ is shown in this appendix using the optimal Mach 10 design as a source for the value of the range factor (RF = 11191 nm) and geometrical shape quantities.

The geometrical shape provides a constant value of the nondimensional volume ($\forall / \ell_1^3 = .2367$) and surface area ($A_w / \ell_1^2 = 4.568$). For a fixed takeoff weight ($W_{to} = 500,000$ lb) Eq E37 (Appendix E) becomes a cubic equation in the unknown scale factor ℓ_1

$$\left(\frac{\forall}{\ell_1^3}\right) \ell_1^3 + \left(\frac{\gamma_s}{\rho_f} \frac{A_w}{\ell_1^2}\right) \ell_1^2 - W_{to} \left[\frac{1}{\rho_f} \left(1 - \frac{W_p}{W_{to}} - \frac{W_e}{W_{to}}\right) + \frac{W_p}{W_{to}} \frac{1}{\rho_p} + \frac{W_e}{W_{to}} \frac{1}{\rho_e} \right] = 0 \qquad (C2)$$

Once the scale factor ℓ_1 is known, the structural weight is determined from

$$W_s = \left(\frac{A_w}{\ell_1^2}\right) \gamma_s \ell_1^2 \qquad (C3)$$

and the fuel weight from

$$W_{f\ell} = W_{to} - W_p - W_e - W_s \qquad (C4)$$

The structural factor of the Breguet range equation SF can now be evaluated from

$$SF = \ln \left[1 + \frac{\frac{W_{fc}}{W_{f\ell}} \quad \frac{W_{f\ell}}{W_{to}}}{\frac{W_p}{W_{to}} + \frac{W_e}{W_{to}} + \frac{W_s}{W_{to}}} \right] \qquad (C5)$$

Thus, the cruise range R can be determined for a constant range factor RF, since

$$R = (RF)\ (SF) \qquad (C6)$$

Figures 36 through 43 were generated by varying the members of the structural parameter set one at a time while fixing the remaining members at the values used in the optimization study as shown in Table III. Since the range factor is constant, the percentage change in cruise range and structural factor is shown on the same ordinate in the figures. Figure 36 shows that the range was insensitive to wide variations of the equipment weight density. The performance is also shown in Fig 37 to be insensitive to payload density for perturbations about $\rho_p = 4.5$ lb/ ft^3 (density of airliner passenger compartments with people aboard).

Although the density of the liquid hydrogen fuel is fixed, Fig 38 is included to show, from a structural standpoint, how the performance increases as the density of hypothetical fuels increases. The fuels would have the same energy content per pound as hydrogen but with different densities. As a means of comparison, jet fuel (JP-4) has a density of approximately 50 lb/ ft^3; whereas, the density of liquid hydrogen is 4.5 lb/ ft^3. Unfortunately, the energy content and heat sink capacity of JP-4 is very much lower than liquid hydrogen so that JP-4 is not considered an attractive fuel for the class of vehicles considered in this study.

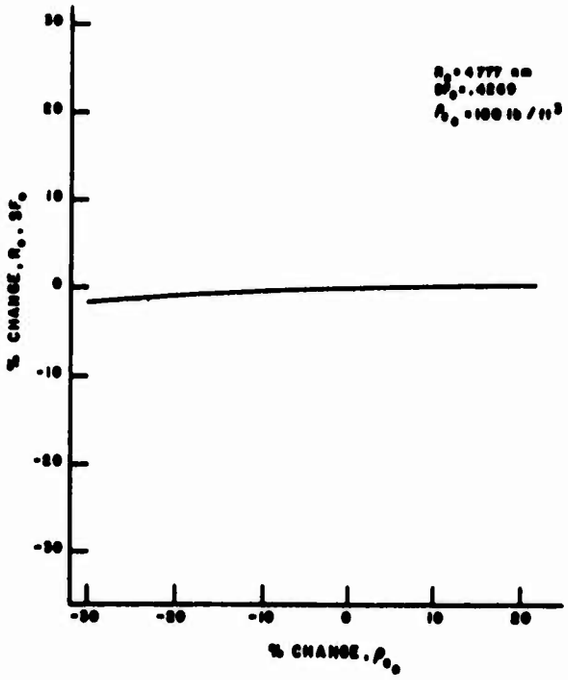

FIG 36 Equipment Density Influence on Performance

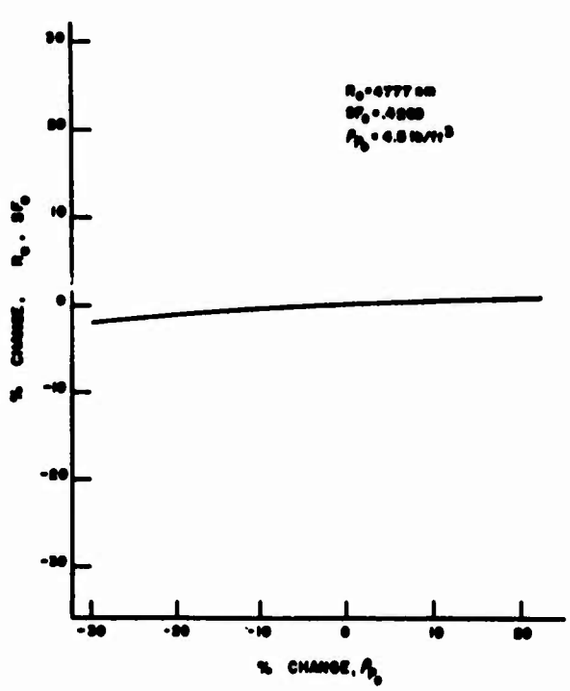

FIG 37 Payload Density Influence on Performance

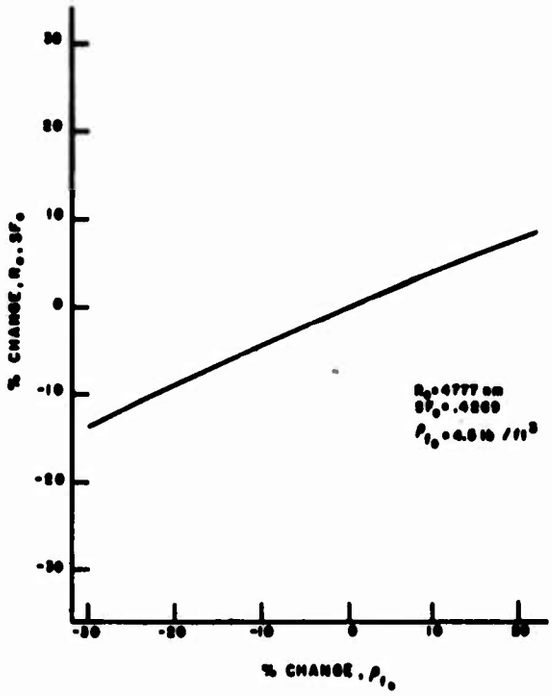

FIG 38 Fuel Density Influence on Performance

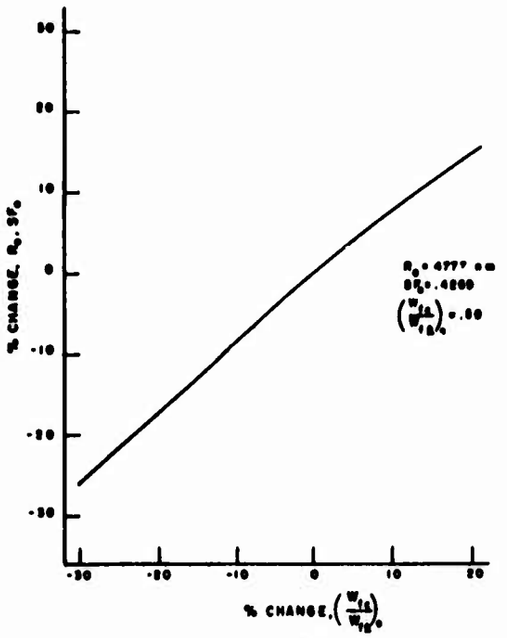

FIG 39 Fraction of Total Fuel Used in Cruise Influence on Performance

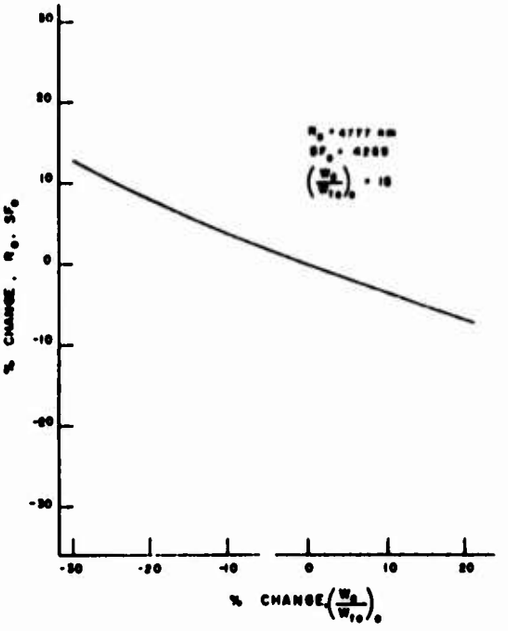

FIG 40 Equipment Weight Fraction Influence on Performance

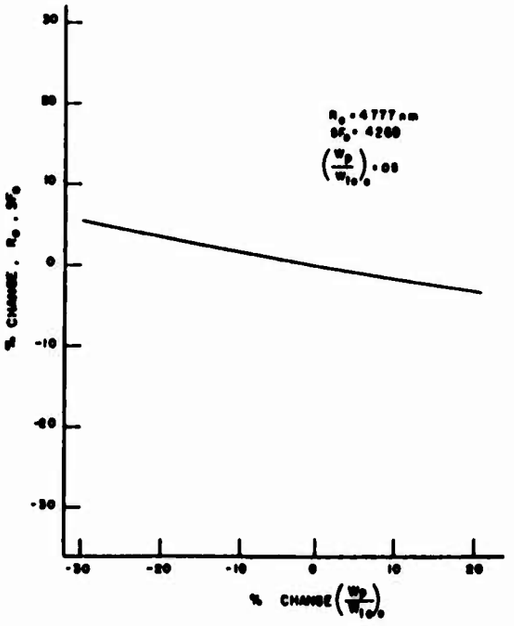

FIG 41 Payload Weight Fraction Influence on Performance

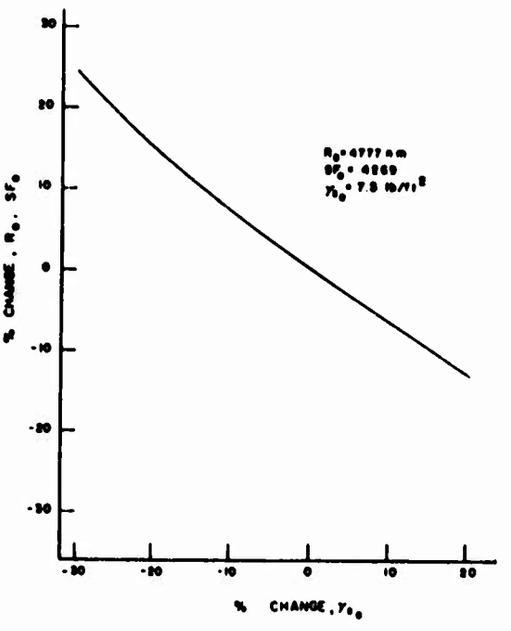

FIG 42 Wetted Area-Structural Weight Parameter Influence on Performance

Figure 39 illustrates that the cruise range increased as the amount of fuel consumed during cruise increased. This parameter, although producing a large change in the level of the range, does not have a large effect on the configuration of the optimized vehicle, since the level of range performance for all trial configurations are affected approximately the same.

Figure 41 illustrates that a 30 percent increase in the nominal payload weight fraction resulted in only about a 5 percent reduction in cruise range. Since the payload and fuel densities are equal, the scale factor (and hence the physical dimensions of the vehicle), remains constant with variations of the payload weight fraction. Passenger compartments and fuel tanks, for example, could be interchanged in a vehicle of fixed dimensions to accomplish a range-payload trade off.

Cruise range variation with the proportionality constant γ_s, which relates surface area of the vehicle to structural weight of the vehicle, is shown in Figure 42. In addition to having a pronounced effect on the level of the cruise range, the area-weight parameter also influences the optimized configuration. The greater the value of the area-weight parameter--the more important the volumetric efficiency, as reflected by the structural factor term of the Breguet range equation, becomes in determining the optimum configuration. Configurations optimized under the higher area-weight parameter would reflect greater volumetric efficiency at the expense of aerodynamic and or propulsive efficiency. For example, an area-weight constant greater than the nominal (7.5 lb/ ft^2) would produce a sharper increase of structural factor with the first inlet ramp angle δ_1 shown in Figure 13. This would result in a higher value of the optimum inlet ramp angle. Thus, the qualitative influence of a value of the area-weight parameter other than the nominal on the configuration can be deduced from an analysis of the performance sensitivities of the independent configuration definition quantities. It can be noted from Figs 10 - 12 that the nominal value of area-weight parameter used in this study resulted in

structural weight fractions for the optimum configuration of W_s / W_{to} = .258, .284, and .296. These values agree with the value of W_s / W_{to} = .27 used as a baseline in a wing structure study of a Mach 8 cruise vehicle (Ref 10).

Appendix D

Vehicle Cooling Requirements

Surfaces of the vehicle which cannot radiate to the surrounding space the heat produced by aerodynamic friction and combustion must be actively cooled. In addition, the aerodynamically sharp leading edges of the vehicle and wing (one-tenth of an inch diameter assumed for this investigation) may also require active cooling.

The purpose of this section is to develop the equations which indicate the amount of fuel needed to regeneratively cool internal surfaces of propulsive components, as well as the leading edges of the vehicle and wings. The fuel-air ratio required to cool the i-th surface is computed by equating the heat absorbing capacity available in the fuel diverted past the area A_{w_i} of the i-th surface

$$\dot{Q}_{c_i} = \dot{w}_{f_i} \zeta = f_{c_i} \dot{w}_{a_i} \zeta = f_{c_i} \rho_i V_i A_{p_i} \zeta \qquad (D1)$$

to the convective heat rate to the i-th surface

$$\dot{Q}_{h_i} = \rho_i V_i S_{t_i} \left(H_{abw_i} - H_{w_i} \right) A_{w_i} \qquad (D2)$$

If the cross sectioned area of the propulsive stream A_{p_i} is evaluated adjacent to the i-th surface being cooled A_{w_i}, then equating Eqs D1 and D2 results in an expression for the fuel-air ratio needed to provide coolant fuel for the i-th surface

$$f_{c_i} = \left(\frac{A_w}{A_{p_i}} \right) \frac{S_{t_i}}{\zeta} \left(H_{abw_i} - H_{w_i} \right) \qquad (D3)$$

or in terms of the equivalence ratio

$$\phi_{c_i} = \frac{f_{c_i}}{f_s} \qquad (D4)$$

Equation D3 and D4 were solved for the following surfaces wetted by the propulsive stream: combustor, second inlet-forebody ramp and fences, inlet cowl and sides, nozzle cowl and sides,

nozzle-aftfuselage back to a point opposite the nozzle cowl.

The Stanton number was computed from the skin friction coefficient using Reynolds analogy $S_{t_i} = C_{f_i} / 2$.

The expression for laminar heat transfer to the stagnation line of an unswept cylindrical leading edge is given by (Ref 22)

$$\dot{q}_{stag} = 627.12 \left(\frac{V_1}{10^4}\right)^{3.15} \sqrt{\frac{\sigma}{r_n}} \qquad (D5)$$

Assuming a cosine distribution of the heating rate about the stagnation point (Ref 23), the heat rate to the surface of the half cylinder leading edge is given by

$$\dot{Q}_{\ell_e} = 2 r_n b_{\ell_e} \dot{q}_{stag} \qquad (D6)$$

where b_{ℓ_e} is the combined leading edge width of the vehicle nose, cowl, and wings. The amount of regenerative cooling needed for the leading edges is found by equating Eq D1 and D6

$$\phi_{\ell_e} = \frac{2 r_n b_{\ell_e} \dot{q}_{stag}}{f_s \rho_1 V_1 \zeta A_c} \qquad (D7)$$

Table IV illustrates for Mach 12 cruise, which is the most severe case, that cooling requirement for the leading edges of the vehicle was small compared to cooling requirements of the other components.

TABLE IV

Component Cooling Data For Mach 12 Configuration

Component	Skin Friction Coefficient C_f	Reynolds Number R_e	Cooling Equivalence Ratio ϕ_c
2nd inlet ramp and fence	$.636 \times 10^{-3}$	1.45×10^{8}	.0687
inlet cowl and sides	1.10×10^{-3}	5.68×10^{7}	.0778
combustor and nozzle cowl	1.6×10^{-3}	3.19×10^{7}	.1598
nozzle-aftfuselage	2.13×10^{-3}	1.72×10^{7}	.0238
vehicle leading edges	------	------	.0015
		Total	.3316

Appendix E

Vehicle Design and Evaluation Computer Program

The problem of formulating the vehicle design and evaluation computer program can be broken down into three areas: first, the identification of quantities needed to define geometrically a configuration in the general class; second, the formulation of methods to predict the flow field properties about the configuration; and third, evaluation of the configuration performance.

Configuration Definition

Some of the quantities necessary to define geometrically a vehicle configuration of the class considered in this investigation can be arbitrarily chosen (independent) while others are calculated (dependent) from constraints. The purpose of this section is to formulate a set of independent configuration design variables and the constraint equations from which the dependent variables can be determined. In order to accomplish this aim, it is convenient to separate the vehicle into components: inlet-forebody , combustor, nozzle-aftfuselage, wing, and fuselage.

Inlet-forebody. In general, six geometric quantities (ℓ_1, ℓ_2, ℓ_3, h_4, δ_1, δ_2) are required to define the inlet-forebody configuration as shown in Figure 43. It is essentially a two-dimensional double ramp inlet with a three-shock wave external compression system, with fences extending from the nose of the vehicle to the leading edge of the inlet cowl to contain the inlet air flow.

If it is assumed that at the design point the shock wave pattern is specified (shock on inlet cowl lip in this study), the number of variables needed to define the inlet configuration is reduced. Once the ramp angles (δ_1, δ_2) are specified, the flow turning angle of the inlet cowl ($\delta_3 = \delta_1 + \delta_2$) is known and the shock wave angles (θ_1, θ_2, θ_3) can be calculated from the oblique shock relations (Ref 24). The variables

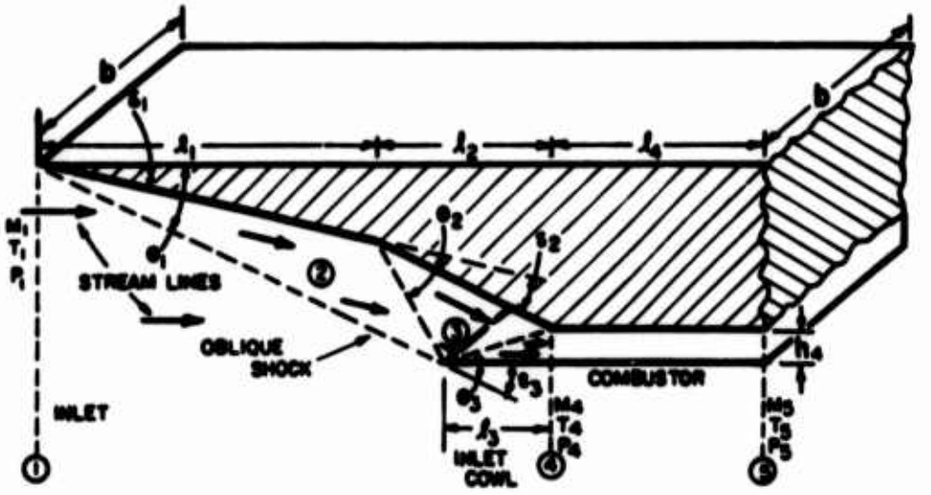

FIG 43 Three Shock Inlet and Combustor

($\ell_1, \ell_2, \ell_3, h_4$) must then be related in such a manner that the shock waves from the double ramp inlet meet and reflect from the edge of the cowl to form a third shock wave. The third shock is cancelled by the appropriate turning angle at the top of the combustor entrance. The relationship among the variables ($\ell_1, \ell_2, \ell_3, h_4$) can be expressed in equation form by using the geometry of Figure 43:

$$(\ell_1 + \ell_2 - \ell_3) \tan \theta_1 = \ell_1 \tan \delta_1 + \ell_2 \tan (\delta_1 + \delta_2) + \ell_3 \tan (\theta_3 - \delta_3) \quad \text{(E1)}$$

$$(\ell_2 - \ell_3) \tan (\theta_2 + \delta_1) = \ell_2 \tan (\delta_1 + \delta_2) + \ell_3 \tan (\theta_3 - \delta_3) \quad \text{(E2)}$$

$$h_4 = \ell_3 \tan (\theta_3 - \delta_3) \quad \text{(E3)}$$

These are three constraint equations which relate four quantities; therefore, only one is independent. The quantity ℓ_1 was arbitrarily chosen to be the independent variable.

Instead of specifying the ramp angle δ_2, the temperature of the air entering the combustor T_4 was chosen as an independent quantity. This was done so that the temperature required for autoignition of

hydrogen and air (2000 R) could be placed directly as a lower bound on the design quantity T_4 to facilitate the optimization process. The ramp angle δ_2 necessary to produce the specified combustor entrance temperature T_4 was calculated using an iterative procedure along with the oblique shock equations. However, in order to calculate the shock angles θ and entrance combustor temperature T_4, the flight Mach number M_1, and ambient temperature T_1 must be specified in addition to the geometric variables, thus

$$\delta_2 = f(T_4, T_1, M_1, \delta_1) \tag{E4}$$

If the ambient temperature T_1 and ambient pressure p_1 are assumed to be functions of altitude H, such as in the set of relationships given by the standard atmosphere (Ref 25), then T_1 becomes a dependent quantity by reason of the following development.

Ambient pressure at start of cruise p_1 is determined from the constraint of equilibrium flight normal to the flight path; hence, p_1 becomes a function of lift L, weight at start of cruise W_i, and cruise velocity V_1,

$$p_1 = f(L, W_i, V_1) \tag{E5}$$

From the standard atmosphere relations

$$H = f(p_1) \tag{E6}$$

and

$$T_1 = f(H) \tag{E7}$$

therefore; the ambient temperature T_1 becomes a dependent quantity. Thus, the final set of independent configuration quantities needed to define the inlet was $(\ell_1, \delta_1, T_4, M_1)$.

A problem arises, however, in the sequences of calculation since it is necessary to know the ambient temperature T_1 before the ambient pressure p_1 is determined from the equilibrium flight constraint

(Equation E5), and T_1 from Equations E6 and E7. The problem can be solved by choosing a reference ambient temperature and assuming an isothermal atmosphere over the range of equilibrium flight altitudes, or by iteration on the equilibrium altitude. The standard atmosphere is isothermal only from approximately 36,000 ft to 88,000 ft at which point temperature begins to increase with altitude at approximately 1.6 R per thousand feet of altitude. Therefore, in the present study, an iteration was performed on the initial equilibrium altitude.

Combustor. The constant area combustor (Fig 43) is formed by the underside of the fuselage and a straight cowl located a distance h_4 from the fuselage. Both the underside of the fuselage and cowl are parallel with the body x-axis reference line. Independent configuration design quantities associated with the constant area combustor are the length ℓ_4 and equivalence ratio ϕ. The length ℓ_4 also determines the length of the vehicle midsection.

Equivalence ratio is defined in terms of stoichiometric fuel-air ratio f_s and actual fuel-air ratio f

$$\phi = \frac{f}{f_s} \tag{E8}$$

where the stoichiometric fuel-air ratio f_s is the ratio of fuel and air which results in all of the available fuel and air entering into the chemical reaction ($f_s = .0292$ for hydrogen). Thus, the equivalence ratio is a measure of the amount of energy added to the propulsive stream.

The equivalence ratio was designated an independent variable to facilitate the search for the optimum nozzle length and wing planform area. Normally, the fuel-air ratio is controlled (by a throttle) to produce unaccelerated flight for a fixed vehicle geometry. In the present formulation, however, it was more efficient, from a computational and search standpoint, to fix the amount of energy added to the propulsive stream and balance the resulting thrust with the drag from an appropriate amount of wing area. As explained in the algorithm at

the end of this section, wing area and performance parameters were calculated as each uprunning characteristic from the trailing edge of the cowl intersected the aftfuselage. Therefore, for one complete nozzle characteristic solution, which was expensive in terms of computation time, many nozzle lengths and wings area combinations were examined. In addition, the nozzle length was terminated when the range performance no longer increased with nozzle length when the situation occurred.

Nozzle-aftfuselage. The two-dimensional nozzle is formed by the aftfuselage and the rear portion of the cowl as shown in Figure 1. Three variables (ℓ_5, ℓ_6, δ_5) are needed to define the geometry of the nozzle-aftfuselage configuration. The maximum length of the nozzle ℓ_5 was constrained such that the base height h_b was equal to or greater than zero. The minimum length of the nozzle cowl ℓ_6 was also constrained as will be discussed later.

Wing. The variables (δ_9, δ_{11}, b_w, c, δ_{12}, ℓ_{e_w}, AR, S_p) can be used to describe the wing geometry and location on the vehicle as shown in Figure 1. However, not all of the variables describing the wing are independent. The first two relationships between the wing variables comes from the definition of aspect ratio

$$AR = \frac{b_w^2}{S_p} \tag{E9}$$

and from the wing geometry

$$\begin{aligned} S_p &= c\,(c \tan \delta_{12}) + c\,(b_w - c \tan \delta_{12}) \\ &= c\, b_w \end{aligned} \tag{E10}$$

The wing planform area S_p was constrained such that the thrust and drag of the wing-body combination were equal (equilibrium flight along the flight path). Thus, the wing planform area S_p becomes a function of the thrust minus body drag

$$S_p = f(\text{thrust} - \text{body drag}) \qquad (E11)$$

The distance from the nose of the vehicle to the leading edge of the wing ℓ_{ew} was determined by a trim requirement such that the pitching moment of the wing-body combination about the center of gravity of the fuselage be zero, hence

$$\ell_{ew} = f(\text{pitching moment about center of gravity}) \qquad (E12)$$

Attachment point of the wing leading edge and fuselage was constrained to be on the fuselage ($\ell_{ew} < \ell_b$) and was chosen to be in the xy-plane of the body axis system. The latter requirement restricted the angle of the top surface of the fuselage to positive values $\delta_7 \geq 0$.

Fuselage. Four independent configuration quantities (α, δ_7, b, W_{to}) are associated with the fuselage. The angle of attack α is the angle between the free stream flow direction and the vehicle reference axis shown in Figure 1. The angle δ_7 is the angle between the x-axis of the vehicle and the top surface of the fuselage; whereas, b is the width of the two-dimensional fuselage. Although δ_7 was constrained to positive values, a variable angle of attack allowed negative angles of incidence of the top surface of the fuselage with respect to the free stream flow.

The center of gravity of the two-dimensional fuselage, which can be controlled to some extent by placement of equipment and fuel in the vehicle, was assumed to coincide with the centriod of the profile area of the fuselage. It is shown in the results, however, that this assumption was not critical since the trim constraint did not seriously limit the range performance of the vehicle.

Although the geometrical shape of the vehicle is defined by the design quantities discussed thus far, the size or physical dimensions are arbitrary. The length of the first inlet ramp ℓ_1 was used as the length scale factor for the vehicle. The equation for calculating ℓ_1 (see Appendix C) can be written as a function of vehicle shape and

takeoff weight W_{to}

$$\ell_1 = f(\text{vehicle shape}, W_{to}) \qquad \text{(E13)}$$

As in the case of altitude it is necessary to specify a reference length ℓ_1 in order to calculate Reynolds numbers needed to determine skin friction in the force calculations.

Independent and dependent quantities used to define the geometrical model of the vehicle investigated in this study are summarized in Table IV. The number of independent quantities used to

TABLE IV

Configuration Definition Quantities

Independent Quantities

$\overline{X} = (\delta_1, T_4, \phi, \ell_4, \delta_5, \ell_5, \ell_6, \delta_9, \delta_{11}, \delta_{12}, AR, b, \delta_7, a, W_{to}, M_1)$

Dependent Quantities

Variable	Calculated From Relation
ℓ_2, ℓ_3, h_4	E1, E2, E3
δ_2	E4
S_p	E11
ℓ_{ew}	E12
b_w	E9
c	E10
p_1	E5
T_1	E7
ℓ_1	E13

define the model is analagous to the number of degrees of freedom used to describe a mechanical system with equality constraints. For the case depicted in Table IV there are N = 27 quantities defining the

configuration model and $m = 11$ equality constraint relations; thus, the degrees-of-freedom n of model is given by

$$n = N - m = 16 \qquad \text{(E14)}$$

which corresponds to the number of independent configuration definition variables.

Flow Field Prediction

Once the vehicle configuration model is defined, the second major step in the problem formulation is the selection of methods to predict flow field properties about the vehicle. The distribution of flow field properties about the vehicle such as temperature, pressure, and velocity is needed to evaluate aerodynamic, propulsive, and cruise range performance. Inviscid flow field property distribution was determined using the following prediction techniques: adiabatic shock, Prandtl-Meyer expansion, one-dimensional constant - area supersonic heat addition, and method of characteristics. Local inviscid properties and turbulent (Ref 26) or laminar (Ref 27) skin friction laws, depending on the local Reynolds number, were used to compute the skin friction coefficient assuming a cold wall condition of $T_w = 2000R$. Appendix D contains typical values of skin friction coefficients obtained for various local surfaces.

Shock Expansion. Oblique shock relations were used to calculate flow field properties for compression surfaces and the Prandtl-Meyer relations for all expansion surfaces except the nozzle-aftfuselage. A constant value of 1.4 was used for the ratio of specific heats in both the oblique shock and Prandtl-Meyer relations.

The underside of the cowl, top surface of the fuselage, and the wing surfaces were treated as compression or expansion surfaces depending on the alignment of the particular surface with the flow. Due to the geometry of the above surfaces only one shock wave or expansion fan calculation per surface was required; however, the oblique shock

relations were also used to calculate the flow field properties in the inlet where three shock waves are involved. Initial conditions for the first shock wave calculation were the free stream properties, and a wedge angle equal to the sum of the first inlet ramp angle and angle of attack. Conditions behind the first shock were used as initial conditions for the second shock along with an assumed value of the second ramp angle δ_2. Initial conditions for the third shock were the conditions behind the second shock, and since the cowl is parallel to the x-body axis, the wedge angle δ_3 for the third shock becomes the sum of the first and second ramp angles. An iterative procedure was used to determine the ramp angle δ_2 which produced the combustor entrance temperature T_4 specified as a design variable.

Constant Area Heat Addition. The combustor inviscid flow calculation procedure from station 4 to 5 (Fig 43) was based on the enthalpy method (Ref 28) and the one-dimensional, shockless, constant area heat addition relations for a mixture of gaseous hydrogen and air. Since the coolant fuel is also used for propulsion, initial conditions for the calculation assume that hydrogen fuel has a temperature of 2000 R (with no axial momentum component). Air flow properties at the combustor entrance were assumed equal to those at final inlet conditions. The gases leaving the combustor at station 5 were assumed to be in chemical equilibrium and produced by 100 per cent combustion efficiency.

Combustion products tables of Ref 29 along with the one-dimensional combustion equations were used to calculate combustor exit flow properties at station 5. This calculation requires an iteration on both the combustor exit pressure p_5 and temperature T_5 since dissociation and ionization of the combustion products are accounted for in the analysis.

Turbulent skin friction effects were superimposed on the inviscid pressure distribution to determine the combustor duct forces. Although

relations were also used to calculate the flow field properties in the inlet where three shock waves are involved. Initial conditions for the first shock wave calculation were the free stream properties, and a wedge angle equal to the sum of the first inlet ramp angle and angle of attack. Conditions behind the first shock were used as initial conditions for the second shock along with an assumed value of the second ramp angle δ_2. Initial conditions for the third shock were the conditions behind the second shock, and since the cowl is parallel to the x-body axis, the wedge angle δ_3 for the third shock becomes the sum of the first and second ramp angles. An iterative procedure was used to determine the ramp angle δ_2 which produced the combustor entrance temperature T_4 specified as a design variable.

Constant Area Heat Addition. The combustor inviscid flow calculation procedure from station 4 to 5 (Fig 43) was based on the enthalpy method (Ref 28) and the one-dimensional, shockless, constant area heat addition relations for a mixture of gaseous hydrogen and air. Since the coolant fuel is also used for propulsion, initial conditions for the calculation assume that hydrogen fuel has a temperature of 2000 R (with no axial momentum component). Air flow properties at the combustor entrance were assumed equal to those at final inlet conditions. The gases leaving the combustor at station 5 were assumed to be in chemical equilibrium and produced by 100 per cent combustion efficiency.

Combustion products tables of Ref 29 along with the one-dimensional combustion equations were used to calculate combustor exit flow properties at station 5. This calculation requires an iteration on both the combustor exit pressure p_5 and temperature T_5 since dissociation and ionization of the combustion products are accounted for in the analysis.

Turbulent skin friction effects were superimposed on the inviscid pressure distribution to determine the combustor duct forces. Although

Geometrically Eq E18 illustrates that the effect of combustor drag on the combustor pressure ratio increases with increasing combustor length to height ratio as expected. For typical values of combustor skin friction coefficients $C_{f_{av}} = .002$ and combustor length to height ratios of $\ell_4 / h_4 = 5$, the term $D_c / p_4 A_4 \gamma_4 M_4^2$ is small compared to unity. Thus, the effect of combustor drag on the pressure ratio is small for the configuration geometries considered.

Method of Characteristics. The method of characteristics (Ref 30) was used to determine the two-dimensional inviscid flow field properties in the nozzle. It was assumed that the flow entering the nozzle is uniform and that the total pressure remains constant during the expansion process. Mach number at the nozzle entrance was based on the frozen speed of sound determined from Ref 29 for the combustion products at combustor exit conditions. The frozen speed of sound at the combustor exit was also used to compute an effective specific heat ratio γ_5 which was then assumed to remain constant for the expansion process. The above method resulted in constant values of specific heats of $\gamma_5 \cong 1.27$ being used in the method of characteristic solutions.

A characteristic net was produced in the nozzle using a grid size of $\Delta\omega = 1.25^{\circ}$. As shown in Fig 44, expansion waves emananting from the sharp corner at ` a´ can either strike the inner surface of the cowl and reflect to the aftfuselage, or miss the cowl and strike the free pressure boundary. Waves missing the cowl and striking the free pressure boundary do not reflect to the aftfuselage before the nozzle length is terminated; however, expansion waves emananting from the trailing edge of the cowl were accounted for when this condition existed. Due to programing considerations, the minimum length of the nozzle cowl was constrained to a length $\ell_{6_{min}}$ at which the first down running characteristic emananting from ` a´ struck the nozzle cowl as shown in Figure 44.

the skin friction drag of the combustor duct was considered in the computation of vehicle drag, the effect of combustor skin friction drag on the inviscid flow field solution of the combustor was neglected, since the effect of skin friction drag on the inviscid solution can be shown to be small.

The pressure ratio p_5 / p_4 across the combustor can be written using the one-dimensional momentum equation and equations of state of a perfect gas at stations 4 and 5

$$\frac{p_5}{p_4} = \frac{\gamma_4 M_4^2 + 1 - \left(\frac{D_c}{p_4 A_4}\right)}{\gamma_5 M_5^2 + 1} \tag{E15}$$

where D_c is the combustor friction drag. Factoring the numerator of Eq E15

$$\frac{p_5}{p_4} = \frac{\gamma_4 M_4^2 \left(1 + \frac{1}{\gamma_4 M_4^2} - \frac{D_c}{p_4 M_4^2 \gamma_4 A_4}\right)}{\gamma_5 M_5^2 + 1} \tag{E16}$$

The term $D_c / p_4 A_4 \gamma_4 M_4^2$ can be compared to unity in order to determine under what conditions the pressure losses due to skin friction are small.

Since the ratio of combustor area wetted by the propulsive stream to the cross sectional area of the stream at station 4 is given by $((2h_4 \ell_4 + 2 \ell_4 b)/ bh_4)$, the combustor drag term can be written as

$$\frac{D_c}{p_4 A_4 \gamma_4 M_4^2} = \left[\frac{\gamma_{c_{av}}}{\gamma_4} \quad \frac{p_{c_{av}}}{p_4} \quad \frac{M_{c_{av}}^2}{M_4^2}\right] \frac{\ell_4}{h_4} \left(1 + \frac{h_4}{b}\right) C_{f_{av}} \tag{E17}$$

Since the term in the brackets on the right side of Eq E17 is on the order of unity, and the height of the combustor to the width of the vehicle is small, Eq E18 can be written

$$\frac{D_c}{p_4 A_4 \gamma_4 M_4^2} \cong \frac{\ell_4}{h_4} C_{f_{av}} \tag{E18}$$

Geometrically Eq E18 illustrates that the effect of combustor drag on the combustor pressure ratio increases with increasing combustor length to height ratio as expected. For typical values of combustor skin friction coefficients $C_{f_{av}} = .002$ and combustor length to height ratios of $\ell_4 / h_4 = 5$, the term $D_c / p_4 A_4 \gamma_4 M_4^2$ is small compared to unity. Thus, the effect of combustor drag on the pressure ratio is small for the configuration geometries considered.

Method of Characteristics. The method of characteristics (Ref 30) was used to determine the two-dimensional inviscid flow field properties in the nozzle. It was assumed that the flow entering the nozzle is uniform and that the total pressure remains constant during the expansion process. Mach number at the nozzle entrance was based on the frozen speed of sound determined from Ref 29 for the combustion products at combustor exit conditions. The frozen speed of sound at the combustor exit was also used to compute an effective specific heat ratio γ_5 which was then assumed to remain constant for the expansion process. The above method resulted in constant values of specific heats of $\gamma_5 \cong 1.27$ being used in the method of characteristic solutions.

A characteristic net was produced in the nozzle using a grid size of $\Delta\omega = 1.25^\circ$. As shown in Fig 44, expansion waves emananting from the sharp corner at ` a´ can either strike the inner surface of the cowl and reflect to the aftfuselage, or miss the cowl and strike the free pressure boundary. Waves missing the cowl and striking the free pressure boundary do not reflect to the aftfuselage before the nozzle length is terminated; however, expansion waves emananting from the trailing edge of the cowl were accounted for when this condition existed. Due to programing considerations, the minimum length of the nozzle cowl was constrained to a length $\ell_{6_{min}}$ at which the first down running characteristic emananting from ` a´ struck the nozzle cowl as shown in Figure 44.

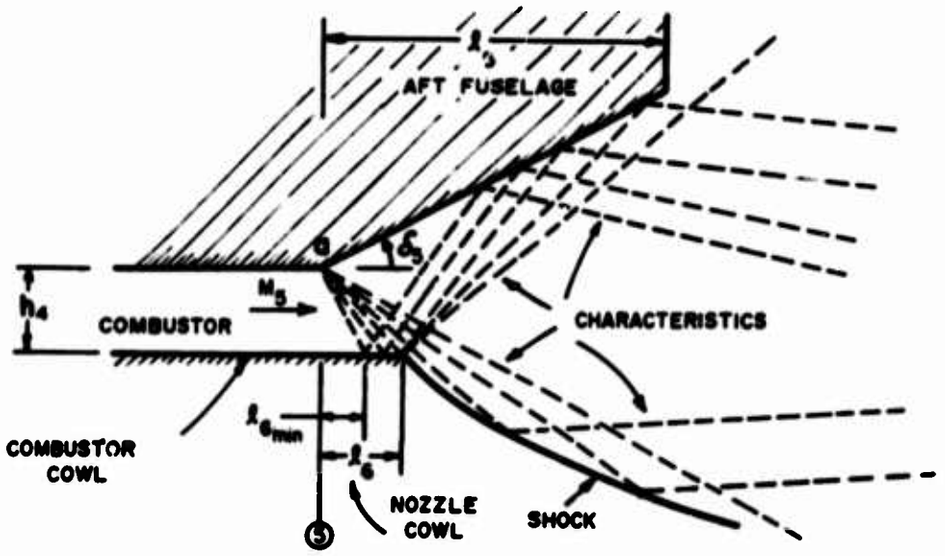

FIG 44 Schematic of Characteristic Net in Nozzle

Performance Evaluation

Once the independent variable design set has been specified and the flow field properties calculated for a configuration, then the performance of the configuration can be evaluated. As pointed out in Chapter II, only the cruise segment of the mission profile was considered in the performance evaluation. This resulted in the Breguet range equation

$$R = \frac{L}{D} \; Isp \; \frac{V_1}{1 - V_1^2 / V_0^2} \; \ell n \frac{W_i}{W_f} \qquad (E20)$$

developed in Appendix A becoming the criterion function in the determination of the optimum configuration. The purpose of this section is to develop the equations which relate the criterion function R to the independent configuration design variables. The Breguet range equation can be divided into two parts: (1) the so called Breguet range factor

$$RF = \frac{L}{D} \; Isp \; \frac{V_1}{1 - V_1^2 / V_0^2} \tag{E21}$$

and (2) the structural factor

$$SF = \ln (W_i / W_f) \tag{E22}$$

Range Factor. The range factor is a measure of combined aerodynamic and propulsive performance for a given cruise speed. Equation (E21) is convenient for calculating range factor from L/ D and Isp if these quantities are known for a configuration. However, to calculate the range factor from the aerodynamic flow field surrounding the vehicle and vehicle geometry, it is convenient to write Eq E21 in another form by retracing two steps in its development. Using the definition of specific impulse

$$Isp = \frac{T}{\dot{w}_f} \tag{E23}$$

and the requirement for equilibrium flight along the flight path of the vehicle

$$T = D \tag{E24}$$

Eq E21 becomes

$$RF = \frac{L}{\dot{w}_f} \; \frac{V_1}{1 - V_1^2 / V_0^2} \tag{E25}$$

where the lift L is determined from the projection, in a direction normal to the flight path, of the pressure p and shear stress τ integrated over all wetted surfaces A_w of the configuration

$$L = \int\int_{\text{all surfaces}} (- p \hat{n} \cdot \hat{k}_w + \tau \hat{t} \cdot \hat{k}_w) \, dA \tag{E26}$$

subject to the requirement for equilibrium flight along the flight path

$$\int\int_{\text{all surfaces}} (- p \hat{n} \cdot \hat{i}_w + \tau \hat{t} \cdot \hat{i}_w) \, dA = 0 \tag{E27}$$

where $\hat{i}_w$, and $\hat{k}_w$ are unit vectors along and normal to the flight path respectively, and $\hat{n}$ and $\hat{t}$ are the surface area normal and tangent unit vectors respectively.

In evaluating the range factor RF from Eq E25, bookkeeping decisions as to which forces are aerodynamic and which are propulsive are not important since the integration of the surface integrals in Eqs E26 and E27 is carried out over the entire surface of the configuration. However, if one wishes to determine classical aerodynamic and propulsive performance separately, a classification or division of the forces must be made. The definition of thrust used in this study is the projection of the nozzle force along the flight path given by

$$T = \int\int_{\text{nozzle surfaces}} (p\,\hat{n} \cdot \hat{i}_w - \tau\,\hat{t} \cdot \hat{i}_w)\, dA \qquad \text{(E28)}$$

Once the I_{sp} has been determined then the L/D can be found from

$$L/D = (L/\dot{w}_f) I_{sp} \qquad \text{(E29)}$$

Structural Factor. The purpose of the development in this section is to relate the structural factor $\ell n(W_i/W_f)$ to configuration design variables in such a manner that the value of the structural factor is related to the configuration volumetric efficiency. Volumetric efficiency as defined in the report, is the ratio of volume V to surface area A_w.

If the takeoff weight W_{to} of the vehicle is assumed to be composed of payload W_p, equipment W_e, fuel W_{fl} and structure W_s, then the structural factor can be written as

$$\ell n \frac{W_i}{W_f} = \ell n \left[1 + \frac{\dfrac{W_{fc}}{W_{fl}} \dfrac{W_{fl}}{W_{to}}}{\dfrac{W_p}{W_{to}} + \dfrac{W_e}{W_{to}} + \dfrac{W_s}{W_{to}}} \right] \qquad \text{(E30)}$$

where $W_{fc}/W_{f\ell}$ is the fraction of total fuel used during cruise.

Two of the terms, $W_{f\ell}/W_{to}$ and W_s/W_{to}, will be shown to be related to the volumetric efficiency of the vehicle. However, in order to evaluate the structural factor, from the set of independent design variables, it is necessary to introduce the structural set $\bar{S}$ as discussed in Chapter II:

$$\bar{S} = \left[\frac{W_p}{W_{to}}, \frac{W_e}{W_{to}}, \frac{W_{fc}}{W_{to}}, \rho_p, \rho_e, \rho_f, \gamma_s \right] \tag{E31}$$

Neglecting the volume required for the structure, the enclosed volume of the vehicle is composed of volume required for payload $\forall_p$, equipment $\forall_e$, and fuel $\forall_{f\ell}$, thus

$$\forall = \forall_p + \forall_e + \forall_{f\ell} \tag{E32}$$

The takeoff weight is given by

$$W_{to} = W_p + W_e + W_{f\ell} + W_s \tag{E33}$$

Introducing ρ_p, ρ_e, and ρ_f from the structural parameter set $\bar{S}$, Eqs E32 and E33 become respectively

$$\forall_{f\ell} = \forall - \frac{W_p}{W_{to}} \frac{W_{to}}{\rho_p} - \frac{W_e}{W_{to}} \frac{W_{to}}{\rho_e} \tag{E34}$$

and

$$\forall_{f\ell} = \frac{1}{\rho_f} \left[W_{to} - \frac{W_p}{W_{to}} W_{to} - \frac{W_e}{W_{to}} W_{to} - W_s \right] \tag{E35}$$

The wetted area of the vehicle is introduced by assuming that the structural weight is a function of the wetted area--in particular a linear function

$$W_s = \gamma_s A_w \tag{E36}$$

Equating and rearranging Eqs E 34 and E35 along with Eq E36, allow the takeoff weight to be written as a function of vehicle volume $\forall$, wetted area A_w, and the structural parameter set $\bar{S}$

$$W_{to} = \frac{\forall + \gamma_s\left(\frac{A_w}{\rho_f}\right)}{\left(1 - \frac{W_p}{W_{to}} - \frac{W_e}{W_{to}}\right)\frac{1}{\rho_f} + \left(\frac{W_p}{W_{to}}\right)\frac{1}{\rho_p} + \left(\frac{W_e}{W_{to}}\right)\frac{1}{\rho_e}} \quad \text{(E37)}$$

For each configuration defined by a set $\bar{X}$ of independent design variables, a relationship exists between $\forall$ and A_w which, along with the additional relationship given by Eq E37, uniquely determines the volume and wetted area of the configuration. Once the vehicle volume $\forall$ is known, the total fuel volume $\forall_{fl}$ can be determined from Eq E34 which along with the fuel density ρ_f enables the total fuel fraction W_{fl}/W_{to} to be calculated.

The structural fraction W_s/W_{to} can be determined from Eq E36 knowing the wetted area A_w and proportionality constant γ_s. All of the terms in the structural factor are now known. The structural factor, and hence, the cruise range R can be evaluated given the set $\bar{X}$ of independent design quantities and the set $\bar{S}$ of structural parameters.

Algorithm. This appendix is summarized by the computational algorithm of the design and evaluation computer program. The purpose of the algorithm is to relate the general formulation contained in this appendix to the subroutines contained in the listing of the program which details the equations used in the vehicle design and evaluation computer program.

For a given set of independent design variables the configuration and performance of a vehicle is determined by the following procedure:

1. Input data including the independent design variables is contained in MAIN.

2. Initial conditions for flow field calculations are set in subroutine RANGE.

3. Inlet-forebody flow field parameters and shock wave angles are calculated in subroutine SHOCK using oblique shock relations.

4. Inlet configuration and combustor height are computed in CONFIG using the constraint of shock on lip.

5. Flow field properties are determined for the underside of cowl, fuselage top, and wing surfaces, by SHOCK or PRANT depending on whether the component is a compression or expansion surface respectively.

6. One-dimensional supersonic heat addition equations are solved in CBMST to determine the inviscid flow properties at the combustor exit.

7. Inviscid and viscid (subroutine SKINF) forces and moment are calculated by subroutine FAM for the inlet, cowl, fuselage top and sides back to the point where the nozzle-aftfuselage begins.

8. Inviscid nozzle flow properties are calculated by the method of characteristics in subroutines NOZZL, STARTC, PMSBR, and LPS.

9. Force and moments are integrated on the nozzle-aftfuselage by subroutine FAM. Integration step size is the axial distance between the intersection of the nozzle-aftfuselage and adjacent up-running characteristics.

10. The following computations are made in subroutine FAM whenever an up-running characteristic strikes the nozzle-aftfuselage.

(a) Thrust forces produced by the nozzle and the drag of the inlet, cowl, and fuselage are compared.

(b) If the thrust is less than body drag, another up-running characteristic is computed which increases the nozzle length.

(c) Steps (a) and (b) continue until: (i) the nozzle reaches the length specified in the design set, or (ii) the nozzle surface intersects the top surface of fuselage (zero base) or (iii) the thrust is greater than the body drag. If conditions (i) or (ii) occur, the

calculation is terminated and the cruise range solution does not exist for the selected set of configuration variables.

(d) If the thrust is greater than body drag, wing forces and moments are determined. A wing area is determined such that the drag of the wing-body combination equals the thrust produced by the nozzle.

(e) The center of force (for the wing-body combination) and center of gravity (based on the center of area of the body profile) is determined. Placement of the wing on the body is then calculated such that the sum of the moments about the center of gravity is zero (trimmed flight condition). If the trim requires a placement of the wing such that the wing is off the body, the calculation returns to step 10 (c).

(f) Scaling or sizing the vehicle is made by relating vehicle volume and wetted area to takeoff weight and the members of the structural parameter set $\bar{S}$.

(g) Ambient pressure at initial cruise altitude is computed from the requirement for equilibrium flight normal to the flight path.

(h) Structural, aerodynamic, propulsive, and cruise range performance (criterion function) are calculated.

(i) Another up-running characteristic is computed which increases the nozzle length.

(j) Steps (d) through (i) are repeated until one of the following case termination conditions are reached: (I) cruise range decreases with increasing nozzle length, (II) nozzle length greater than length specified in design set or (III) intersection of the nozzle-aftfuselage surface and fuselage upper surface (zero base).

11. If the case is terminated by condition (I), the performance value of the point before the decrease in performance was noted is used as the final performance value.

12. If the case is terminated by conditions (II) or (III), between the current point (exceeded constraint) and previous point (within)

constraint), a linear interpolation is performed in subroutine NOZZL to adjust configuration performance and parameters to satisfy the constraints.

13. Cooling requirements of the combustor and portions of the inlet and nozzle as well as the leading edge are determined in subroutine COOL.

14. Configuration performance and parameters are printed in subroutine MAIN.

```
C                          APPENDIX E(CONTINUED)

C                VEHICLE DESIGN AND EVALUATION PROGRAM
C                      COMPUTER LISTING



$IBJOB
$IBFTC MAIN
C THE VEHICLE DESIGN AND EVALUATION PROGRAM DEFINES THE CONFIGURATION
C AND COMPUTES THE PERFORMANCE FOR A SET OF INDEPENDENT DESIGN QUANTITIES

      COMMON /VAR/ P(13),DEL(13),DELD(13),LAM(13),THETA(13),XCWL,P2(13),
     1X(6),Q,V4,V5,CFX(13),CFY(13),DEL5,ALPHAR,CACAP,TLAP(13),PXCESS,
     2EA,APS,P
      COMMON /NAMEC/ TEMP5,V4,V5,MINF5,GAM5,BD1,CAV45,A5,AM5,TEMP45
      COMMON /VAR1/ VOLABA,VLTABA,VLWABA,PWW,CDLW,CF
      COMMON /VAR2/ P12,PASPR,HP,PDES,PALT,WTOD,WTOT,CWT,PALTT,CPALT,X50
      COMMON /REF/ CC
      COMMON /CON1/ L,MCON,IPATH
      COMMON /PRNT/ SEPCV,STPRAC,XCM,YCM,BWDC,AWNG,VTD120,ATGD12,CDSF,
     1RLWLEV,PCW,XW,AISPT,AISPL,ALOBL,ALOBT,RAMP,FDW,CDW,CDLEW,
     2PCI12,PDI12,D3,PDTP,CDLEDC,CLW,VWD120,ABGD12,XCPLEV,CDD,CLD,TWL,
     3T5C,CLP(33),XCK
      COMMON /ACC1/ DLE,D1,WTO
      COMMON /SOK/ TCMOST
      COMMON/PRP/AMET
      COMMON /COSF/ ST(10)
      DATA P1,P2 /.0174533292,57.2957779/
      REAL P,P2,LAM
      RAD(Z)=Z*P1
      DEG(Z)=Z*P2
C INPUT DATA

C INDEPENDENT DESIGN QUANTITIES
C   DESIGN PACH NUMBER
      P(1)=13.
C   INLET-FIRST RAMP ANGLE(DEG) AND COMBUSTOR ENTRANCE TEMP(R)
      DELC(1)=8.21
      TCMPST=2500.
C   COMBUSTOR-EQUIVALENCE RATIO AND LENGTH/HEIGHT RATIO
      EA=.93
      CPLR=9.
C   NOZZLE-HALF ANGLE(DEG),LENGTH(INCH-D),COWL LENGTH(INCH-D)
      DELC(9)=14.02
      XSC=1.29
      XCWL=C.
C   FUSELAGE-ANGLE OF ATTACK(DEG),UPPER FUSELAGE SURFACE(DEG),WIDTH/HEIGHT
C   RATIO,TIME OFF WEIGHT(LB)
      ALPHAC=1.01
      DELC(7)=0.
      FWP=1.33
      WTC=9.55
C   WING-SURFACE ANGLES(DEG),ASPECT RATIO
      DELC(9)=-5.21
      DELD(11)=7.41
      DELC(12)=0.
C REFERENCE QUANTITIES TO COMPUTE SKIN FRICTION AND
      PASPR=.2403
C FREE STREAM PROPERTIES--HP=ALTITUDE(FT), D1=SCALE FACTOR(FT)
      HP=1.15E5
      D1=60.
C     DIAMETER OF LEADING EDGES(FT)
      DLE=.1/12.
C CAV45-COEFFICIENT FOR DETERMINING AVERAGE COMBUSTOR PROPERTIES
      CAV45=.5
C COMPUTATION CONTROL CARDS
C   PCON-WING PLACEMENT CONTROL--IF MCON NOT EQUAL 1-COMPUTE WING
C   PLACEMENT FROM MOMENT ABOUT CG EQUAL ZERO REQUIREMENT-MCON EQUAL 1
C   FIX WING POSITION
C   ST(2)-SKIN FRICTION COMPUTATION CONTROL-IF ST(2) LESS THAN ZERO
C   COMPUTE SKIN FRICTION FOR LOCAL SURFACES-ST(2) EQUAL ZERO OR GREATER-
C   USE VALUE OF ST(2) AS SKIN FRICTION COEFFICIENT FOR ALL SURFACES
      ST(2)=-2.
      MCON=0
      ALPHAR=RAD(ALPHAD)
      DEL5=RAD(DELD(5))
      P12=-1.
      PALT=0.
      A=0.
      L=0
      XCK=0
C DETERMINE CONFIGURATION AND PERFORMANCE FOR ABOVE INPUT DATA
      CALL RANGE
C DETERMINE REGENERATIVE COOLING REQUIREMENTS
      CALL CCOL(BWDC)
      STOP
      END


$IBFTC RAN      DECK
      SUBROUTINE RANGE

C THIS SUBROUTINE CALLS COMPUTATIONAL SUBROUTINES IN PROPER SEQUENCE
C WITH PROPER INITIAL CONDITIONS

      COMMON /VAR/P(13),DEL(13),DELC(13),LAM(13),THETA(13),XCWL,P2(13),
     1X(6),Q,V4,V5,CFX(13),CFY(13),DEL5,ALPHAR,CACAP,TLAP(13),PXCESS,
     2EA,APS,P
      REAL P,P2,LAM
      DATA P1,P2/.0174533292,57.2957779/
      RAD(Z)=Z*P1
      DEG(Z)=Z*P2
C X(I),LAP(I),TLAP(I) ARE NON-DIMENSIONAL LONGITUDINAL LENGTH-L(I)/D1,
C PRESSURE-P(I)/P1,AND TEMPERATURE-T(I)/T1 RESPECTIVELY
C COMPUTE INLET FLOW FIELD PROPERTIES
C   INITIAL CONDITIONS
  169 X(1)=1.
      LAP(1)=1.
      TLAP(1)=1.
C   ADJUST FIRST RAMP ANGLE FOR ANGLE OF ATTACK
      ALPHAC=DEG(ALPHAR)
      DEL(1)=RAD(DELD(1))+RAD(ALPHAC)
      DEL(2)=RAD(DELD(1))
C   SOLVE OBLIQUE SHOCK WAVE EQUATIONS FOR INLET SHOCK SYSTEM
      CALL SHOCK(1.3,617)
      DELC(2)=DEG(DEL(2))
```

```
C   REFERENCE SHOCK WAVE TO BODY AXIS SYSTEM
      DEL(I)=RAD(DELD(I))
      THETA(I)=THETA(I)-RAD(ALPHAD)
C COMPUTE INLET GEOMETRY
      CALL CONFIG
C COMPUTE FLOW FIELD-UNDERSIDE OF COWL
      M2(9)=M2(1)
      LAM(9)=LAM(1)
      TLAM(9)=TLAM(1)
      DEL(9)=ALPHAR
      CALL SHOCK(9,9,817)
C COMPUTE FLOW FIELD-UPPER FUSELAGE SURFACE(7),UPPER WING(9)
      DO 5 I=7,9,2
      LAM(I)=LAM(1)
      M2(I)=M2(1)
      TLAM(I)=TLAM(1)
      DEL(I)=RAD(DELD(I))-ALPHAR
      IF(DEL(I).LT.0.) GO TO 5
C   IF COMPRESSION SURFACE-OBLIQUE SHOCK
      CALL SHOCK(I,I,817)
      GO TO 4
C   IF EXPANSION SURFACE-PRANDTL-MEYER
 3    CALL PRANT(I)
 4    CONTINUE
 5    CONTINUE
C   UNDERSURFACE OF  WING
      M2(11)=M2(1)
      LAM(11)=LAM(1)
      TLAM(11)=TLAM(1)
      DEL(11)=RAD(DELD(11))+ALPHAR
      CALL SHOCK(11,11,817)
C COMPUTE COMBUSTOR FLOW FIELD PROPERTIES
      CALL COMBST(817)
C COMPUTE NOZZLE FLOW FIELD PROPERTIES
      CALL NOZZL(818)
 17   CONTINUE
 18   CONTINUE
      RETURN
      END


SUBROUTINE SHOCK(I1,I2,I3)
      DIMENSION DEL(13),DELD(13),LAM(13),THETA(13),M2(13),
     1P(13),T(13),RHO(13),CPR(13),CPV(13),DEL9,ALPHAR,CACAP,TLAM(13),PRCESS,
     2RO,GM1,G
      COMMON/SHOCK/TCPOST
      COMMON /V84/M(13),DEL(13),DELD(13),LAM(13),THETA(13),RCWL,M2(13),
     1P(13),T(13),RHO(13),CPR(13),CPV(13),DEL9,ALPHAR,CACAP,TLAM(13),PRCESS,
     2RO,GM1,G
      COMMON/FLOW/P12,PAIRM,PF,PDES,PALT,WTOT,WTOT,CWT,PALTT,CPALT,RSC
      DIMENSION ACCT(3),W(3)
      REAL M,M2,LAM
      DATA PI,R2D,D2R/3.1415926536,57.2957795/
      RAD(I)=I*D2R
      DEG(I)=I*R2D
      DATA G1/2.4/,GM1/0.4/
C DETERMINE AMBIENT TEMPERATURE FROM 1959 STANDARD ATMOSPHERE
C SUBROUTINE ATMOS IS A LIBRARY ROUTINE
      CALL ATMOS(H,TM,SIGMA,RHO,THETT,DELTA,CO,AML,K)
      P2(I)=P(I)*2
```

```
C IF INLET SURFACE USE TRIAL VALUE OF 2ND INLET RAMP ANGLE AS SHOWN
      IF(I).EQ.1) DEL(2)=RAD(DELD(1))/2.
 19   CONTINUE
      DEL(9)=RAD(DELD(1))+DEL(2)
C SOLVE OBLIQUE SHOCK EQUATIONS
      DO 200 I=11,12
      PP=-((M2(I)+2.0)/M2(I)+1.4*SIN(DEL(I))**2)
      QQ=(2.0*M2(I)+1.0)/M2(I)**2+(1.4+1.40/M2(I))*SIN(DEL(I))**2
      RR=-COS(DEL(I))**2/M2(I)**2
      A=(3.0*QQ-PP**2)/3.0
      B=(2.0*PP**3-9.0*PP*QQ+27.0*RR)/27.0
      DIS=B**2/4.0+A**3/27.0
      IF(DIS.LT.0.) GO TO 99
      IF(DIS.GT.1.0E-5) GO TO 200
      PHI=0.0
      GO TO 100
99    PHI=ARCOS(-B/(2.0*SQRT(-A**3/27.0)))
100   DO 101 J=1,3
      Z=J-1
101   ROOT(J)=2.0*SQRT(-A/3.0)*COS(PHI/3.0+PI23*Z)
      W(1)=AMAX1(ROOT(1),ROOT(2))
      W(2)=AMAX1(ROOT(2),ROOT(3))
      W(3)=AMAX1(ROOT(1),ROOT(3))
      Y=AMIN1(W(1),W(2),W(3))-PP/3.0
C SHOCK WAVE ANGLE
      THETA(I)=ARSIN(SQRT(Y))
C FLOW PROPERTIES BEHIND SHOCK
      P2(I+1)=(M2(I)*Y*5.0)/((7.0*M2(I)*Y-1.0)*(SIN(THETA(I)-DEL(I))**2)
     1)
      LAM(I+1)=((7.0*M2(I)*Y-1.0)/6.0)*LAM(I)
      M(I+1)=SQRT(M2(I+1))
      TLAM(I+1)=(((7.0*M2(I)*Y-1.)*(M2(I)*Y+5.))/(36.*M2(I)*Y))*TLAM(I)
200   CONTINUE
      IF(I1.NE.1) GO TO 300
C TEST TO DETERMINE IF TRIAL DELD(2) PRODUCED DESIRED COMBUSTOR ENTRANCE
C TEMPERATURE- TCPOST
      T1=TCPOST/TM-TLAM(6)
      IF(ABS(T1).LE.1.E-2) GO TO 300
C COMPUTE NEW TRIAL DELD(2)
      C=2./57.3
      DEL(2)=DEL(2)+C*T1
      DELD(2)=DEG(DEL(2))
      IF(DEL(2).LT.0.) GO TO 400
      IF(DELD(2).GT.60.) GO TO 400
C CONTINUE ITERATION
      GO TO 19
 710  FORMAT(1X,11HTEMP RATIO=,F13.6//)
 300  CONTINUE
      RETURN
603   FORMAT(3H I=I2,2X,7HMROOTS=3F10.5,2X,7HPICDLE=F10.5,
     12X,6HTHETA=F10.5,2X,12HLAMBDA(I+1)=F10.5,2X,7HM(I+1)=F10.5)
 711  FORMAT(1X,F17.6)
500   WRITE(6,605)
605   FORMAT(1H 26HROT A 3 REAL RCOT EQUATION)
      RETURN 1
 400  CONTINUE
      WRITE(6,606)
 606  FORMAT(1H 6HDEL2=0)
      RETURN 1
      END
```

```
$IBFTC CONFG   DECK
      SUBROUTINE CONFIG

C THIS SUBROUTINE COMPUTES INLET CONFIGURATION AND COMBUSTOR LENGTH
C USING SHOCK ON INLET COWL LIP CONSTRAINT

      COMMON /VAR/M(13),DEL(13),DELC(13),LAM(13),THETA(13),XCWL,M2(13),
     1X(6),P,V4,V5,CFX(13),CFY(13),CEL5,ALPHAR,CACAP,TLAM(13),FXCESS,
     2ER,AP5,P
      COMMON /VAR1/VOLACA,VLTAD4,VLWAD4,CMW,CBLM,CF
      REAL P,M2,LAM
C INLET LENGTHS
      X(3)=((TAN(THETA(1))-TAN(CEL(1)))*(TAN(THETA(2)+DEL(1))-TAN(DEL(3)
     1)))/((TAN(THETA(2)+DEL(1))-TAN(THETA(1)))*(TAN(THETA(3)-DEL(3)))+TA
     2N(CEL(3))))
      X(2)=X(3)*(TAN(THETA(1))-TAN(CEL(1)))/(TAN(THETA(2)+DEL(1))-TAN(TH
     1ETA(1)))
C NON-DIMENSIONAL FREE STREAM CAPTURE AREA
      CACAP=((1.+X(2)-X(3))/COS(THETA(1)))*SIN(THETA(1)+ALPHAR)
C COMBUSTOR HEIGHT
      V4=X(2)*TAN(THETA(3)-CEL(3))
C COMBUSTOR LENGTH
      X(4)=CBLM*V4
      RETURN
      END



      SUBROUTINE PRANT(I)

C THIS SUBROUTINE COMPUTES INVISCID FLOW FIELD FOR EXPANSION SURFACES
C FROM PRANDTL-MYER RELATIONS

      COMMON /VAR/M(13),DEL(13),DELC(13),LAM(13),THETA(13),XCWL,M2(13),
     1X(6),P,V4,V5,CFX(13),CFY(13),CEL5,ALPHAR,CACAP,TLAP(13),FXCESS,
     2ER,AP5,P
      REAL P,M2,LAM
      EPSCHF(A,B)=SQRT((2.*(A**2))/((B+1.))/(1.-((B-1.)/(B+1.))*(A**2)))
      PRTIOF(A,B)=(1.+((B-1.)/2.0))**(B/(B-1.))
      O SOAF(A, )=SQR ((B+1.)/(B-1.))*ATAN(SQRT((A**2-1.)/((B+1.)/(B-1.)
     1-A**2)))-ATAN(SQRT(((B+1.)/(B-1.))*((A**2-1.)/((B+1.)/(B-1.)-A**2)
     2)))
      EPASTF(A,B)=SQRT((0.5*(B+1.)*(A**2))/(1.+0.5*(B-1.)*(A**2)))
      TEMPF(A,B)=1.+((B-1.)/2.)*A**2
      GAMMAP=1.4
      M(I)=SQRT(M2(I))
      EPS=EPASTF(P(I),GAMMAP)
      Z=OMEGAF(EPS,GAMMAP)
      Z2=EPS*.02
      Z1=Z-CEL(I)
 61   Z3=OMEGAF(Z2,GAMMAP)
      IF(ABS(Z1-Z3)-1.90E-6)63,63,62
 62   Z2=Z2+((Z1-Z3)/(Z3-OMEGAF(EPS,GAMMAP)))*(Z2-EPS)
      GO TO 61
 63   CONTINUE
C PROPERTIES BEHIND EXPANSION FAN
      M(I+1)=EPACHF(Z2,GAMMAP)
      LAP(I+1)=PRTIOF(M(I),GAMMAP)/PRTIOF(M(I+1),GAMMAP)
      LAP(I+1)=LAP(I+1)*LAM(I)
      TLAP(I+1)=TEMPF(M(I),GAMMAP)/TEMPF(M(I+1),GAMMAP)
      TLAP(I+1)=TLAP(I+1)*TLAM(I)
      RETURN
      END
$IBFTC CMST    DECK
      SUBROUTINE CMPST(*)

C THIS SUBROUTINE SOLVES ONE-DIMENSIONAL,SUPERSONIC,CONSTANT AREA
C HEAT ADDITION EQS TO DETERMINE INVISCID COMBUSTOR FLOW FIELD PROPERTIES

      COMMON /VAR/M(13),DEL(13),DELC(13),LAM(13),THETA(13),XCWL,M2(13),
     1X(6),P,V4,V5,CFX(13),CFY(13),CEL5,ALPHAR,CACAP,TLAP(13),FXCESS,
     2ER,AP5,P
      COMMON/VAR2/P12,PASPR,HF,PDES,PALT,WTOO,WTOT,CWT,PALTT,CPALT,X5C
      COMMON/VAREC/ TEMP5,V4,V5,MINF5,GAM5,BD1,CAV45,R5,AP6,TEMP65
      COMMON/BCD1/CLE,D1,WTO
      REAL P,M2,LAM
      PRTIOF(A,B)=(1.+((B-1.)/(2.0C))*A**2)**(B/(B-1.))
C FST-STOICHIOMETRIC FUEL-AIR RATIO
      FST=.0292
      U=1.+ER*FST
      CF=2.
C HFAB-ABSOLUTE ENTHALPY OF FUEL BEFORE COMBUSTION
      HFAB=6000.
C DETERMINE PRESSURE,TEMPERATURE,AND ABSOLUTE ENTHALPY OF AIR AT STATION 4
      CALL ATMOS(HF,TM,SIGMA,RHO,THETT,DELTA,CC,MU,K)
      P4=DELTA*LAP(4)
      TEMP4=TLAM(4)*TM
      CALL AIRTAB(TEMP4,H4)
C DETERMINE PRESSURE AND TEMPERATURE OF COMBUSTION PRODUCTS AT
C EXIT OF COMBUSTOR BY ITERATION ON PRESSURE AND TEMPERATURE
 13   CONTINUE
      PP=0
C INITIAL TRIAL PRESSURE OF COMBUSTION PRODUCTS
      P5=P4*2.
 12   CONTINUE
      GAP4=1.4
      BARP4=28.9
      RACT=49719.
      R4=RACT/BARP4
      GJ2=32.2*778.*2.
C INITIAL TRIAL TEMPERATURE OF COMBUSTION PRODUCTS
      TEMP5=5000.
C COMPUTE VELOCITY RATIO V5/V4 WHICH SATISFIES CONTINUITY
C AND MOMENTUM EQUATIONS
      V4=M(4)*SQRT(GAP4*R4*TEMP4)
      AA=0
      A=V4*V4
      B=(1.+R4*TEMP4)/U
C DETERMINE MOLECULAR WEIGHT OF PRODUCTS OF COMBUSTION
 6    CALL PCLWT(TEMP5,ER,P5,PARM5)
C SUBROUTINE MOLWT CONTAINS MOLECULAR WEIGHT OF PRODUCTS AS A
C FUNCTION OF EQUIVALENCE RATIO, PRESSURE, AND TEMPERATURE(REF 29)
      C=RACT*TEMP5/PARM5
C CHOOSE POSITIVE SIGN OF SQUARE ROOT IN FOLLOWING EQUATION WHICH
C CORRESPONDS TO A WEAK DETONATION WAVE(NEGATIVE ROOT-STRONG DETONATION)
C FOR HEAT ADDITION TO A SUPERSONIC STREAM OF AIR
      V5V4=(B+SQRT(B**2-4.*A*C))/(2.*A)
C COMPUTE VELOCITY RATIO-V5/V4-SQUARED FROM ENERGY EQUATION WRITTEN IN
C TERMS OF ABSOLUTE ENTHALPY OF THE REACTANTS AND PRODUCTS

C DETERMINE ABSOLUTE ENTHALPY OF PRODUCTS OF COMBUSTION
      CALL THAPY(TEMP5,ER,P5,H5)
C SUBROUTINE THAPY CONTAINS ABSOLUTE ENTHALPY OF HYDROGEN-AIR
C AS A FUNCTION OF EQUIVALENCE RATIO, PRESSURE, AND TEMPERATURE(REF 29)
```

```
      F2=(GJ2/(V4*V4+U))*(P4+V4*V4/GJ2*HFAB*ER*FST)-H5*GJ2/(V4*V4)
C TEST TO DETERMINE IF VELOCITY RATIO WILL SATISFY MOMENTUM,ENERGY AND
C CONTINUITY EQUATIONS SIMULTANEOUSLY
      F1=V5/V4*V5/V4
      F=F1-F2
      IF(ABS(F).LT.1.E-3) GO TO 8
C COMPUTE NEW TRIAL TEMPERATURE USING NEWTON-RAPHSON TECHNIQUE
      R5=R*CT/P144
      FDOT=-(R5*2)/(A*SQRT(P*R-4.*A*C))-R5/A+GJ2*CP5/(V4*V4)
      C1=1.
      TEMP5=TEMP5-C1*F/FDOT
C CONTINUE TEMPERATURE ITERATION
      NN=NN+1
      IF(NN.GT.40)GO TO 40
      GO TO 6
 8    V5=V5/V4*V4
      P5P4=L*(TEMP5/TEMP4)*(BARM4/BARM5)*(V4/V5)
      P=P5P4
C TEST TO DETERMINE IF TRIAL AND CALCULATED PRESSURE ARE WITHIN LIMITS
      P5C=P4*P
      IF(ABS((P5C-P5)/P5).LT..001) GO TO 11
C CONTINUE PRESSURE ITERATION
      P5=P5+(P5C-P5)*.9
      MM=MM+1
      IF(MM.GT.40) GO TO 40
      GO TO 12
 11   CONTINUE
C DETERMINE FROZEN SPEED OF SOUND
      CALL SPEED(TEMP5,ER,P5,CAF5)
C SUBROUTINE SPEED CONTAINS FROZEN SPEED OF SOUND OF COMBUSTION GASES
C AS A FUNCTION OF EQUIVALENCE RATIO, PRESSURE, AND TEMPERATURE(REF 29)
C COMPUTE MACH NUMBER STATION 5
      AM5=V5/CAF5
C COMPUTE RATIO OF SPECIFIC HEATS AT STATION 5
      GAM5=CAF5*CAF5/(R5*TEMP5)
      PO5=P5*PRTIOF(AM5,GAM5)
      HINF5=H5
      IF(AM5.LT.1.05) GO TO 50
      RETURN
 40   WRITE(6,31)
 31   FORMAT(2X,40HPRESS OR TEMP FAILED TO CONVERGE AT ST 5,/)
      RETURN 1
 50   WRITE(6,51)
 51   FORMAT(2X,16HCOMBUSTOR CHOKED,/)
      RETURN 1
      END


$IBFTC NOZZ
      SUBROUTINE NOZZL(*)

C THIS SUBROUTINE CONTROLS NOZZLE FLOW FIELD AND FORCE CALCULATIONS

      COMMON /VAR/M(13),DEL(13),DELD(13),LAM(13),THETA(13),XCWL,M2(13),
     1X(6),R,Y4,Y5,CFX(13),CFY(13),DEL5,ALPHAR,CACAP,TLAM(13),FXCESS,
     2ER,AM5,P
      COMMON/VAR2/P12,PASPR,HF,PDES,PALT,WTOD,WTOT,CWT,PALTT,CPALT,X5D
      COMMON/ADD1/DLE,D1,WTO
      COMMON/SAMEC/ TEMP5,V4,V5,HINF5,GAM5,BD1,CAV45,R5,AM6,TEMP65
      COMMON/NEF/DC
      COMMON/PRNT/SEFCY,STFRAC,XCM,YCM,BWBC,AWNG,VTD12B,ATGD12,CDSF,
     $XLWLEV,PDW,XW,AISPT,AISPL,ALODL,ALODT,RANF,FDW,CDW,CDLEW,
     $FDI12,PDI12,D3,PDTP,CDLEBC,CLW,VWD12B,AWGD12,XCPLEV,CDB,CLB,TWL,
     $TWC,CUM(33),KCK
      DIMENSION PMB(060,4,35),PO(4),P1(4),P2(4),P3(4),LPT(33,2)
      EQUIVALENCE (LPT(1,1),SEFCY)
      REAL M,M2,LAM,LPT
      PRTIOF(A,B)=(1.-((B-1.)/(B+1.))*A**2)**(B/(B-1.))
      EMACHF(A,B)=SQRT(((2.*(A**2))/(B+1.))/(1.-((B-1.)/(B+1.))*(A**2)))
      EMASTF(A,B)=SQRT((0.5*(B+1.)*(A**2))/(1.+0.5*(B-1.)*(A**2)))
      N6=0
      I=0
      K=0
      DXCWL=XCWL
      PIS=.5
      BETA=0.
      X5L=0.
      Y5L=0.
      PALTL=0.
      DCL=0.
      GAMMAP=GAM5
      RL=0.
      EM1P=AM5
 600  EMS1P=EMASTF(EM1P,GAMMAP)
      ANGLE=-DELD(5)
      N1=1
C COMPUTE DOWN RUNNING CHARACTERISTICS EMANATING FROM NOZZLE EXPANSION
C CORNER
      CALL PMSUB (1,GAMMAP,EM1P,N1,ANGLE,BETA,K,PMB)
C COMPUTE STARTING LINE FOR CHARACTERISTICS SOLUTION
      CALL STARTC (EM1P,EMS1P,PMB)
C COMPUTE PROPERTIES AT LATTICE POINTS ALONG FIRST 9 UPRUNNING
C CHARACTERISTICS ORIGINATING ON STARTING LINE
      DO 5 I=9
      DO 6 J=1,K
      DO 7 L=1,4
      P1(L)=PMB(J,L,I)
   7  P2(L)=PMB(J+1,L,I-1)
C COMPUTE FLOW PROPERTIES AT INTERIOR LATTICE POINTS OF FLOW FIELD
      CALL LPS (1,GAMMAP,ANGLE,P1,P2,P3)
      DO 8 L=1,4
   8  PMB(J+1,L,I)=P3(L)
   6  CONTINUE
      DO 9 L=1,4
      P2(L)=PMB(K+1,L,I-1)
   9  P1(L)=PMB(K+1,L,I)
C COMPUTE FLOW PROPERTIES AT LATTICE POINT ON NOZZLE-FUSELAGE SURFACE
      CALL LPS (2,GAMMAP,ANGLE,P1,P2,P3)
      L1=K+2
      I5=I
      PP4=57.2957795*P3(4)
      PP3=EMACHF(P3(3),GAMMAP)
  11  DO 12 L=1,4
  12  PMB(K+2,L,I)=P3(L)
   5  K=K+1
      N1=1
C COMPUTE PROPERTIES AT LATTICE POINTS ALONG UPRUNNING CHARACTERISTICS
C ORIGINATING FROM NOZZLE COWL OR TRAILING EDGE OF NOZZLE COWL
      DO 50 J1=N1,10000
      DO 70 L=1,4
      P1(L)=PMB(J1,L,I)
  70  P2(L)=PMB(J1+1,L,I)
C COMPUTE PROPETIES AT SURFACE OF NOZZLE COWL
      CALL LPS (3,GAMMAP,ANGLE,P1,P2,P3)
```

```
C TEST TO DETERMINE IF X-COORDINATE OF PROPOSED UPRUNNING
C CHARACTERISTIC IS GREATER THAN DESIRED LENGTH OF THE NOZZLE COWL
      IF(P3(1).GE.DXCWL) GO TO 31
C DETERMINE FORCE AND MOMENTS OF NOZZLE COWL
      CALL FAM (1,GAMMAP,P1,P2,P3,I,N6,$777,$778)
      L2=J1+1
      I6=I+1
      PP4=57.2957795*P3(4)
      PP3=EPACHF(P3(3),GAMMAP)
      DO 80 L=1,4
   80 PMB(J1+1,L,I+1)=P3(L)
      N2=N1+1
      DO 60 J2=N2,K
      DO 71 L=1,4
      P1(L)=PMB(J2,L,I+1)
   71 P2(L)=PMB(J2+1,L,I)
C INTERIOR LATTICE POINT
      CALL LPS (1,GAMMAP,ANGLE,P1,P2,P3)
      L7=J2+1
      I7=I+1
      PP3=EPACHF(P3(3),GAMMAP)
      PP4=57.2957795*P3(4)
      DO 81 L=1,4
   81 PMB(J2+1,L,I+1)=P3(L)
   60 CONTINUE
      DO 90 L=1,4
      P2(L)=PMB(K+1,L,I)
   90 P1(L)=PMB(K+1,L,I+1)
C NOZZLE-FUSELAGE SURFACE LATTICE POINT
      CALL LPS (2,GAMMAP,ANGLE,P1,P2,P3)
C SAVE OLD VALUES OF CONFIGURATION AND PERFORMANCE PARAMETERS
      DCL=DC
      X5L=X(5)
      Y5L=Y5
      RL=R
      PALTL=PALT
      DO 92 L=1,33
   92 LPT(L,2)=LPT(L,1)
C DETERMINE FORCES AND MOMENTS ACTING ON THE VEHICLE
      CALL FAM (2,GAMMAP,P1,P2,P3,I,N6,$777,$778)
      L1=K+2
      I5=I+1
      PP4=57.2957795*P3(4)
      PP3=EPACHF(P3(3),GAMMAP)
      DO 120 L=1,4
  120 PMB(K+2,L,I+1)=P3(L)
C TEST TO DETERMINE IF GEOMETRIC CONSTRAINTS(ZERO BASE OR NOZZLE
C LENGTH EXCEEDING DESIRED LENGTH)HAVE BEEN EXCEEDED
      IF (Y5.LE.0.00) GO TO 500
      IF (X(5).GT.X5D) GO TO 502
      I=I+1
      N1=N1+1
   50 K=K+1
      GO TO 400
   31 CONTINUE
      XCWL=PMB(N1,1,I)
      KK=K
C COMPUTE FORCE AND MOMENT ON NOZZLE COWL
      CALL FAM (3,GAMMAP,P1,P2,P3,I,N6,$777,$778)
C COMPUTE UPRUNNING CHARACTERISTICS EMANATING FROM CENTERED EXPANSION
C ABOUT TRAILING EDGE OF THE NOZZLE COWL
      CALL EMSBR (2,GAMMAP,EM1P,N1,ANGLE,BETA,K,PMB)
      K=KK
   15 DO 61 J=N1,K
      DO 72 L=1,4
      P1(L)=PMB(J,L,I+1)
   72 P2(L)=PMB(J+1,L,I)
C COMPUTE INTERIOR LATTICE POINT
      CALL LPS (1,GAMMAP,ANGLE,P1,P2,P3)
C COMPUTE FLOW FIELD PROPETIES
      L1=J+1
      I5=I+1
      PP4=57.2957795*P3(4)
      PP3=EPACHF(P3(3),GAMMAP)
      DO 82 L=1,4
   82 PMB(J+1,L,I+1)=P3(L)
   61 CONTINUE
      DO 91 L=1,4
      P2(L)=PMB(K+1,L,I)
   91 P1(L)=PMB(K+1,L,I+1)
      CALL LPS (2,GAMMAP,ANGLE,P1,P2,P3)
C SAVE OLD VALUES OF CONFIGURATION AND PERFORMANCE PARAMETERS
      PALTL=PALT
      RL=R
      X5L=X(5)
      DCL=DC
      Y5L=Y5
      DO 93 L=1,33
   93 LPT(L,2)=LPT(L,1)
C DETERMINE FORCES AND MOMENTS ACTING ON THE VEHICLE
      CALL FAM (2,GAMMAP,P1,P2,P3,I,N6,$777,$778)
      K5=K+2
      I7=I+1
      PP4=57.295779*P3(4)
      PP3=EPACHF(P3(3),GAMMAP)
      DO 121 L=1,4
  121 PMB(K+2,L,I+1)=P3(L)
      I=I+1
      K=K+1
C TEST TO DETERMINE IF CONSTRAINTS HAVE BEEN EXCEEDED
      IF (Y5.LE.0.00) GO TO 500
      IF (X(5).GT.X5D) GO TO 502
      GO TO 15
C LINEAR INTERPOLATION BETWEEN CURRENT AND PREVIOUS POINT
  400 RETURN
C   ZERO BASE SOLUTION
  500 DY5=-Y5L/(Y5-Y5L)
      DCS=DCL+(DC-DCL)*DY5
      PALTS=PALTL+(PALT-PALTL)*DY5
      X5S=X5L+(X(5)-X5L)*DY5
      IF (KCK.EQ.1) GO TO 699
      RS=RL+(R-RL)*DY5
      DO 501 L=1,33
  501 LPT(L,1)=LPT(L,2)+(LPT(L,1)-LPT(L,2))*DY5
      R=RS
      Y5=0.
      X(5)=X5S
  698 WRITE (6,700) PALTS,PDES,DCS,C1
      IF(X(5).GT.X5D) GO TO 502
  700 FORMAT (2X,18HZERO BASE SOLUTION//2X,19HPALT,PALTD,DIC,D1
     $1P4E15.7//)
      RETURN
C   NOZZLE LENGTH EQUAL DESIRED LENGTH
  699 IF (ABS(X(5)-X5D) .LE. 0.05) GO TO 698
```

```
      R=0.0
      WRITE (6,700) PALTS,PDES,DCS,D1
      RETURN
  502 DX5=(X5D-X5L)/(X(5)-X5L)
      DCS=CCL+(DC-DCL)*DX5
      PALTS=PALTL+(PALT-PALTL)*DX5
      IF (RCK.EQ.1) GO TO 705
      RS=RL+(R-RL)*DX5
      DO 503 L=1,33
  503 LPT(L,1)=LPT(L,2)+(LPT(L,1)-LPT(L,2))*DX5
      R=RS
      X(5)=X5D
  505 WRITE(6,701) PALTS,PDES,DCS,D1
  701 FORMAT(2X,18HX5.GT.X5D          ,//2X,19HPALT,PALTD,D1C,D1   ,
     $1P4E15.7//)
      RETURN
  705 IF (ABS(X(5)-X5D) .LE. 0.05) GO TO 505
      R=0.0
      WRITE(6,701) PALTS,PDES,DCS,D1
      RETURN
  777 WRITE(6,703) PALTL,PDES,DCL,D1
  703 FORMAT(2X,18HX5 OPT LENGTH      ,//2X,19HPALT,PALTD,D1C,D1   ,
     $1P4E15.7//)
      R=RL
      YS=Y5L
      X(5)=X5L
      DO 702 L=1,33
  702 LPT(L,1)=LPT(L,2)
      RETURN
  778 WRITE (6,704)
  704 FORMAT(1H 13HNEGATIVE CORC)
      RETURN 1
      END


$IBFTC PRAP    DECK
      SUBROUTINE PPSBR(K2,GAMMAP,EM1P,M1,ANGLE,BETA,K,PMB)

C THIS SUBROUTINE COMPUTES CHARACTERISTICS EMANATING FROM COMBUSTOR-NOZZLE
C EXPANSION CORNNER AND TRAILING EDGE OF NOZZLE COWL

      COMMON/PRM/ANET
      DIMENSION PMB(060,4,35)
      REAL M,M2,LAM
      OMEGAF(A,B)=SQRT((B+1.)/(B-1.))*ATAN(SQRT((A**2-1.)/((B+1.)/(B-1.)
     1-A**2)))-ATAN(SQRT(((B+1.)/(B-1.))*((A**2-1.)/((B+1.)/(B-1.)-A**2)
     2)))
      EMASTF(A,B)=SQRT((0.5*(B+1.)*(A**2))/(1.+0.5*(B-1.)*(A**2)))
      EMRSF(A,B)=SQRT(((B+1.)/(B-1.))*(1.-A**((B-1.)/B)))
  101 FORMAT(5X,13HPRANCTL-MEYER,//)
  100 FORMAT(5F13.6)
      GO TO(1,2),K2
C   COMBUSTOR-NOZZLE CORNNER
    1 CONTINUE
      T=OMEGAF(EMASTF(EM1P,GAMMAP),GAMMAP)
C   CHARACTERISTIC NET SPACING CONTROL
      ANET=1.25
      K=ABS(ANGLE/ANET)
      C=K
      DELTA=ANGLE/(C*57.295779)
      PPB(1,1,1)=0.0
      PPB(1,2,1)=-1.0
      PPB(1,3,1)=EMASTF(EM1P,GAMMAP)
      PPB(1,4,1)=BETA
      DO 50 I=1,K
      PPB(I+1,1,1)=PMB(I,1,1)
      PPB(I+1,2,1)=PMB(I,2,1)
      PMB(I+1,4,1)=PMB(I,4,1)+DELTA
      Y1=T-(PMB(I+1,4,1)-PMB(1,4,1))
      Y2=PPB(I,3,1)+0.02
   51 Y3=OMEGAF(Y2,GAMMAP)
      IF (ABS (Y1-Y3)-1.50E-6) 53,53,52
   52 Y2=Y2+((Y1-Y3)/(Y3-OMEGAF(PMB(I,3,1),GAMMAP)))*(Y2-PMB(I,3,1))
      GO TO 51
   53 CONTINUE
      PPB(I+1,3,1)=Y2
   50 CONTINUE
      GO TO 400
C   TRAILING EDGE OF NOZZLE COWL
    2 I1=N1+8
      DO 54 I=I1,34
      Z=OMEGAF(PMB(N1,3,I1),GAMMAP)
C   CHARACTERISTIC NET SPACING CONTROL
      DELTA=ANET/57.29577
      PPB(N1,1,I+1)=PMB(N1,1,I)
      PPB(N1,2,I+1)=PMB(N1,2,I)
      PMB(N1,4,I+1)=PMB(N1,4,I)+DELTA
      Z1=Z+PMB(N1,4,I+1)-PMB(N1,4,I1)
      Z2=PPB(N1,3,I)+.02
   61 Z3=OMEGAF(Z2,GAMMAP)
      IF(ABS(Z1-Z3)-1.50E-6)63,63,62
   62 Z2=Z2+((Z1-Z3)/(Z3-OMEGAF(PMB(N1,3,I1),GAMMAP)))*(Z2-PMB(N1,3,I1))
      GO TO 61
   63 CONTINUE
      PPB(N1,3,I+1)=Z2
   54 CONTINUE
  400 CONTINUE
      RETURN
      END


$IBFTC START   DECK
      SUBROUTINE STARTC(EM1P,EMS1P,PMB)

C THIS SUBROUTINE COMPUTES STARTING LINE FOR CHARACTERISTICS SOLUTION

      COMMON /VAR/M(13),DEL(13),DELC(13),LAM(13),THETA(13),XCWL,M2(13),
     1X(6),R,Y4,Y5,CFX(13),CFY(13),CEL5,ALPHAR,CACAP,TLAM(13),FXCESS,
     2ER,AM5,P
      DIMENSION PMB(060,4,35)
      REAL M,M2,LAM
      Y=1./SQRT(EM1P**2-1.)
      PPB(1,1,1)=0.0
      PPB(1,2,1)=-1.0
      PPB(1,3,1)=EMS1P
      PPB(1,4,1)=0.0
      DR=1./8.
      DX=DR/Y
      DO 1 I=2,9
      PPB(1,1,I)=PMB(1,1,I-1)+DX
      PPB(1,2,I)=PMB(1,2,I-1)+DR
      PPB(1,3,I)=EMS1P
      PPB(1,4,I)=0.0
  101 FORMAT(5X,13HSTARTING LINE,//)
```

```
 100  FORMAT(5F13.6)
    1 CONTINUE
      RETURN
      END


$IBFTC LATIS   DECK
      SUBROUTINE LPS(RG,GAMMAP,ANGLE,P1,P2,P3)

C THIS SUBROUTINE COMPUTES PROPERTIES AT LATTICE POINTS IN NOZZLE FLOW FIELD
C NOTATION FOLLOWS THAT OF SHAPIRO(REF 30)

      COMMON /VAR/M(13),CEL(13),DELC(13),LAM(13),THETA(13),XCWL,M2(13),
     1R(6),P,Y4,Y5,CFX(13),CFY(13),CEL5,ALPHAR,CACAP,TLAM(13),FXCESS,
     2ER,AP5,P
      DIMENSION P1(4),P2(4),P3(4)
      REAL M,M2,LAM
      EMACHF(A,B)=SQRT(((2.+(A**2))/(B*1.1)/(1.-((B-1.)/(B+1.))*(A**2)))
      ALPHAF(C)=ATAN(SQRT(1./(C**2-1.)))
      OMEGAF(A,B)=SQRT((B+1.)/(B-1.))*ATAN(SQRT((A**2-1.)/((B+1.)/(B-1.)
     1-A**2)))-ATAN(SQRT(((B+1.)/(B-1.))*((A**2-1.)/((B+1.)/(B-1.)-A**2)
     2)))
      D=57.29577
C PHYSICAL COORDINATES OF POINTS (1) AND (2)
      X1=P1(1)
      X2=P2(1)
      Y1=P1(2)
      Y2=P2(2)
C M STAR AT POINTS (1) AND (2)
      EPS1=P1(3)
      EPS2=P2(3)
C INCLINATION OF FLOW DIRECTION AT POINTS (1) AND (2)
      THET1=P1(4)
      THET2=P2(4)
C CHARACTERISTIC COORDINATES AT POINTS (1) AND (2)
      OMEG1=OMEGAF(EMS1,GAMMAP)
      OMEG2=OMEGAF(EMS2,GAMMAP)
      EII=(1000.+OMEG1+D+THET1+D)/2.
      EII2=(1000.-OMEG2+D+THET2+D)/2.
      GO TO (1,2,3),KE
C HODOGRAPH SOLUTION OF INTERIOR POINT (3) KNOWING POSITION AND PROPERTIES
C  AT POINTS (1) AND (2)
    1 EI3=EII
      EII3=EII2
      THET3=(EI3+EII3-1000.)/D
      OMEG3=(EI3-EII3)/D
C INITIAL TRIAL VALUE FOR M STAR AT (3)
      EPS3=(EMS1+EMS2)/2.
   40 COMEG=OMEGAF(EMS3,GAMMAP)
      DOMEG=OMEG3-COMEG
      T1=ABS(DOMEG)
      IF(T1-1.E-4)20,20,30
   30 C=(GAMMAP+1.)/(GAMMAP-1.)
      T2=EMS3+EMS3
      T3=C/(2.+SQRT(T2-1.)+SQRT(C-T2))
      T4=1.-1./(T2+SQRT(C))
      F1=T3+T4
      DMS32=DOMEG/F1
      EMS32=T2+2.+DMS32
C  NEW TRIAL VALUE OF M STAR AT 3
      EPS3=SQRT(EMS32)
      GO TO 40
   20 ALPH3=ALPHAF(EMACHF(EMS3,GAMMAP),GAMMAP)
      ALPH1=ALPHAF(EMACHF(EMS1,GAMMAP),GAMMAP)
C LOCATE POINT (3) IN PHYSICAL PLANE
      ALPH2=ALPHAF(EMACHF(EMS2,GAMMAP),GAMMAP)
      ANG1=(THET3-ALPH3+THET1-ALPH1)/2.
      ANG2=(THET3+ALPH3+THET2+ALPH2)/2.
C AVERAGE SLOPES OF MACH LINES FROM (1-3) AND (2-3)
      BI=TAN(ANG1)
      BII=TAN(ANG2)
      GO TO 39
C HODOGRAPH SOLUTION OF NOZZLE-FUSELAGE BOUNDARY POINT WHERE FLOW ANGLE
  AND ONE COORDINATE IN HODOGRAPH PLANE IS KNOWN
    2 THET3=ANGLE/D
      EI3=EII
      OMEG3=(2.+EI3-1000.-THET3+D)/C
      EPS3=(EMS1+EMS2)/2.
   41 COMEG=OMEGAF(EMS3,GAMMAP)
      DOMEG=OMEG3-COMEG
      T1=ABS(DOMEG)
      IF(T1-1.E-4)21,21,31
   31 C=(GAMMAP+1.)/(GAMMAP-1.)
      T2=EPS3+EMS3
      T3=C/(2.+SQRT(T2-1.)+SQRT(C-T2))
      T4=1.-1./(T2+SQRT(C))
      F1=T3+T4
      DMS32=DOMEG/F1
      EMS32=T2+2.+DMS32
      EPS3=SQRT(EMS32)
      GO TO 41
   21 ALPH3=ALPHAF(EMACHF(EMS3,GAMMAP),GAMMAP)
      ALPH1=ALPHAF(EMACHF(EMS1,GAMMAP),GAMMAP)
      ALPH2=ALPHAF(EMACHF(EMS2,GAMMAP),GAMMAP)
      ANG1=(THET3-ALPH3+THET1-ALPH1)/2.
      ANG2=(THET3+ALPH3+THET2+ALPH2)/2.
      BI=TAN(THET3)
      GO TO 39
C HODOGRAPH SOLUTION OF NOZZLE COWL BOUNDARY POINT WHERE FLOW ANGLE
C AND ONE COORDIDATE IN HODOGRAPH PLANE IS KNOWN
    3 THET3=0.
      EII3=EII2
      OMEG3=(1000.-2.*EII3+THET3)/D
      EPS3=(EMS1+EMS2)/2.
   42 COMEG=OMEGAF(EMS3,GAMMAP)
      DOMEG=OMEG3-COMEG
      T1=ABS(DOMEG)
      IF(T1-1.E-4)22,22,32
   32 C=(GAMMAP+1.)/(GAMMAP-1.)
      T2=EMS3+EMS3
      T3=C/(2.+SQRT(T2-1.)+SQRT(C-T2))
      T4=1.-1./(T2+SQRT(C))
      F1=T3+T4
      DMS32=COMEG/F1
      EMS32=T2+2.+DMS32
      EPS3=SQRT(EMS32)
      GO TO 42
   22 ALPH3=ALPHAF(EMACHF(EMS3,GAMMAP),GAMMAP)
      ALPH1=ALPHAF(EMACHF(EMS1,GAMMAP),GAMMAP)
      ALPH2=ALPHAF(EMACHF(EMS2,GAMMAP),GAMMAP)
      ANG1=(THET3-ALPH3+THET1-ALPH1)/2.
      ANG2=(THET3+ALPH3+THET2+ALPH2)/2.
      BI=TAN(THET3)
```

```
      BII=TAN(ANG2)
   39 CONTINUE
C LOCATION AND FLOW PROPERTIES OF POINT (3)
      Y3=(BI*(Y2-BII*X2)-BII*(Y1-BI*X1))/(BI-BII)
      X3=(Y2-BII*X2-Y1+BI*X1)/(BI-BII)
      P3(1)=X3
      P3(2)=Y3
      P3(3)=EMS3
      P3(4)=THET3
      RETURN
      END


SIBFTC FORCE   DECK
      SUBROUTINE FAM(KB,GAMMAP,P1,P2,P3,I,N6,*,*)

C THIS SUBROUTINE COMPUTES FORCES AND MOMENTS ACTING ON THE VEHICLE AS
C WELL AS VEHICLE PERFORMANCE--ALL FORCES BODY AXIS SYSTEM EXCEPT
C WHERE NOTED

      COMMON /VAR/M(13),DEL(13),DELC(13),LAM(13),THETA(13),XCWL,P2(13),
     1X(6),A,Y4,Y5,CFX(13),CFY(13),DEL5,ALPHAR,CACAP,TLAM(13),EXCESS,
     2ER,AP5,P
      COMMON /VAR1/ VOLADA,VLTADA,VLWADA,FWM,CBLM,CF
      COMMON/VAR2/P12,PASPR,HF,PDES,PALT,WTOD,WTOT,CWT,PALTT,CPALT,X50
      COMMON/NAMEC/ TEMP5,V4,V5,MINF5,GAM5,BD1,CAV45,R5,AP6,TEMP65
      COMMON /CON1/ L,PCON,IPRTN
      COMMON/PRNT/SEFCV,STFRAC,XCM,YCM,BWBC,AWNG,VTD12B,ATGD12,CDSF,
     $BLWLEV,PDW,XW,AISPT,AISPL,ALOCL,ALOOT,RANF,FDW,CDW,CDLEW,
     $FCI12,PUI12,CD,PDTP,CDLERC,CLW,VWD12B,AWGD12,XCPLEV,CDB,CLB,TWL,
     $TWC,CUP(33),WCK
      COMMON/ABD1/CLE,C1,WTO
      COMMON/SEF/CC
      DIMENSION P1(4),P2(4),P3(4)
      REAL M,M2,LAM
      EMACHF(A,D)=SQRT(((2.+(A**2))/(D*1.))/(1.-((D-1.)/(D*1.))*(A**2)))
      PRTIOF(A,D)=(1.+((D-1.)/(2.CO))*A**2)**(D/(D-1.))
      TEMPF(A,D)=(1.+((D-1.)/(2.CO))*A**2)
      L=L+1
      IF(L.EC.1) CALL  ATMOS(HF,TM,SIGMA,RHO,THETT,DELTA,CO,APU,K)
      PCES=DELTA*2116.17
      IF(L.EC.1) WRITE(6,340)
      IF(L.EC.1) ANOZZL=0.
340   FORMAT(2X,49HSKIN FRICTION REF DATA M,T-WALL,T-STREAM,RL,RT,CF,//)
      ALAST=0.
      EP1P=AP5
      AAA=0
      GAMMAP=GAM5
      GP=GAMMAP
      EMACH1=EMACHF(P1(3),GAMMAP)
      EMACH2=EMACHF(P2(3),GAMMAP)
      EMACH3=EMACHF(P3(3),GAMMAP)
      PRTIC1=1./PRTIOF(EMACH1,GAMMAP)
      PRTIC2=1./PRTIOF(EMACH2,GAMMAP)
      PRTIC3=1./PRTIOF(EMACH3,GAMMAP)
      GO TO(1,2,3),KB
C INCREMENT    OF PRESSURE FORCE  AND MOMENT  ON NOZZLE COWL- FRICTION.
C ACCOUNTED FOR IN COMPUSTOR CALCULATION
1     PRPAV=PRTIO3
      CF=0.
      DELX=P3(1)-P1(1)
      IF(I.NE.9) GO TO 32
      CFYU1=-PRTIU1*P1(1)
      CFYU1=-CFYU1*P1(1)/2.
      CFYU2=-DELX*PRPAV
      CFYU2=-CFYU2*(DELX/2.+P1(1))
      CFY=0.
      CFX=0.
      CFXU1=-PRTIC1*P1(1)*GAMMAP*(EMACH1**2.)*CF/2.
      CFXU2=-PRPAV*DELX*GAMMAP*(EMACH3**2.)*CF/2.
      CF1=0.
      CF2=0.
      CFT=0.
      GO TO 60
32    CFYU2=-DELX*PRPAV
      CF=0.
      CFYU2=-CFYU2*(DELX/2.+P1(1))
      CFYU1=0.
      CFXU1=0.
      CFXU2=-PRPAV*DELX*GAMMAP*(EMACH3**2.)*CF/2.
      CFYU1=0.
      GO TO 60
C INCREMENT    OF FORCES AND MOMENTS ON NOZZLE AFTFUSELAGE SURFACE
2     PRPAV=PRTIO3
      DELX=P3(1)-P2(1)
      DELY=P3(2)-P2(2)
      AP6=EMACH2
      TRAT6=TEMPF(EMACH2,GM)
      TRAT5=TEMPF(AP5,GM)
      TEMP65=TRAT5/TRAT6
C COMPUTE STATIC WALL PRESSURE RATIO DELD(4),AND GEOMETRIC QUATITIES
      DELC(4)=PRPAV*LAM(4)*P*PRTIOF(EM1P,GAMMAP)
      X(5)=P3(1)*Y4
      DEL1=DELC(1)/57.29775
      M1=TAN(DEL1)
      M2=X(2)*TAN(DEL(3))
      M3=M1+M2
      DEL7=DELC(7)/57.29775
      Y5=XL*TAN(DEL7)+M3-X(5)*TAN(DEL5)
      M5=(1.+X(2)+X(4))*TAN(DEL7)+M2+Y4
      BC1=FWM+M5
      X(6)=XCWL*Y4
C  DETERMINE QUANTITIES NEECED TO DETERMINE SKIN FRICTION COEFFICIENT-
C  WALL TEMPERATURE-TW IS SPECIFIED AS IS TRANSITION REYNOLDS NUMBER-RT
      TW=2000.
      RT=1.E3
      T=TEMP5*TEMP65
      P6=PCES*PRPAV*LAM(4)*P*PRTIOF(EM1P,GAMMAP)
      XMU=2.27E-8*T**1.5/(198.6+T)
      X(5)=P3(1)*Y4
      RENZ=P6*EMACH1*49.2*SQRT(T)*(X(4)+X(5))*D1/(1718.*T*XMU)
      CALL SKINF(RENZ,EMACH2,TW,T,GAM5,RT,10,CF)
      IF( I.EC.9) WRITE(6,341) EMACH1,TW,T,RENZ,RT,CF
      IF(I.EC.9)CFFST=CF
      IF(I.EC.9)DPFST=EMACH2**2.*PRPAV
341   FORMAT(2X,10HNOZZLE     ,1P6E15.7)
      IF(I.NE.9) GO TO 33
      CFYL1=PRTIC2*P2(1)-TAN(P3(4))*P2(1)*GAMMAP*EMACH2**2.*PRTIO2*CF/2.
      CFYL1=-CFYL1*P2(1)/2.
      CFYL2=PRPAV*DELX-TAN(P3(4))*PRPAV*DELX*GM*EMACH3**2.*CF/2.
      CFYL2=-CFYL2*(DELX/2.+P2(1))
      CFXL1=-PRTIC2*P2(1)*TAN(P3(4))-PRTIO2*P2(1)*GM*EMACH2**2.*CF/2.
      CFXL2=-PRPAV*DELX*TAN(P3(4))-PRPAV*DELX*GM*EMACH3**2.*CF/2.
      CFXL1=-CFXL1*(1.-(P2(2)-1.)/2.)
```

```
      CFXL2=CFXL2+(CELY/2.*P2(2))
      CFUP=CF
      GO TO 65
   33 CONTINUE
      CFYL2=PRPAV*CELX-TAN(P3(4)))*PRPAV*DELX*GM*EMACH3**2.*CF/2.
      CMYL2=-CFYL2*(CELX/2.*P2(1))
      CFXL2=-PRPAV*CELX*TAN(P3(4))-PRPAV*DELX*GM*EMACH3**2.*CF/2.
      CMXL2=CFXL2*(CELY/2.*P2(2))
      CFYL1=0.
C     COMPUTE NOZZLE FENCE DRAG
      DPAV=(EMACH3**2.*PRPAV*CPFST)/2.
      AWNOZ=(Y4+X(6)*TAN(DEL5))*X(5)/BD1
      CFNOZ=CF
      FNOZ=-DPAV*CFNOZ*GM*(AWNOZ-AWNOZL)/(2.*Y4)
      CFXL2=CFXL2+FNOZ
      AWNOZL=AWNOZ
      CFXL1=0.
      CMXL1=0.
      CMYL1=0.
      GO TO 65
C FORCE AND MOMENT CALCULATION WHEN FIRST DOWN RUNNING CHARACTERISTIC
C STRIKES TRAILING EDGE OF NOZZLE COWL
    3 IF(I.NE.9) GO TO 40
      N6=N6+1
      IF(N6.GE.2) GO TO 60
      CFYU1=-PATIO1*P1(1)
      CMYU1=-CFYU1*P1(1)/2.
      CFXU1=0.
      CFYU2=0.
      CFXU2=0.
      CMYU2=0.
      CMY=0.
      CMX=0.
      CF2=0.
      CF1=0.
      CMT=0.
      GO TO 60
   40 CFYU1=0.
      CMYU1=0.
      CFXU1=0.
      CFXU2=0.
      CMYU2=0.
      CFYU2=0.
      GO TO 60
C ADD FORCE AND MOMENT INCREMENTS TO OBTAIN INTEGRATED VALUES
   65 CF1=CF1+CFXL1+CFXL2+CFXU1+CFXL2
      CF2=CF2+CFYU1+CFYU2+CFYL1+CFYL2
      CMY=CMY+CMYU1+CMYU2+CMYL1+CMYL2
      CMX=CMX+CMXL1+CMXL2
      XL=L.*X(2)+X(4)+X(5)
   77 XTAN9=TAN(DELC(9)/57.29775)
      XTAN11=TAN(DELC(11)/57.29775)
      GM=1.4
C FIRST TIME THROUGH SUBROUTINE COMPUTE FORCES ACTING ON VEHICLE
      IF(I.NE.9) GO TO 233
C   UNDERSIDE OF FOREBODY WETTED BY PROPULSIVE STREAM
      XI1=X(1)/COS(DEL1)
      XI2=X(2)/COS(DEL3))
C    COMPUTE AVERAGE PROPERTIES FOR SKIN FRICTION COMPUTATION
      XI12=XI1+XI2
      T=TM*(TLAM(2)*XI1+TLAM(3)*XI2)/XI12
      AMI2=(M(2)*XI1+M(3)*XI2)/XI12
      PI12=PDES*(LAM(2)*XI1+LAM(3)*XI2)/XI12
      RCI12=PI12/(1718.*T)
      XMU=2.27E-8*T**1.5/(198.6+T)
      VI12=(M(2)*SQRT(TM*TLAM(2))*XI1+M(3)*SQRT(TM*TLAM(3))*XI2)*49.2/XI
     *12
      REI12=RCI12*VI12*XI12*D1/XMU
      TW=2000.
      RT=1.E6
      CALL SKINF(REI12,AMI12,TW,T,GM,RT,1,CF)
      WRITE(6,342) AMI12,TW,T,REI12,RT,CF
  342 FORMAT(2X,10HFORE BODY ,1P6E15.7)
C   DETERMINE FORCE COEFFICIENTS IN THE BODY AXIS SYSTEM
      AWFI1=X(1)*(X(1)*X(2)-X(3))*(TAN(THETA(1))-H1)/BD1
      DF1=AWFI1*CF*M2(2)*LAM(2)/2.
      DC=LAM(2)*M2(2)*GM*CF/2.
      CFX(1)=LAM(2)*TAN(DEL1)*DC+DF1*COS(DEL1)
      AWFI2=(Y4+X(3)*TAN(DEL(3)))*X(2)/BD1
      DF2=AWFI2*CF*M2(3)*LAM(3)/2.
      D2=X(2)*LAM(3)*M2(3)*GM*CF/2.
      CFX(2)=LAM(3)*X(2)*TAN(DEL(3))+D2+DF2*COS(DEL(3))
      CFY(1)=LAM(2)*LAM(2)*M2(2)*GM*TAN(DEL1)*CF/2.-DF1*TAN(DEL1)
      CFY(2)=LAM(3)*X(2)-LAM(3)*M2(3)*X(2)*TAN(DEL(3))*GM*CF/2.-DF2*TAN(
     *DEL(3))
      FCI12=CD+D2
      PCI12=CFX(1)+CFX(2)-FCI12
C LEADING EDGE DRAG
C      INLET FENCES
      CLED1=CLE/D1
      CDLFF=2.*.8*1.4*M(1)**2.*SIN(THETA(1))**2.*DLED1*M3/(BD1*D1)
C  INLET COWL WETTED BY PROPULSIVE STREAM
      T=TM*TLAM(4)
      AP3=P(4)
      REI3=PDES*LAM(4)*X(3)*C1*M(4)*SQRT(T)*49.2/(1718.*T*XMU)
      CALL SKINF(REI3,AM3,TW,T,1.4,RT,3,CF)
  343 FORMAT(2X,10HINLET COWL,1P6E15.7)
      WRITE(6,343) AM3,TW,T,REI3,RT,CF
      CFX(3)=LAM(4)*M2(4)*GM*CF*(X(3)+Y4*X(3)/BD1)/2.
      CFY(3)=(LAM(6)-LAM(4))*X(3)
C  COMBUSTOR FORCE CALCULATION-VALUE OF CAV45 DETERMINES WEIGHTING
C  OF PROPERTIES AT STATIONS (4) AND (5) IN DETEMINING AVERAGE PROPERTIES
C   TRANSITION REYNOLDS NUMBER OF RT=1000. WILL GIVE PREDOMINATELY
C   TURBULENT VALUE OF SKIN FRICTON
      T=T*(1.-CAV45*(1.-TEMP5/T))
      AP45=P(4)*(1.-CAV45*(1.-AM5/M(4)))
      VC45=V4*(1.-CAV45*(1.-V5/V4))
      RT=1.E3
      PAV45=PDES*LAM(4)*(1.-CAV45*(1.-P))
      XMU=2.27E-8*T**1.5/(198.6+T)
      RE4=PAV45*VC45*(X(4)+X(3)/2.)*D1/(1718.*T*XMU)
      GAM45=1.4*(1.-CAV45*(1.-GAM5/1.4))
      CALL SKINF(RE4,AM45,TW,T,GAM45,RT,4,CF)
  344 FORMAT(2X,10HCOMBUSTOR ,1P6E15.7)
      WRITE(6,344) AM45,TW,T,RE4,RT,CF
      CFX(4)=CF*(PAV45/PDES)*AM45*AM45*GAM45*(X(4)+X(4)*Y4/BD1+X(6)/2.*X
     2(6)*Y4/(2.*RD1))
      CFY(4)=LAM(6)*X(4)
C  CALCULATION OF FORCES ON UNDER SIDE OF INLET COMBUSTOR AND NOZZLE COWL
      RT=1.E6
      XL36=X(3)+X(4)+X(6)
      T=TM*TLAM(6)
      AP36=P(6)
      XMU=2.27E-8*T**1.5/(198.6+T)
```

```
      RE36=PCES*LAM(6)*XL36*D1*M(6)*SQRT(T)*49.2/(1718.*T*XMU)
      CALL SKINF(RE36,AM36,TW,T,1.4,RT,5,CF)
      CFX(6)=LAM(6)*M(6)*M(6)*1.4*CF*XL36/2.
      CFY(6)=LAM(6)*X(6)
  233 CONTINUE
C  CALCULATION OF FORCES ON UPPER SURFACE OF FUSELAGE
      RT=1.E6
      T=TP*TLAM(8)
      APT=P(8)
      XMU=2.27E-8*T**1.5/(198.6+T)
      RETP=PCES*LAM(8)*XL*D1*M(8)*SQRT(T)*49.2/(1718.*T*XMU)
      CALL SKINF(RETP,AMT,TW,T,1.4,RT,6,CF)
      IF(I.EQ.9) WRITE(6,345) AMT,TW,T,RETP,RT,CF
  345 FORMAT(2X,10HTOP OF FUS,1P6E15.7)
      D3=LAP(8)*M(8)*M(8)*XL*GM*CF/2.
      CFX(7)=LAM(8)*XL*TAN(DEL7)+D3
      PCTP=CFX(7)-D3
      CFY(7)=-LAM(8)*XL*LAM(8)*M(8)*M(8)*XL*TAN(DEL7)*GM*CF/2.
C  CALCULATION OF BASE PRESSURE DRAG, BASE PRESSURE IS ZERO
      PB=0.
      CFX(8)=-PB*Y5
C  FORCE ON SIDES OF VEHICLE IN WIND AXIS SYSTEM
      X4=1.+X(2)+X(4)
      B=X4*TAN(DEL7)+H3
      VOL2B=.5*H1*H1*X(2)+.5*X(2)*H2*(H3)*X(4)+(B+Y5)*X(5)/2.+.5*X4*X4*T
     1AN(DEL7)
      T=TP
      RESI=RHO*M(1)*CO*D1*XL/AMU
      APSI=P(1)
      CALL SKINF(RESI,AMSI,TW,T,1.4,RT,7,CF)
      IF(I.EQ.9) WRITE(6,346) AMSI,TW,T,RESI,RT,CF
      CDSF=VOL2B*M(1)*M(1)*GM*CF/BD1
      CDFNS=P(1)**2.*GM*CF*(AWNOZ+AWFI1+AWFI2)
      CDSF=CDSF+CDFNS
  346 FORMAT(2X,10HFUSE SIDES,1P6E15.7)
C  TRANSFORM BODY FORCE COEFFICIENTS TO WIND AXIS SYSTEM
      CA=CFX(1)+CFX(2)+CFX(3)+CFX(4)+CFX(6)+CFX(7)+CFX(8)
      CN=CFY(1)+CFY(2)+CFY(3)+CFY(4)+CFY(6)+CFY(7)
      SA=SIN(ALPHAR)
      CDSA=CDS(ALPHAR)
C     VEHICLE NOSE AND EDGE OF INLET COWL LEADING EDGE DRAG
      CDLEPC=.6*1.4*M(1)**2.*DLED1*2.
      CDB=CA*CDSA+CN*SA+CDSF+CDLEBC+CDLEF
      CLB=-CA*SA+CN*CDSA
C  REFFERENCE NOZZLE FORCE COEFFICIENTS TO SAME QUANTITIES AS BODY FORCES
      CFX(5)=CF1*PRTIOF(EMIP,GAMMAP)*Y4*LAM(4)*P
      CFY(5)=CF2*PRTIOF(EMIP,GAMMAP)*Y4*LAM(4)*P
C     TRANSFORM TO WIND AXIS SYSTEM
      TWL=CFY(5)*CDSA+CFX(5)*SA
C  COMPUTE FLOW PROPERTIES FOR SIDE SURFACE OF WING
      IF(P12.GT.-1.) GO TO 41
      T12=TLAM(12)
      P12=LAP(12)
      AP122=P2(12)
      LAP(12)=1.
      P2(12)=M(1)*M(1)
      DEL(12)=DELD(12)/57.29775
      IF(DEL(12).LE.0.) GO TO 19
      CALL SHOCK(12,12,88)
      GO TO  41
   19 CALL PRANT(12)
   41 CONTINUE
      T9T11=XTAN9*XTAN11
      TWD=CFX(5)*CDSA-CFY(5)*SA
C  TEST TO DETERMINE IF CONSTRAINTS HAVE BEEN EXCEEDED AND WHETHER THE
C  PROJECTION OF NOZZLE FORCE ALONG VELOCITY VECTOR EXCEEDS BODY DRAG
      IF(X(5).LT.X5C.AND.Y5.GT.0..AND.(TWD-CDB).LT..05) RETURN
      IF((TWD-CDB).LT..05)GOTO334
C  ITERATE TO SIZE NON-DIMENSIONAL WING AREA-AWNG-FOR UNACCELERATED FLIGHT
C   COMPUTE TRIAL VALUE OF WING AREA
      AWNG=(TWD-CDB)/(DELD(11)*ABS(CELD(12)))
      XTAN12=ABS(TAN(CEL(12)))
      XCOS12=COS(DEL(12))
      ATRAT=XTAN12/PASPR
    5 CONTINUE
C   DIVICE WING AREA INTO TRIANGULAR AND RECTANGULAR SECTION
      ATRI=ATRAT*AWNG
      AREC=AWNG-ATRI
C   DETERMINE NON-D WING LENGTH,XW, AND WIDTH,BWBC=BW/B,OF RECTANGULAR SEC
      XW=SQRT(ABS(BC1*AWNG/PASPR))
      BWBC=AREC/XW
C   COMPUTE FORCES ON UPPER WING SURFACE
      AP10=P(10)
      T=TP*TLAM(10)
      XMU=2.27E-8*T**1.5/(198.6+T)
      REUW=PCES*TLAM(10)*XW*C1*49.2*M(10)*SQRT(T)/(1718.*T*XMU)
      CALL SKINF(REUW,AP10,TW,T,1.4,RT,8,CF)
      FDUW=LAM(10)*AWNG*M(10)*M(10)*GM*CF/2.
      CFX(9)=LAM(10)*AWNG*XTAN9+FDUW
      PDUW=CFX(9)-FDUW
      CFY(9)=LAM(10)*AWNG*(-1.*M(10)*M(10)*GM*CF*XTAN9/2.)
C   COMPUTE FORCES ON LOWER WING SURFACE
      T=TP*T12
      XMU=2.27E-8*T**1.5/(198.6+T)
      AP12=SQRT(AP122)
      RELW=PCES*P12*XW*C1*AM12*49.2*SQRT(T)/(1718.*T*XMU)
      CALL SKINF(RELW,AM12,TW,T,1.4,RT,9,CF)
      FDLW=P12*AWNG*AM122*GM*CF/2.
      CFX(10)=P12*AWNG*XTAN11+FDLW
      PDLW=CFX(10)-FDLW
      CFY(10)=P12*AWNG*(1.-AM122*XTAN11*GM*CF/2.)
      IF(CELC(12).LE.0.) GO TO 55
C COMPUTE PRESSURE FORCES ON SIDES AND BASE OF WING
      CFX(11)=-PB*T9T11*(AREC+2.*ATRI)
      CFX(12)=LAM(13)*ATRI*T9T11
      GO TO 20
   55 CFX(11)=-PB*T9T11*AREC
      CFX(12)=LAM(13)*ATRI*T9T11*(-1.)
   20 CONTINUE
      CAW=CFX(9)+CFX(10)+CFX(11)+CFX(12)
      CNW=CFY(9)+CFY(10)
C     WING LEADING EDGE DRAG
      CDLEW=.6*1.4**M(1)**2.*DLED1*BWBC
C   TRANSFORM WING FORCES FROM BODY AXIS TO WIND AXIS SYSTEM
      CLW=-CAW*SA+CNW*COSA
C   TEST FOR UNACCELERATED FLIGHT
      CDW=CAW*COSA+CNW*SA+CDLEW
      EXCESS=TWD-CDP-CDW
      IF(ABS(EXCESS).LT..001) GO TO 6
C   COMPUTE NEW TRIAL WING AREA
      AWNG=AWNG+.1*EXCESS
C   CONTINUE ITERATION ON WING AREA
      GO TO 5
    6 CONTINUE
```

```
      IF(AWNG.LE.0.) RETURN
C COMPUTATION TO FIND LONGITUDINAL WING PLACEMENT SUCH THAT THE SUM OF
C THE PITCHING MOMENTS ABOUT THE CENTER OF GRAVITY IS ZERO
C  COMPUTE MOMENTS ABOUT LEADING EDGE OF VEHICLE(PITCH UP IS POSITIVE)
      CMX5=CMX*PRTIOF(EM1P,GM)*Y4*Y4*LAM(4)*P
      CMY5=CMY*PRTICF(EM1P,GM)*Y4*Y4*LAM(4)*P
      CMX1L=-CFX(1)*H1/2.
      CMX2L=-CFX(2)*(H1+H2/2.)
      CMX3L=-CFX(3)*(H3+Y4)
      CMX4L=-CFX(4)*(H3+Y4)
      CMX6L=-CFX(6)*(H3+Y4)
      CMX7L=CFX(7)*(XL+TAN(DEL7)/2.)
      CMX5L=CMX5+CFX(5)*(H3+Y4)
      CMY1L=-CFY(1)*X(1)/2.
      CMY2L=-CFY(2)*(1.+X(2)/2.)
      CMY3L=-CFY(3)*(1.+X(2)-X(3)/2.)
      CMY4L=-CFY(4)*(1.+X(2)+X(4)/2.)
      CMY6L=-CFY(6)*(1.+X(2)+X(4)+X(6)/2.)
      CMY7L=-CFY(7)*XL/2.
      CMY5L=CMY5-CFY(5)*(1.+X(2)+X(4))
      CFYTCL=CN+CFY(5)
      CFXTCL=CA-CFX(8)-CFX(5)
      CMXLE=CMX1L+CMX2L+CMX3L+CMX4L+CMX5L+CMX6L+CMX7L
      CMYLE=CMY1L+CMY2L+CMY3L+CMY4L+CMY5L+CMY6L+CMY7L
C  COMPUTE CENTER OF FORCE LOCATION
      YCF=CMXLE/CFXTOL
      XCF=-CMYLE/CFYTOL
C  COMPUTE CENTER OF GRAVITY LOCATION(ASSUMED TO BE CENTROID OF PROFILE AREA)
      A1=H1/2.
      A2=H1+X(2)
      A3=H2*X(2)/2.
      A4=(H1+H2)*X(4)
      A5=(B+Y5)*X(5)/2.
      A6=X4*X4+TAN(DEL7)/2.
      RHRV=1.
      XC5=X(5)*(B+2.*Y5)/(3.*(B+Y5))+X4
      YC5=(H3+XL*TAN(DEL7))*(B+2.*Y5)/(3.*(B+Y5))*(B-Y5)/3.-H3
      XC6=2.*X4/3.
      YC6=X4*TAN(DEL7)/3.
      ATCL=A1+A2+A3+A4+A5+A6
      XCT=2.*A1/3.*(1.+X(2)/2.)*A2+(1.+2.*X(2)/3.)*A3+(1.+X(2)+X(4)/2.)*
     2A4+A5*XC5+A6*XC6
      YCT=-H1*A1/3.-A2*H1/2.-(H1+H2/3.)*A3-(H1+H2)*A4/2.+A5*YC5+A6*YC6+A
     2WT*XL*XTAN9/3.
C  LOCATION OF CG
      XCM=XCT/ATCL
      YCM=YCT/ATCL
      CMYCM=(XCM-XCF)*CFYTOL
      CMXCM=(YCM-YCF)*CFXTOL
C  TOTAL MOMENT PRODUCED BY BODY FORCES
      CMTCM=CMYCM+CMXCM
C  MOMENT PRODUCED BY AXIAL FORCE OF OF WING SURFACES
 88   IF(DEL(12).LE.0.) XCPLEW=((.5*AREC+1.*ATRI/3.)/AWNG)*XW
      IF(DEL(12).GT.0.) XCPLEW=((.5*AREC+2.*ATRI/3.)/AWNG)*XW
      CMCAW=CFX(9)*(XCPLEW*XTAN9-YCM)+CFX(10)*(-XCPLEW*XTAN11-YCM)+CFX(1
     $1)*(XW*(XTAN9-XTAN11)-YCM)+C*X(12)*(2.*X0*(XTAN9-XTAN11)*3.-YCM)
C  LONGITUDINAL POSITION OF WING NORMAL FORCE TO PRODUCE ZERO MOMENT ABOUT
C  THE CENTER OF GRAVITY
      XCPCM=(CMTCM+CMCAW)/CNW
      XCPLEV=XCM+XCPCM
      XLWLEV=XCPLEV-XCPLEW
C  PCON IS EXTERNAL CONTROL-IF PCON EQUAL 1 DISREGARD ABOVE WING PLACEMENT
C  CALCULATION AND POSITION WING SUCH THAT TRAILING EDGE OF WING AND
C  VEHICLE ARE EQUAL
      IF(PCON.EQ.1) XLWLEV=XL-XW
C  COMPUTE NON-DIMENSIONAL SURFACE AREA AND VOLUME
      XCOS9=COS(DEL(9)/57.29775)
      XCOS11=COS(DELD(11)/57.29775)
C   BODY WETTED AREA
      AWD12=2.*VD12B+BD1*(1./COS(DEL1)+X(2)/COS(DEL(3))+X(4)+X(5)/COS(DE
     2L5)+XL/COS(DEL7)+Y5)
      AWRD12=XW*(XTAN9+XTAN11)*(0.+1.*BWBC*BD1)+XW*(1./COS(DELD(9)/57.2
     29775)+1./COS(DELD(11)/57.29775))*BWBC*BD1
C   WING WETTED AREA
      AWTC12=XW*XW*XTAN12*(1./XCOS9+1./XCOS11)+XW*XW*T9T11*(2.*XTAN12+1.
     2/XCOS12)
      IF(XLWLEV.GT.XL) AWTCV=0.
      IF(XLWLEV.GT.XL) GO TO 335
C   ADJUST TOTAL WETTED AREA FOR WING AREA COVERING FUSELAGE
      IF((XLWLEV+XW).GE.XL) XCOVER=XL-XLWLEV
      IF((XLWLEV+XW).LT.XL) XCOVER=XW
      XTE=XL-(XLWLEV+XW)
      IF(XTE.LT.0.) XTE=0.
      HUP=(-1.)*(XCOVER*XTAN9)
      HLC=XCOVER*XTAN11
      BTST=H3+TAN(DEL5)*(XTE-X(5))
      BY5=H3-X(5)*TAN(DEL5)
      XUMAX=(BY5+(XCOVER+XTE)*TAN(DEL5))/(TAN(DEL5)-XTAN9)
      XLMAX=(BY5+(XCOVER+XTE)*TAN(DEL5))/(TAN(DEL5)+XTAN11)
      IF(HUP.LT.BTST.AND.HLO.LT.BTST)AWTCV=XCOVER**2*T9T11
      IF(HUP.LT.BTST.AND.HLO.GE.BTST)AWTCV=XCOVER**2*T9T11-(HLO-BTST)*((
     $(XCOVER-XTE)*XTAN11-BY5)/(TAN(DEL5)+XTAN11)-XTE)
      IF(HUP.GE.BTST.AND.HLO.GE.BTST)AWTCV=XLMAX**2*XTAN11+XUMAX**2*XTAN
     $9-(XUMAX-XLMAX)*XUMAX*T9T11
 335  CONTINUE
      IF(X(5).GE.X5C.OR.Y5.LE.0..AND.XLWLEV.GT.XL)WRITE(6,992)
C     FENCE AREA
      AWFN=(AWNOZ+AWFI1+AWFI2)*BD1
C   WING VOLUME
      IF(DEL(12).GE.0.) VTC12B=2.*XW**3.*T9T11*XTAN12/3.
      IF(DEL(12).LT.0.) VTD12B=1.*XW**3.*T9T11*XTAN12/3.
      VRC12B=.5*XW*XW*BWBC*(XTAN9+XTAN11)
 75   VWC12B=VRD12B+VTC12B
      AWGC12=AWRC12+AWTC12-AWTCV
      IF(AWGC12.LE.0.) GO TO 79
C   TOTAL VOLUME
 79   VTC12B=VC12B+VWC12B
C   TOTAL WETTED AREA
      ATGC12=AWD12+AWGC12+AWFN
C STRUCTUAL SET MEMBERS
C  DENSITIES- FUEL, PAYLOAD, EQUIPMENT
      RDEFL=4.5
      RDEPA=4.5
      RDEEC=40.*RDEPA
C  AREA-WEIGHT PARAMETER
      RDEST=7.5
C  PAYLOAD AND EQUIPMENT FRACTIONS
      PCTP=.05
      PCTE=.15
C PER CENT  OF TOTAL FUEL TO BE USED IN CRUISE
      PCTFCR=.5
C CALCULATE SCALE FACTOR-LENGTH OF FIRST INLET RAMP- BY ITERATION
      CCE1=7.5*VTC12B*BD1
      CCE2=ATGC12*RDEST
```

```
C  ESTIMATE TRIAL VALUE
       DC=(WTO/(VTD12B*BD1*11.))**.333
C  CALCULATE TAKE OFF WEIGHT
 16    WTC=(VTD12B*BC1*DC*DC*DC*ROEST*ATGD12*DC*DC/ROEFL)/((1.-PCTP-PCTE
      $/ROEFL*PCTP/ROEPA*PCTE/ROEEQ)
       FC1=WTC-WTO
C  TEST TO DETERMINE IF CALCULATED IS WITHIN 10 LB OF SPECIFIED TAKE OFF
C  WEIGHT
       IF(ABS(FD1).LE.10.) GO TO 17
C  DETERMINE NEW TRIAL SCALE FACTOR USING NEWTON-RAPHSON METHOD
       FDDT=3.*COE1*DC**2.+2.*COE2*DC
       DC=DC-FD1/FDDT
C  CONTINUE ITERATION
       GO TO 16
C DETERMINE STRUCTUAL WEIGHT FRACTION
 17    STFRAC=COE2*DC**2./WTO
C DETERMINE FUEL WEIGHT FRACTION
       PCTVF=1.-STFRAC-PCTE-PCTP
C EVALUATE LOG TERM OF BREQUET RANGE EQUATION(STRUCTUAL FACTOR)
       SF=ALOG(1.+PCTFCR*PCTVF/(PCTE+PCTP+STFRAC))
C COMPUTE CRUISE VELOCITY BASED ON CRUISE MACH AND SPEED OF SOUND AT
C REFERENCE  ALTITUDE-V12- CRUISE VELOCITY(FT/SEC) SQUARED
       V12=CO*CO*M(1)*M(1)
C COMPUTE RANGE FACTOR OF BREQUET RANGE EQUATION-RF (NAUTICAL MILES)
C VC2-ORBITAL VELOCITY(FT/SEC) SQUARED
       VC2=26000.*26000.
       FULAR=ER*.0292
       R1=V12/((1.-V12/VO2)*64.34*FULAR*6076.)
       Y6=CLP*CLW*TWL
       DELD(8)=(1.428*Y6)/(M(1)*M(1)*CACAP)
       RF=R1*DELD(8)
       RLAST=R
C COMPUTE CRUISE RANGE
       R=RF*SF
C COMPUTE PRESSURE AT CRUISE ALTITUCE WHERE PCTFA IS PER CENT OF TOTAL
C FUEL USED DURING TAKE OFF, CLIMB AND ACCELERATION
       PCTF=.5*PCTVF
       PALT=(1.-PCTFA)*WTO*(1.-V12/VO2)/(Y6*DC*DC*BD1)
       FCW=FCLW+FCUW
       KCK=KCK+1
C COMPUTE SPECIFIC IMPULSE
       AISPT=CO*M(1)*TWD/(32.17*FULAR*1.4*P(1)*P(1)*CACAP)
C COMPUTE POWER ON LIFT-DRAG RATIO
       RANF=RF*6076.
       ALCCT=RANF*(1.-V12/VO2)/(CO*M(1)*AISPT)
C TEST FOR DECREASE IN CRUISE RANGE IF SO-OPTIMUM NOZZLE LENGTH OBTAINED
       IF(KCK.EQ.1)WRITE(6,600)
 600   FORMAT(2X,5HSCALE,3X,4HPALT,3X,3HISP,3X,3HL/D,3X,1HR,3X,2HRF,2X,2H
      $SF,3X,2HPF,3X,2HX5,/)
       RANF=RF
       SEFCV=SF
       IF(RLAST.GT.R.AND.DELD(4).LT.5.) RETURN 1
       RETURN
 992   FORMAT(2X,51HGEOMETRICAL CONSTRAINT AND EDGE OF WING OFF VEHICLE.)
 721   FORMAT(3X,1P7E15.7)
 334   CONTINUE
       WRITE(6,350)
 350   FORMAT(2X,41HGEOMETRICAL CONSTRAINT AND THRUST NE DRAG.)
       RETURN
 8     CONTINUE
 60    RETURN
       END
```

```
$IBFTC SKIN    DECK
       SUBROUTINE SKINF(RX,EM,TW,T,GAMF,RT,I,CF)

C THE PURPOSE OF THIS SUBROUTINE IS TO CALCULATE SKIN FRICTION
C AND HEAT TRANSFER COEFFICIENTS

       COMMON/COSF/ ST(10)
       DIMENSION G(10)
       DATA G/-5.811434E1,3.7558925E1,-1.0779506E1,1.1521712,-1.78021280E
      $-1,1.1999272E-2,-5.3483789E-4,1.5214431E-5,-2.5064468E-7,1.821E-9/
       IF(ST(2).GT.(-1.1) GO TO 33
C  CALCULATION  OF AVERAGE TURBULENT VALUE OF SKIN FRICTION BY SPALDING-CHI
C  METHOD(REF26/40)-NOTATION FOLLOWS REF 26
       XMU=2.27E-8*T**1.5/(198.6+T)
       RECOV=.89
       A=TW/T
       C=RECOV*EM*EM*.5*(GAMF-1.)/(-2.)
       B=1.-C-A
       RAD=SQRT(B**B-4.*A*C)
       TABW=T*(1.-C)
       FC=((ARSIN(-(2.*C+B)/RAD)-ARSIN(-B/RAD))/SQRT(-C))**(-2.)
       FRTATA=(A**(-.702))*((TABW/TW)**.772)
       FRX=FRTATA/FC
       XX=ALOG(FRX*RX)
       PCLYB=G(1)+G(2)*XX+G(3)*XX**2.+G(4)*XX**3.+G(5)*XX**4.+G(6)*XX**5+
      $G(7)*XX**6.+G(8)*XX**7.+G(9)*XX**8.+G(10)*XX**9.
C   AVERAGE SKIN FRICTION COEFFICIENT ASSUMING TURBULENT FLOW FOR ENTIRE
C   SURFACE
       CFTS=(1./FC)*2.72**POLYB
C  CALCULATION OF AVERAGE LAMINAR VALUE OF SKIN FRICTION BY INCOMPRESSIBLE
   LAMINAR BLASIUS SOLUTION MODIFIED BY REFERENCE TEMPERATURE METHOD
   TO ACCOUNT FOR COMPRESSIBILITY(REF 15)
C   COMPUTE REFERENCE TEMPERATURE
       IF(EM-5.12,2,3
 2     TPL=T*(1.+.032*EM*EM+.58*(TW/T-1.))
       GO TO 4
 3     TPL=T*(.7+.023*EM*EM+.58*(TW/T))
 4     CONTINUE
       XMUPL=2.27E-8*TPL**1.5/(198.6+TPL)
       XKL=.441*(T*XMUPL/(TPL*XMU))
       IF(RT-RX)5,25,25
C   COMPUTE SKIN FRICTION COEFFICIENT FOR ENTIRELY LAMINAR BOUNDARY LAYER
 5     CFL=2.*SQRT(XKL/RX)
C COMPUTE AVERAGE SKIN FRICTION COEFFICIENT FOR TRANSITIONAL BOUNDARY
C LAYER BASED ON TRANSITION REYNOLDS NUMBER-RT
       CFTRS=CFTS*(1.-RT/RX+(CFL/CFTS)**1.25*(RT/RX)**.625)**.8
       CF=CFTRS
       GO TO 30
C USE LAMINAR SKIN FRICTION COEFFICIENT IF REYNOLDS NUMBER IS LESS THAN
C TRANSITION REYNOLDS NUMBER
 25    CFL=2.*SQRT(XKL/RX)
       CF=CFL
 30    CONTINUE
       ST(I)=CF
       RETURN
 33    ST(I)=ST(2)
       CF=ST(I)
       RETURN
       END
```

```
      SUBROUTINE CCCL(BWBC)

C THIS SUBROUTINE COMPUTES FUEL FLOW REQUIRED TO PROVIDE REGENERATIVE
C CCCLING FOR COMBUSTOR AND PORTIONS OF THE INLET AND NOZZLE, ALSO THE
C     LEADING EDGES OF THE VEHICLE AND WINGS

      COMMON /VAR/M(13),DEL(13),DELC(13),LAM(13),THETA(13),XCWL,M2(13),
     1X(6),R,Y4,Y5,CFX(13),CFY(13),CEL9,ALPHAR,CACAP,TLAP(13),FXCESS,
     2ER,AP5,P
      COMMON /VAREC/ TEMP5,V4,V5,HINF5,GAM5,BD1,CAV45,R5,AM6,TEMP65
      COMMON /VAR2/ P12,PASPR,MF,PDES,PALT,WTOD,WTOT,CWT,PALTT,CPALT,XSD
      COMMON /ADC1/ DLE,D1,WTO
      COMMON /CONSF/ ST(10)
      REAL M,M2,LAM
C  CONSTANTS USED IN SUBROUTINE
      GAP=1.4
      RACT=49719.
C   CPH2-SPECFIC HEAT CAPACITY OF LIQUID HYDROGEN(BTU/LB)
      CPH2=6000.
C   GJ2-USED IN COVERSION OF UNITS OF ENTHAPY FROM MECHANICAL TO THERMAL
      GJ2=32.17*778.07.
C   FST-STOCHIMETRIC FUEL-AIR RATIO- HYDROGEN-AIR
      FST=.0292
C   PR-RECOVERY FACTOR USED IN DETERMINATION OF ADIBATIC WALL ENTHALPY
      PR=.89
      R3=RACT/28.9
C  DETERMINE AMBIENT TEMPERATURE AT REFERENCE ALTITUDE
      CALL ATMOS(MF,TM,SIGMA,RHO,THETT,DELTA,CO,AMU,K)
      C2=1.+(CPH2*FST*2.)
      RLE=DLE/2.
      GSTAG=.725*865.*(M(1)*CO/1.E4)**3.15*(SIGMA/RLE)**.5
      DLE=DF1*(2.*PWBC)*2.*RLE*D1*QSTAG
      EPCLE=CLE/(FST*RHO*CO*M(1)*CACAP*D1*D1*6D1*CPH2*32.2)
      WRITE(6,45) GSTAG,DLE,EPCLE
C  COMPUTE COOLING REQUIREMENT FOR UNDER SURFACE OF FUSELAGE OPPOSITE
C  INLET COWL
C   DETERMINE RATIO OF COOLED AREA TO PROPUSIVE STREAM TUBE AREA IN PLANE
C   NORMAL TO COOLED SURFACE
      AIAC3=X(2)/(COS(DEL(3))*(Y4+X(3)*TAN(DEL(3))))
C   DETERMINE VELOCITY IN PROPULSIVE STREAM TUBE
      T3=TLAP(3)*TM
      V3=M(3)*SQRT(GAM*R3*T3)
      V32=V3*V3
C   DETERMINE STATIC ENTHALPY IN STREAM TUBE(SUBROUTINE AIRTAB TABLES BASED
C   ON DATA FROM REF 29 AT ZERO EQUIVALANCE RATIO)
      CALL AIRTAB(T3,H3)
      HABW3=H3+PR*V32/GJ2
      TW3=2000.
C   WALL ENTHALPY
      CALL AIRTAB(TW3,HW3)
      HW=HW3
      C3=ST(1)/C2
C   CCOLING EQUIVALENCE RATIO FOR SURFACE
      FERCI=C3*AIAC3*(HABW3-HW)/COS(DEL(3))
      IF(FERCI.LT.0.) FERQI=0.
C     COMPUTE COOLING REQUIREMENT FOR INLET FENCE ALONG SHOCK FROM
C     SECOND INLET RAMP
      AFAC3=X(2)/(BD1*COS(DEL(3)))
      FERCFI=C3*AFAC3*(HABW3-HW)
C  COMPUTE COOLING REQUIREMENTS FOR INLET COWL AND SIDES
      ALEAC4=(X(3)*(1.+1.*Y4/BD1))/Y4
      TEMP4=TLAM(4)*TM
      CALL AIRTAB(TEMP4,H4)
      HABW4=H4+PR*V4*V4/GJ2
      C3=ST(3)/C2
C   CCOLING REQUIREMENT FOR SURFACE
      FERCLE=C3*ALEAC4*(HABW4-HW)
C  COMPUTE COOLING REQUIREMENTS FOR COMBUSTOR
      ASCAC4=2.*X(4)*(1./Y4+1./BD1)
      HABW5=HINF5+PR*V5*V5/GJ2
C   AVERAGE ADIBATIC WALL ENTHALPY BETWEEN ENTRANCE AND EXIT OF COMBUSTOR
      HABW45=HABW4-(1.-CAV45*(1.-HABW5/HABW4))
      C3=ST(4)/C2
C   CCOLING REQUIRE FOR COMBUSTOR
      FERCCP=C3*ASCAC4*(HABW45-HW)
C  CCCLING REQUIRED FOR NOZZLE COWL AND SIDES
      ATEAC5=(X(6)*(1.+Y4/BD1))/Y4
C   CCOLING REQUIRED
      FERCTE=C3*ATEAC5*(HABW5-HW)
C  CCOLING REQUIRED FOR AFT-FUSELAGE SURFACE OPPOSITE NOZZLE COWL
      ANZAC6=X(6)/(COS(DEL5)*(Y4+X(6)*TAN(DEL5)))
      TEMP6=TEMP5*TEMP65
      V6=AP6*SQRT(GAM5*R5*TEMP6)
      HABW6=HABW5
      C3=ST(10)/C2
      FERCNZ=C3*ANZAC6*(HABW6-HW)
      FERCAF=C3*(HABW6-HW)*X(6)/(BD1*COS(DEL5))
C  TOTAL COOLING REQUIREMENT FOR SURFACES CONSIDERED
      TFERC=FERQI+FERCLE+FERQCB+FERCTE+FERQNZ+FERCFI+FERCAF+ERCLE
      WRITE(6,700) FERQI,FERCLE,FERQCB,FERQTE,FERQNZ,TFERC
 700  FORMAT(2X,36HPHI'S FROM INLET TO NOZZLE AND TOTAL,//,2X,6F13.6//)
      RETURN
      END
C**********************END OF PROGRAM LISTING*****************************
```

Unclassified

Security Classification

DOCUMENT CONTROL DATA - R & D

(Security classification of title, body of abstract and indexing annotation must be entered when the overall report is classified)

1. ORIGINATING ACTIVITY (Corporate author)	2a. REPORT SECURITY CLASSIFICATION
Aerospace Research Laboratories Hypersonic Research Laboratory Wright-Patterson AFB, Ohio 45433	Unclassified 2b. GROUP

3. REPORT TITLE

Configuration Optimization of a Class of Hypersonic Cruise Vehicles

4. DESCRIPTIVE NOTES (Type of report and inclusive dates)

Scientific Interim

5. AUTHOR(S) (First name, middle initial, last name)

Richard C. Walker

6. REPORT DATE	7a. TOTAL NO. OF PAGES	7b. NO. OF REFS
December 1970	135	30

8a. In-house Research	9a. ORIGINATOR'S REPORT NUMBER(S)
b. PROJECT NO. 7064-00-02	
c. DoD Element 61102F	9b. OTHER REPORT NO(S) (Any other numbers that may be assigned this report)
d. DoD Subelement 681307	ARL 70-0342

10 DISTRIBUTION STATEMENT

1. This document has been approved for public release and sale; its distribution is unlimited.

11 SUPPLEMENTARY NOTES	12. SPONSORING MILITARY ACTIVITY
TECH OTHER	Aerospace Research Laboratories (LH) Wright-Patterson AFB, Ohio 45433

13 ABSTRACT

An optimization of air breathing hypersonic cruise vehicles was performed in order to determine basic configuration characteristics and performance trends. A distinctive feature of the investigation is that prediction techniques such as the method of characteristics were used to determine the flow field surrounding the vehicle; therefore, any interaction between the aerodynamic and propulsive flow fields is accounted for in a fundamental manner. The general class of vehicles considered in the study cruise in the Mach 8-12 speed regime, utilize a hydrogen fueled supersonic combustion ramjet engine, and can be geometrically characterized as two-dimensional wedgelike shapes. Configurations were optimized for maximum cruise range as determined from the Breguet range equation which incorporates a measure of the aerodynamic, propulsive, and volumetric efficiencies of a configuration. A generalized configuration model was defined by a discrete parameters which transformed the variational problem to a static or discrete optimization problem. The direct method of function optimization, utilizing search algorithms such as random point and adaptive creeper techniques, was employed to determine the value of the parameters defining the optimum configuration for cruise at design Mach numbers of 8, 10, and 12. The design parameter space in the vicinity of the optimum point was explored to show performance sensitivity. Results of this study showed that optimum cruise configurations are characterized by small wings. Approximately three-fourths of the total lift is provided directly from the propulsive system in accordance with an expression for optimum propulsive force vectoring derived in the study. The results

DD FORM 1 NOV 68 1473

Unclassified

Security Classification

also indicated that Breguet range factors of approximately 10,000 nautical miles are attainable by vehicles which cruise in the Mach 8 to 12 speed regime.

Security Classification

14 KEY WORDS	LINK A		LINK B		LINK C	
	ROLE	WT	ROLE	WT	ROLE	WT
Configuration optimization						
Hypersonic vehicles						
Computer-aided design						
Direct search						

Security Classification